NTNU – Trondheim
Norwegian University of
Science and Technology

Alternating Current Corrosion of Aluminium Sacrificial Anodes

Kari Forthun

Chemical Engineering and Biotechnology
Submission date: June 2013
Supervisor: Kemal Nisancioglu, IMTE
Co-supervisor: Sven Morten Hesjevik, Statoil

Norwegian University of Science and Technology
Department of Materials Science and Engineering

Declaration

I hereby declare that this work has been carried out independently and according to the examination regulations of the Norwegian University of Science and Technology (NTNU).

Trondheim, 10.06.13

Kari Forthun

Preface

This master thesis has been written in the course TMT4900 Materials Chemistry and Energy Technology, during spring 2013 at the Department of Materials Science and Engineering at NTNU. The experimental work in relation to this project has been performed at the corrosion laboratory in KII at the Department of Materials Science and Engineering, between 15 January and 01 June 2013.

I thank my supervisor Professor Kemal Nisancioglu at the Department of Materials Science and Engineering at NTNU and co-supervisor Sven Morten Hesjevik at Statoil (Rotvoll) for guidance and sharing their knowledge throughout this project.

My gratitude goes to Staff Engineer Kjell Røkke for technical assistance throughout the project. He has always been available for valuable help and support in my day-to-day work. I thank Asbjørn Fjellvikås at the Technical Section of the faculty of Natural Science and Technology for help in development and implementation of new software and logging instrument.

Thanks are due to Statoil at Rotvoll for the supply of anode materials. Special credit goes to Jack Monsen at BEME Corrosion International for providing me with anode materials. His genuine interest in helping me has been invaluable. I also wish to thank SINTEF for the supply of the steel materials and the workshop at the Faculty for Natural Science and Technology at NTNU, for machining of the test materials and supply of test equipment.

Last, but not least, I would like to thank fellow students, for sharing knowledge, good stories and gossip in countless coffee breaks. You have been an inspiration, motivation and valuable support, and the main reason for five years with happiness in Trondheim.

Trondheim, June 2013

Abstract

Direct Electric Heating (DEH) is applied to subsea oil production and transmission pipelines to prevent freezing of hydrates as wax during productions shut downs, or during other conditions where the temperature is low. To prevent clogging, the pipes are heated by application of alternating current (AC) voltage. As a result, a risk for AC corrosion is introduced, which is the motivation and subject of this thesis. The steel pipes are coated and applied conventional cathodic protection (CP) by use of AlZnIn sacrificial anodes. Earlier project and thesis work at NTNU indicate that the steel pipes are well protected during application of AC. Therefore, the present work focused on the risk of increased rates of AC influenced corrosion of the AlZnIn anodes. Anode samples coupled to steel samples were investigated under applied AC by use of laboratory scale test cells in synthetic seawater at room temperature. In these experiments, which lasted for one week, the applied AC was varied in the range 0.5 to 150 A m^{-2}, and the anode-steel area ratio (AR) was set to either 10:1 or 100:1. Corrosion rates were assessed by weight loss measurements and properties of surface deposits and corroded surfaces were analyzed by X-ray diffraction (XRD) and scanning electron microscopy (SEM), respectively. For better assessment of anode-steel coupling in practice and the significance of anode-steel area, similar tests were performed by using a connection of two identical pairs of parallel-coupled anode-steel, with area ratio of 100:1. This configuration is thought to simulate the connection of the DEH system to two bracelet anode pairs located at a distance to one another along the pipeline length to be heated. Equipment and methodology for investigation of AC corrosion were developed and evaluated.

Results show that the anode corrosion rate increased with increasing applied AC level, while steel is sufficiently protected under the experimental conditions specified above. Anode corrosion rate was influenced both by current provided for the protection of the steel and self-corrosion, and the attack was characterized by pit formation and coalescence of these at higher AC levels. High self-corrosion rates were attributed to successive alkalization, explained by hydrogen evolution, and acidification of the anode surface at each AC cycle, which destabilized the protective oxide layer. Corrosion was limited at high AC levels, explained by hydrogen blanketing of the anode surface and by hydrogen trapped within pores of the hydroxide surface film. AC corrosion of the anodes depended strongly on the anode-steel area ratio. In experiments with electrode pair configuration as described above, the significance of the steel samples vanished by increasing the anode-steel area ratio to 100:1. The system functioned as an anode – anode galvanic couple, which caused a significant decrease in the potential of the anodes, giving rise to runaway self-corrosion rates.

In experiments with one anode-steel couple, the couple potential also decreased once AC was applied, increasingly in extent with applied AC potential. This further increased the current requirement by increasingly cathodic steel, thereby resulting in extreme anode corrosion at high AC levels ($\geq$ 2 V RMS) in experiments with AR of 10:1. A subsequent positive shift in the couple potential to a stable level lower than the DC operation potential (-1.05 V_{SCE}) of the AlZnIn anode was observed within 20 hours, caused by hydrogen evolution on steel. The time until the positive shift increased with applied AC level and larger steel area (i.e. decreased AR).

Formation of calcareous deposits on the steel surface under DC conditions is an important aspect of CP in seawater because the deposits reduce the current requirement significantly. Such deposits did not appear to have a similar significance in the presence of applied AC. Increased water reduction by AC, causing pH increase on the steel surface higher than the DC case, reduced the protectiveness of the deposits by inhibition of electrically insulating $CaCO_3$ formation. Preconditioning of the steel surface by CP under usual DC conditions to form the desired deposits did not have a clear influence on the AC corrosion of anodes. The decrease of both the AC and DC components of the cell current as a function of time under moderate applied AC levels, however, indicated the formation of calcareous deposits on steel. No calcareous scales were found to deposit on the anode surface. The decrease of cell current with time can also be attributed to the development of corrosion products on the anode surface. Decrease in the cell current was not appreciable for high AC levels ($\geq$ 2 V RMS) with an AR of 10:1, explained by the destruction and instability of the calcareous deposits due to vigorous gas evolution. In conclusion, these results suggest that the lifetime of the CP system at high levels of applied AC ($V_{AC} \geq 2$ V AC or $i_{AC} \geq 30$ A m^{-2}) may become significantly reduced in relation to the expected lifetime under DC conditions.

Sammendrag

Direkte elektrisk oppvarming (DEH) benyttes på undervannsrørledninger innen oljeproduksjon for å forhindre frys av hydrater og voksdannelse ved produksjonsstans eller ved andre forhold hvor temperaturen er lav. For å forhindre tilstoppelse, varmes rørene opp ved bruk av vekselstrøm (AC) spenning. Dette resulterer i en risiko for AC korrosjon, som utgjør motivasjonen bak, og temaet for dette prosjektet. Stålrørene er overflatebeskyttet og under konvensjonell katodisk beskyttelse (CP) ved bruk av AlZnIn offeranoder. Tidligere prosjekt og masteroppgaver ved NTNU indikerer at stålrørene er godt beskyttet ved påtrykk av AC. Denne avhandlingen fokuserte derfor på risiko for økte korrosjonsrater under påvirking av AC for AlZnIn anodene. Anodeprøver koblet til stålprøver ble undersøkt under påtrykt AC ved bruk av testceller på laboratorieskala, i syntetisk sjøvann ved romtemperatur. Påtrykt AC ble variert mellom 0.5 til 150 A m^{-2}, og anode-stål arealforholdet (AR) ble satt til enten 10:1 eller 100:1, i eksperimentene som alle varte en uke. Korrosjonsrater ble evaluert ved vekttapsmålinger og ved analyse av egenskaper ved overflatebelegg og korroderte overflater ved bruk av henholdsvis røntgendiffraksjon (XRD) og SEM. For en forbedret evaluering av en realistisk anode-stål kobling og betydningen av anode-stål areal, ble lignende tester gjennomført på en kobling av to identiske par av parallellkoblet anode-stål, med et arealforhold på 100:1. En slik konfigurasjon er antatt å simulere koblingen av et DEH system til to ringformete anoder som omslutter det oppvarmede stålrøret, og som er plassert med en avstand fra hverandre langs lengden av røret. Utstyr og metode for undersøkelse av AC korrosjon ble utviklet og evaluert.

Resultater gjør det klart at anode korrosjonsraten øker med økende påtrykt AC nivå, mens karbonstål er tilstrekkelig beskyttet ved de eksperimentelle betingelser spesifisert over. Anode korrosjonsraten var påvirket av både strøm for beskyttelse av stålet samt selv-korrosjon, og korrosjonen var karakterisert ved gropdannelse og koalesens av disse ved høyere AC nivå. Høye selv-korrosjonsrater ble tilskrevet en suksessiv alkalisering, forklart ved hydrogenutvikling, og forsuring av anodeoverflaten ved hver AC syklus, som videre destabiliserte det beskyttende oksidlaget. Korrosjon ble funnet å være begrenset ved høye AC nivå, forklart ved dannelse av et hydrogen teppe på anodeoverflaten samt hydrogen fanget i porene i hydroksidfilmen på overflaten. AC korrosjon av anodene var sterkt avhengig av anode-stål arealforholdet. I eksperimenter med en konfigurasjon som beskrevet ovenfor med to elektrodepar, hadde stålprøvene ingen betydning ved et arealforhold på 100:1. Systemet fungerte med andre ord som en anode – anode galvanisk kobling, som medførte et signifikant fall i anodepotensialet og videre en sterkt økende selv-korrosjonsrate ved økt AC nivå.

I eksperimenter med kun en anode-stål kobling, falt også koblingspotensialet umiddelbart etter påtrykk av AC, og da i økende omfang med påtrykt AC potensial. Dette førte videre til økte strømbehov fra økende katodisk stål som resulterte i ekstrem anodekorrosjon ved høyt AC nivå ($\geq$ 2 V RMS) i eksperimenter med arealforhold 10:1. Et påfølgende positivt skift i koblingspotensialet til et mer stabilt nivå sammenlignbart med, men lavere enn, DC potensialet til en AlZnIn anode under drift (-1.05 V_{SCE}) ble observert innen 20 timer, forårsaket av hydrogenutvikling på stål. Tiden inntil det positive skiftet økte med påtrykt AC nivå og økt størrelse på stålet (dvs. lavere arealforhold).

Dannelse av kalkbelegg på ståloverflaten under likestrømsforhold (DC) er et viktig aspekt av katodisk beskyttelse i sjøvann fordi belegget reduserer strømbehovet i betydelig grad. Slike overflatebelegg synes ikke å ha en lignende betydning ved tilstedeværelse av påtrykt AC. Økt pH på ståloverflaten sammenlignet DC tilfellet som følge av økt vannreduksjon ved påtrykk av AC, reduserte beskyttelsen av beleggene ved å inhibere dannelse av elektrisk isolerende $CaCO_3$. Forbehandling av ståloverflaten ved katodisk beskyttelse under konvensjonelle DC forhold for å danne ønsket belegg synes ikke å ha en klar påvirkning på AC korrosjon av anodene. Nedgangen i både AC og DC komponenter av cellestrømmen som funksjon av tid under moderate nivå av påtrykt AC, indikerte likevel dannelse av kalkbelegg på stål. Kalkbelegg ble ikke funnet dannet på anodeoverflaten. Nedgangen i cellestrøm med tid kan også skyldes utvikling av korrosjonsprodukt på anodeoverflaten. For høyt nivå av påtrykt AC ($\geq$ 2 V RMS) og et arealforhold lik 10:1, var ikke nedgangen i cellestrømmen betydelig, og dette ble forklart ved ødeleggelse og ustabilitet av kalkbelegg som følge av kraftig gassutvikling. Som en konklusjon tyder resultatene på at levetiden til et katodisk beskyttelsessystem ved påtrykk av høye nivå av AC ($V_{AC} \geq 2$ V AC or $i_{AC} \geq 30$ A m^{-2}) kan bli betydelig redusert i forhold til forventet levetid ved likestrømsforhold (DC).

Contents

Appendices

1 Introduction

1.1 Motivation

When a metal structure is exposed to an Alternating Current (AC) source, its electrochemical behaviour will be altered. Although its effect on electrochemical processes is small compared to a Direct Current (DC) of the same magnitude, AC influenced corrosion of the structure occurs. The application of Direct Electric Heating (DEH) system to ensure flow inside subsea oil production and transmission pipelines introduces the risk for this type of corrosion. DEH has proven a cost efficient and environmentally friendly alternative to chemical treatment of the multi-phase flow [1]. It involves the application of an AC voltage on the pipeline that, due to resistivity effects, induces heating of the pipeline. The system is relevant during shutdown of oil well production or during other abnormal process conditions where the temperature in the produced well fluids is low. Although the DEH system functions adequately by heating the fluid flowing in the pipelines, a risk for AC corrosion of surrounding sacrificial anodes and the pipeline itself at coating defects is introduced.

There is a lack of understanding of the mutual effect that a cathodic protection (CP) system and an applied AC voltage has for the corrosion behaviour of both the steel structure and the sacrificial anode, and the general mechanism that underlies AC corrosion remains to be clarified. In earlier work by the author [2], steel was found to be sufficiently protected by CP in synthetic seawater. However, corrosion of the anodes resulting from both current provided for protection of the steel and self-corrosion occurred at a significant rate under the influence of AC. Under the application of AC, a successive alkalization and acidification of the anode surface at each cycle was suggested to destabilize the protective oxide. In accordance with findings presented by Lilleby in her master thesis [3], AC was found to impede the formation, and deteriorate the protectiveness, of the calcareous deposits on steel. Therefore, the results questioned the role of calcareous deposits in a CP system under the influence of AC. Earlier work of another former master student suggested that AC corrosion is caused by DC induced by partial conversion of AC, which increased in proportion to the increasing AC [4].

1.2 Aim of work

The principal goal of this project is to understand the mechanism of corrosion of carbon steel, cathodically protected by AlZnIn sacrificial anodes in seawater, in the presence of applied AC. This work focuses on the effect of AC on the corrosion of AlZnIn anodes in contrast to the earlier focus on the effect of AC on corrosion of steel [2]. However, the effect of galvanic coupling of the anodes to steel is still considered by investigating the area ratio between the galvanically coupled anode and steel under applied AC. The possible effect of calcareous deposits in reducing the corrosion rate and current requirement is evaluated for the anode-steel couple rather than for each metal alone, as was the usual approach in earlier studies.

AC corrosion of the anodes will be investigated based on the available literature and own laboratory scale corrosion experiments for the anode-steel couple. The evaluation will be based on the corrosion rate and the properties of surface deposits and corroded surfaces, achieved by weight loss measurements and surface analyses, respectively.

The work intends to contribute to the development and evaluation of equipment and methodology for investigation of AC corrosion, a relatively unexplored area compared with DC corrosion. In particular, equipment for measuring and recording the DC and AC components of the response of the test samples to applied AC is investigated.

2 Theoretical background

The first part of this section contains relevant theory on sacrificial AlZnIn anodes and CP of steel. Firstly, the electrochemical properties and corrosion behaviour of aluminium and the AlZnIn alloy is presented and then, the role and characteristics of calcareous deposits on steel for CP in seawater is explained. The second part of this section presents literature in relation to AC corrosion in seawater.

2.1 The sacrificial anode – AlZnIn

Well-established standards and recommended practices [5-7] exist for CP of subsea pipelines of carbon steel in seawater by use of sacrificial anodes of AlZnIn. The operating potential of the anodes in seawater is in the range -1.0 to -1.1 $V_{Ag/AgCl}$ and the anode capacity is in the range 2300 to 2650 Ah kg^{-1} [8]. This section elucidates thermodynamic and kinetic aspects that are characteristic for aluminium and AlZnIn alloys, and further of relevance for the corrosion behaviour of sacrificial anodes in seawater.

2.1.1 Electrochemical and corrosion characteristics of aluminium

Even though pure Al is electrochemically active, the formation of a passive oxide layer (Al_2O_3) on the surface renders its performance as a sacrificial anode inadequate (2.1).

$$2Al + 3H_2O \rightarrow Al_2O_3 + 6H^+ + 6e^- \tag{2.1}$$

The oxide film forms spontaneously and is only a few nanometres thick. It consists of two layers [9]. The protective part of the oxide layer, the so-called barrier layer, is a compact and amorphous inner layer. In addition, an outer, thicker, and more porous layer forms, which at ambient temperature can crystallize into bayerite ($Al_2O_3 \cdot 3H_2O$). As evident from the Pourbaix diagram of Figure 2-1a), aluminium is thermodynamically unstable, and it corrodes in both acidic and alkaline environments. The pH level thus has a critical role on the thermodynamic stability of aluminium.

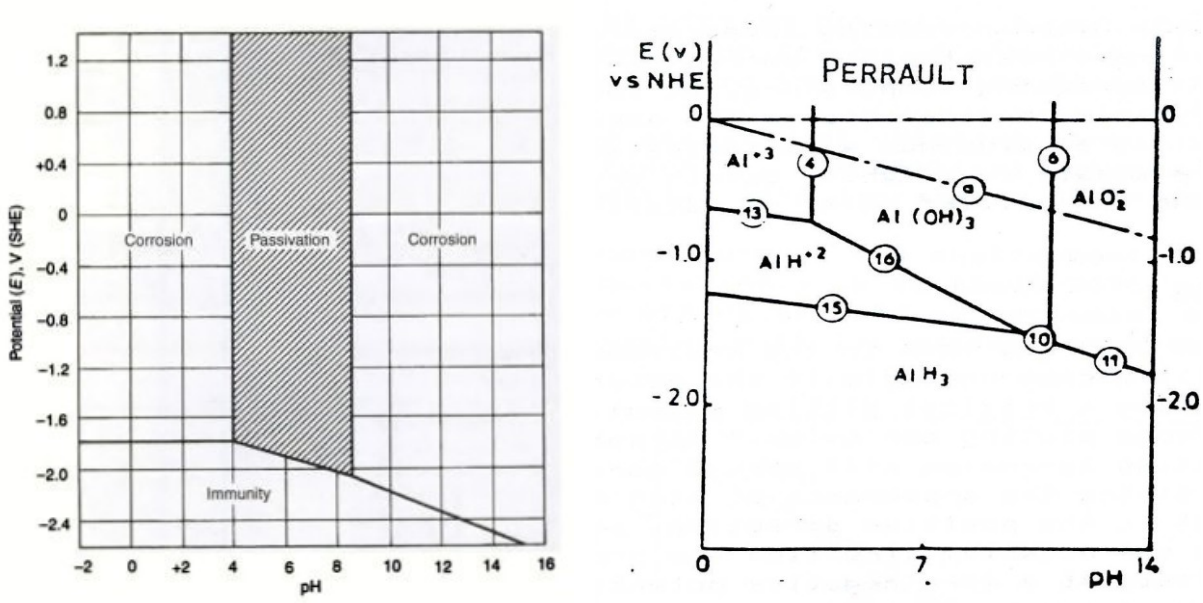

a) **b)**

Figure 2-1. a) The classical Pourbaix diagram of pure aluminium in water at 25 °C [9]. b) Pourbaix diagram where the immune (and partly the passive) region of Al is modified by considering the formation of hydrides [10].

Figure 2-1b) shows a modified form of the classical diagram (Figure 2-1 a), constructed by assuming the formation of hydrides [10]. The diagram indicates that hydride formation with decreasing potential may cause thermodynamic instability of the oxide, and lack of immunity. With increasing temperature, the passive region in the Pourbaix diagram shifts in the direction of lower pH level. Therefore, aluminium is more susceptible to corrosion as the temperature increases, and in addition the rate of attack increases [9].

The mechanism by which aluminium corrodes depends upon environmental factors such as pH level, presence of aggressive species and potential level. Like other active-passive metals, the corrosion mechanism of aluminium in chloride-containing solutions is characterized by pitting corrosion. When discussing the corrosion mechanism of aluminium alloys, the amphoteric and highly insulating properties of the oxide layer of aluminium are important, giving the aluminium surface a poor ability to act as a cathode. The low conductivity of the oxide layer leads to initiation of localized corrosion in the vicinity of impurities and particles with regard to impure and alloyed aluminium, which themselves act as cathodic sites due to their higher noble character [11]. Surface particles arise due to alloying and trace elements. Some of these elements also function as to activate the surface, and the presence of these for the corrosion behaviour of aluminium alloys is important. The reader is referred to section 2.1.2 for a discussion of this aspect. In the immediate vicinity of the cathodic sites, the pH will increase due to the water/oxygen reduction reaction. The increase destabilizes the oxide layer and causes formation of pits by local etching of the surrounding matrix [11].

Microgalvanic couplings that form between particles and the alloy matrix thus promote pitting corrosion. The fact that the cathodic reaction is confined to impurities and particle sites distinguishes aluminium from other active-passive metals such as stainless steel.

Pitting corrosion can occur both at low and high potential levels [12]. In cases where the protective oxide layer is unstable and the surface becomes activated, aluminium appears to corrode uniformly. An example of this relates to the alkalization of the surface when a high reduction reaction rate causes accumulation of OH^- ions, e.g. during cathodic polarization. A hydration of the oxide film occurs as a result of the alkalization at the oxide-solution interface, leading to a decrease in the resistance of the surface film [13]. A proposed mechanism for this type of corrosion involves a combined process of oxidation of aluminium to form oxide/hydroxide at the aluminium-oxide interface, as given by (2.1) or (2.2) and chemical dissolution of the oxide film at the oxide-solution interface (2.3). The latter is promoted by the corresponding water reduction reaction, which also cause hydrogen evolution (2.4) or oxygen reduction (2.5).

$$Al + 3H_2O \rightarrow Al(OH)_3 + 3H^+ + 3e^- \tag{2.2}$$

$$Al(OH)_3 + OH^- \rightarrow Al(OH)_4^- \tag{2.3}$$

$$2H_2O + 2e^- \rightarrow 2OH^- + H_2 \tag{2.4}$$

$$O_2 + 2H_2O + 4e^- \rightarrow 4OH^- \tag{2.5}$$

The experimental and calculated Pourbaix diagram by Perrault [10] (Figure 2-1b) led to an alternative mechanism for the alkaline dissolution of aluminium, where both the interfacial pH and the formation of hydride as an intermediate play central roles for the reaction mechanism. The electrochemical part (2.2) of the mechanism presented above is now broken down into three elementary steps and the kinetics is thus altered. Adhikari, Hebert and Lee [14, 15] have investigated this alternative mechanism during alkaline dissolution. By analytical methods, the authors detected surface particles of aluminium hydride with a hydroxide coverage. According to their study (in 1 M NaOH test solution at open-circuit conditions), etching of aluminium by produced hydrogen yields AlH_3 continuously at the surface (2.6). In the corresponding anodic process aluminium hydride oxidizes and eventually forms aluminate ions ($Al(OH)_4^-$) (2.7).

$$Al + 3H_{(ads)} \rightarrow AlH_3 \tag{2.6}$$

$$AlH_3 + 7OH^- \rightarrow Al(OH)_4^- + 3H_2O + 6e^- \quad (2.7)$$

In combination with water reduction (2.4) the resulting alkaline dissolution of aluminium occurs as given by (2.8).

$$2Al + OH^- + 3H_2O \rightarrow Al(OH)_4^- + AlH_3 \quad (2.8)$$

With regard to this mechanism, dissolution of aluminium competes with the recombination of (adsorbed) hydrogen. Adhikari and Hebert elucidated further the role of pH level on the mechanism of aluminium dissolution, and found two different processes to control the alkaline dissolution [15]. At pH 11, the observation of a surface film of high resistivity indicated direct oxidation of aluminium into oxide (2.2) whereas at pH levels above 11.75, they found a reduction in the surface film resistivity in combination with increased water permeability. Moreover, the dissolution rate increased drastically, at a rate affected by both mass transport and ohmic resistance. The authors suggested that the structural changes at pH > 11.75 correlated with the formation of interfacial AlH_3 (2.6). Aluminium hydride formation at cathodic potentials has been indicated and discussed also by others [16, 17].

2.1.2 Effect of alloy elements

The purpose of adding alloying elements is to modify the passivation- and surface properties of pure aluminium in seawater. The AlZnIn sacrificial anode is a commercial alloy widely used in marine environments. Although the mechanism by which the two elements, zinc and indium, alter the electrochemical characteristics is not fully understood, several studies have elucidated the role of both elements in the corrosion mechanism and for the electrochemical behaviour of the AlZnIn alloy [18-27].

The role of indium

Indium is in general an element of higher noble character and of low solubility in aluminium. Addition of indium (i.e. ppm level) results in a cathodic shift in the pitting potential and a resulting reduction of the region of passivity, see Figure 2-2. As a result, the surface is activated by destabilizing the oxide layer [8]. In addition, the open-circuit potential of pure aluminium is reported to shift in cathodic direction, both when In^{3+} ions is added to an aqueous chloride solution [21] and when aluminium is alloyed with small additions of indium [28]. The given effect is explained by a higher dissolution rate and an increased overpotential for hydrogen evolution in presence of indium [24]. In other words, indium functions poorly as a cathodic site.

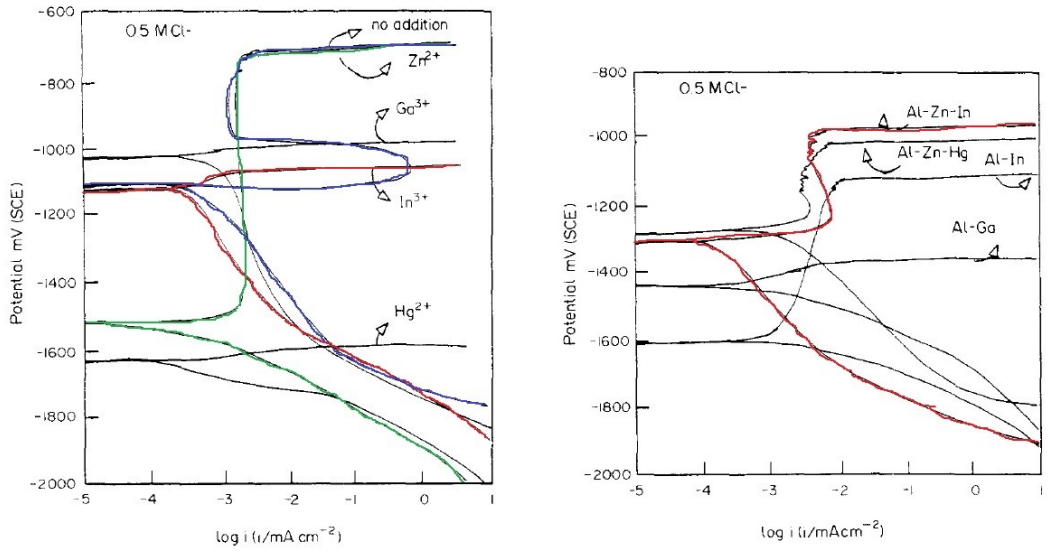

a) **b)**

Figure 2-2. Polarization plots in 0.5 M Cl^- test solution. a) Pure Al (green line) with addition of 5 x 10^{-3} M In^{3+} (red line) and Zn^{2+} (blue line). b) Al alloys. AlZnIn (red line). Adapted from Carrol and Breslin [21].

A proposed mechanism for these changes in electrochemical characteristics involves initiation of selective dissolution of the more active aluminium by the deposition of indium at defective sites in the oxide layer [21]. Two aspects support the central role of defective sites. A flawless oxide layer is of high ionic and electronic resistance, and a correlation (established experimentally [21]) between a smoother surface finish - and hence less defective sites- and longer times prior to onset of attack.

Activation of the surface is a combination of increased dissolution of aluminium and enrichment of indium at the surface. The enrichment is attributed to segregation, and if indium ions are present, reduction and deposition of indium at the surface [29]. In studies by Graver et al.[26, 27], indium, alloyed in small amounts in aluminium, was reported to segregate easily and enrich the surface, which in turn activated the aluminium surface. The authors further suggested that the trace element forms a liquid phase alloy with aluminium, enabled by two processes; heat developed during surface oxidation and a melting point depression because of small particle sizes. With regard to the segregation of alloying elements, Muños et al.[24] reported that the attack of the alloy occurred primarily at grain and cell boundaries and interdendritic zones, as these regions were indium- and zinc rich zones. It is well known that such boundaries function as favourable sites for segregation of inclusions. Contrary to the activation by other activator ions (such as mercury), a synergistic effect is stated to take place between indium and chlorides, meaning that activation by indium *only* occurs in chloride-containing solutions. In relation to this observation, Carroll and Breslin proposed that deposition of indium enable a higher surface concentration of the aggressive

chloride ions, of which play a crucial role for pitting attack. Further, experimental studies have revealed that pits that form during localized attack of aluminium in an indium-containing chloride solution do contain indium [18, 21].

The role of zinc

The role of zinc as an element in aluminium alloys is not understood completely. Contrary to indium, zinc has a significant solubility in aluminium. Its effect is to impede highly localized corrosion by decreasing the reduction rate [8]. This is explained by the low exchange current density, associated with H_2 evolution on zinc [30]. The effect of zinc ions alone is little as shown by the polarization plot in Figure 2-2 a). Based on the resemblance between the oxidation peak of the polarization curve when Zn^{2+} ions is present and the polarization curve for pure zinc, Breslin and Carroll suggested that zinc precipitates on the aluminium surface. In a ternary alloy however, the addition of zinc has a more pronounced effect. For AlZnIn, alloying with zinc displaces the pitting potential in a noble direction as compared to AlIn, see Figure 2-2 b). There is a synergistic interaction between indium and zinc, illustrated by the potential-time plot for pure aluminium by Breslin and Friery [18] in Figure 2-3. The authors reported of higher dissolution rates, reduced extent of repassivation and shorter time prior to onset of attack when comparing the activation of aluminium by indium and zinc salts to the activation by indium salts only.

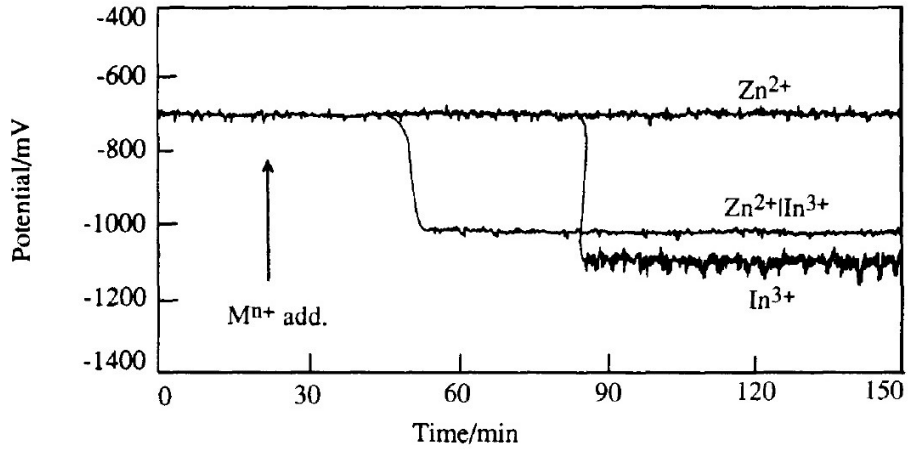

Figure 2-3. Open circuit potential-time plot for pure aluminium in 0.5 M NaCl solution on addition of 0.01 M $ZnSO_4$, 0.005 M $In_2(SO_4)_3$ or 0.005 M $ZnSO_4$ and 0.0025 M $In_2(SO_4)_3$ solutions. Addition of zinc leads to a more efficient attack by indium, seen by reduced time prior to onset of attack and reduced amount of repassivation. From Breslin and Friery [18].

Breslin and Friery further proposed a mechanism where zinc deposits on the surface and causes a higher rate of cracking and rupture of the oxide layer (and hence an increased

instability of the oxide film), which in turn promotes an increased indium enrichment. The cracking has been proposed to relate to the formation of $ZnAl_2O_4$ spinel of higher molar volume than that of the aluminium oxide, at which the difference gives rise to stress corrosion cracking of the oxide film [18, 19].

2.2 Cathodic protection of steel

Carbon steels are susceptible to corrosion in most environments and will, unless protected, oxidize spontaneously into states of higher thermodynamic stability (Figure 2-4). A way to ensure the integrity of steel structures in marine environments is by Cathodic Protection (CP) [31]. In order to ensure a general protection of carbon steel immersed in seawater, a protection potential E_p equal to -850 mV_{SCE} is needed [32]. The cathodic current supply to the steel structure under CP ensures that oxygen reduction (2.5) or water reduction (2.4) takes place at the steel surface, which in turn leads to a local pH increase. This so-called *alkalization mechanism* plays a crucial role for the CP system of steel in seawater, as it results in formation of calcareous scales on the steel surface. The formation of these deposits and its protective properties are explained in this section.

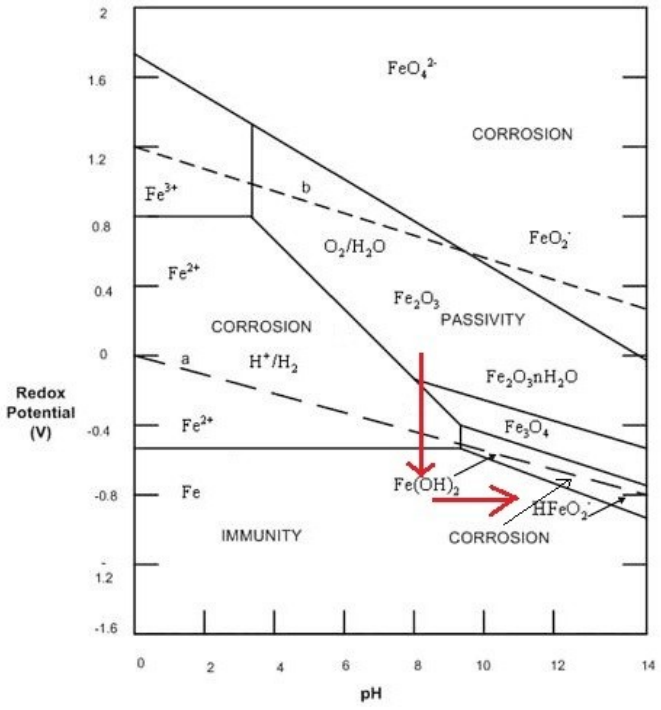

Figure 2-4. Pourbaix diagram for iron in water showing area of immunity, passivity and corrosion. Shift in the potential as indicated due to CP. The potential is given vs. standard hydrogen electrode (SHE). Adapted from Ahmad [33].

Whether O_2 reduction, or water reduction, will dominate as cathodic reactions on the steel surface, depend on several factors such as the potential level, temperature, presence of O_2, and the formation of surface deposits. The O_2 reduction reaction is mass transfer controlled at potentials associated with CP, which implies that when the limiting current density (i_{lim}) is reached at a given overpotential (2.9), any further increase in cathodic potential will have no effect on the rate of O_2 reduction.

$$i_{\text{lim}} = \frac{D \cdot z \cdot F \cdot C_0}{\delta} \tag{2.9}$$

where D is the diffusion constant, z is the electrical equivalent, F is the Faraday constant, C_0 is the bulk concentration of O_2,and δ is the diffusion layer thickness. In contrast, the water reduction, being activation controlled, will act in an increasing manner and eventually dominate at lower potentials. This is evident by the increasing amount of gas development (i.e. H_2 evolution) at the steel surface.

2.2.1 Formation of calcareous deposits

Calcareous deposits - a generic term for a mixture of $CaCO_3$ and $Mg(OH)_2$ - will form spontaneously on a steel surface subjected to CP in seawater. Presence of Mg(II)- ions in seawater allow for a shift in the equilibrium and formation of hydroxides (2.10).

$$\mathrm{Mg^{2+} + 2OH^- \rightarrow Mg(OH)_2} \tag{2.10}$$

$Ca(OH)_2$ does not form because of higher solubility and lower concentrations of Ca(II) ions in seawater [34]. However, the pH increase associated with the alkalization mechanism also alters the inorganic carbon equilibrium (including CO_2) and favours the formation of carbonate ions, as given by (2.11)-(2.13), which in turn enables the formation of carbonate salts at the steel surface (2.14). The solubility of $CaCO_3$ is significantly lower than that of $MgCO_3$ [34] and the composition of calcareous deposits at the steel surface is therefore dominated by $Mg(OH)_2$ and $CaCO_3$ [35].

$$\mathrm{CO_2 + H_2O \leftrightarrow H_2CO_3} \tag{2.11}$$

$$\mathrm{H_2CO_3 + OH^- \leftrightarrow H_2O + HCO_3^-} \tag{2.12}$$

$$\mathrm{HCO_3^- + OH^- \leftrightarrow H_2O + CO_3^{2-}} \tag{2.13}$$

$$\mathrm{Ca^{2+} + CO_3^{2-} \rightarrow CaCO_3} \tag{2.14}$$

In seawater the formation of calcareous deposits play a crucial role for (the lifetime of) the CP system. It acts as a physical barrier against O_2 diffusion, and thus hinders the O_2 reduction (2.5). This limitation lowers the current requirements for protection of the steel structure and thus increases the lifetime of the sacrificial anodes [36]. In a study by Okstad et al. [37, 38], the impeding effect was not seen for the diffusion of water, which suggests that the calcareous deposits do not control the rate of water reduction in the same manner.

2.2.2 The crystal morphology of calcareous deposits

Vast amounts of papers are devoted to the study of the composition and crystal morphology of the calcareous deposits. Essential for the structure of the calcareous deposits and the explanation that follows below, is the fact that the kinetics for the formation of $Mg(OH)_2$ is assumed to be faster than for the formation of $CaCO_3$. A recently presented mathematical model for the formation of calcareous deposits on cathodically protected steel in seawater supports this [39]. The model predicts a dominating formation of $Mg(OH)_2$ in the initial stage followed by an increase in both the content of $CaCO_3$, the electric resistance and also the thickness with time. Whereas the stable polymorph of $Mg(OH)_2$ is brucite, $CaCO_3$ can take different forms, e.g. calcite and aragonite. Although calcite is associated with a higher stability, $CaCO_3$ will rather precipitate as aragonite in seawater, as presence of Mg(II) ions induce a strong inhibiting effect on the crystal growth of calcite. In contrast to calcite, Mg(II) ions cause only a *reduction* in crystal nucleation and growth of aragonite. According to Berner, the inhibition of calcite formation is attributed to the easy fit of Mg(II) ions in the crystal lattice of calcite and the adsorption of Mg(II) ions on the surface of calcite. Both effects cause the Mg-containing calcite to be more soluble [40]. At present, there exists no agreement as to the exact mechanism for this inhibiting effect of Mg. There is however a general agreement that the composition of the calcareous deposits has a uniform inner Mg-rich layer and a thicker outer layer of imbricated aragonite needles [41]. Furthermore, whereas the crystal morphology of brucite is undefined and difficult to identify, the crystal morphology of aragonite has a characteristic flower shape [42].

2.2.3 The protectiveness of calcareous deposits

The protectiveness of calcareous deposits on a steel surface in seawater is largely given by the Ca/Mg ratio. The improved protection with a higher value of the ratio, is attributed to the increased impediment of oxygen diffusion [36, 37]. A lower solubility of Ca(II) as opposed to Mg(II) or poor coating properties of $Mg(OH)_2$ are proposed causes to the superior protection provided by $CaCO_3$ [35]. Yet another proposition relates to the fact that as the formation of $Mg(OH)_2$ is favoured at lower potentials, so is also the hydrogen evolution,

which will act in an increasing manner, and possibly mechanically damage and reduce the adhesion of the calcareous deposits [36]. Recall also that the deposits appear to hinder only the O_2 diffusion and hence not the water reduction reaction. Others have emphasized that the reduced protection provided by a low Ca/Mg ratio attributes to the semiconducting properties of $Mg(OH)_2$ [30] as compared to the superior insulating properties of $CaCO_3$ [43]. The characteristics of the calcareous scale are dependent on parameters such as the potential level, morphology of the steel surface, temperature, pH, flow rate and chemistry of the seawater. Note that the interpretation of these in terms of their influence on the calcareous scale is complicated as parameters are interrelated. A brief introduction to factors considered relevant for the present project follows.

pH and potential

Considering the equilibrium reactions for the formation of calcareous deposits (2.10)-(2.14), it is evident that the pH level on the surface largely affects the composition of the calcareous deposits. In general, the Ca/Mg ratio decreases with increasing current densities, explained by the increase in pH that favours the formation of $Mg(OH)_2$ [44]. The pH needed for precipitation to take place, has been calculated by thermodynamics to be 7.5 for $CaCO_3$ and 9.5 for $Mg(OH)_2$ [31, 41]. Analogous, the properties of the calcareous deposits are dependent on the applied potential in that increased cathodic potential levels increase the cathodic reaction rates. In a study by Okstad et al. [37], the Ca/Mg ratio, and thus the protective properties, was found to be maximized at intermediate potential levels, see Figure 2-5.

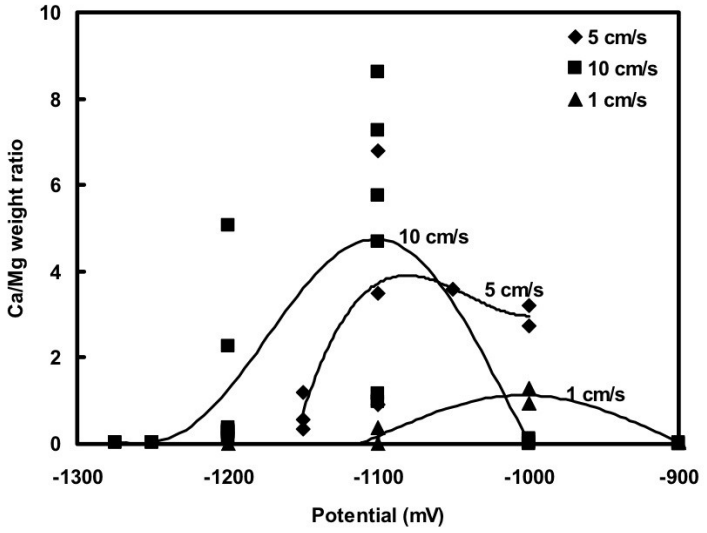

Figure 2-5. The Ca/Mg ratio as a function of applied potential and flow rate. Work by Okstad et al. [37].

According to the study of Okstad [38] there is a balance between too low potential levels (i.e. more negative cathodic potentials) where an increased pH level promotes precipitation of $Mg(OH)_2$, and too high potential levels where the pH is not high enough for $CaCO_3$ to precipitate. At too low pH levels, precipitation of $Mg(OH)_2$ dominates, even though thermodynamic considerations predicts otherwise, because of the slow kinetics associated with the precipitation of $CaCO_3$.

Temperature

The solubility product of $CaCO_3$ and $Mg(OH)_2$ is dependent on temperature. In general, the calcareous scale forms more readily at higher temperatures [44]. Contrary to the solubility of $Mg(OH)_2$, the solubility of $CaCO_3$ decreases with increasing temperature. Hence the Ca/Mg ratio and resulting protectiveness of the deposits improves at higher temperatures [43]. Nevertheless, Barchiche et al. have emphasized that this effect is not present at higher cathodic potentials where high pH levels favour the formation of $Mg(OH)_2$ regardless temperature level [45].

2.3 The system response of an AC perturbation

An AC signal with amplitude ΔV provides a sinusoidal voltage and when impressed on a DC signal, the two are added. The result will be a sinusoidal voltage (2.15) alternating in anodic and cathodic direction with time t, relative to the original DC potential level, E_{DC}.

$$E(t) = E_{DC} + \Delta V \cdot \cos(\omega \cdot t) \tag{2.15}$$

where ω ($=2\pi f$) is the angular frequency with units of s^{-1}. This further gives rise to an alteration in the current. The system response of an AC perturbation and resulting corrosion is understood by considering the fundamental nature and characteristics of a metal-solution interface. It is useful to introduce an electrical equivalent circuit as a model for the metal-solution interface. An example is the simplified Randles circuit, see Figure 2-6, where the interface is modelled as a capacitance (C) in parallel with a polarization resistance (R_f). The ohmic resistance (R_e) refers to the potential drop through the electrolyte. The interfacial capacitance, C, arises from the charge redistribution that takes place in the electrical double layer and the dielectric capacitance associated with a stable oxide layer on the metal surface. The two coupled in series can be modelled as a constant phase element (CPE) that deviates

from an ideal capacitor because of e.g. non-uniform current distribution (discussed below). The impedance Z_{CPE} of the CPE component is given by

$$Z_{CPE} = \frac{1}{(j\omega)^n \cdot C} \tag{2.16}$$

where C is the capacitance, j is the imaginary unit and n is a constant of about 0.8-0.9 (n = 1 for an ideal capacitor). The polarization resistance R_f on the other hand, represents the charge transfer across the interface, and thus any electrochemical process at the metal surface.

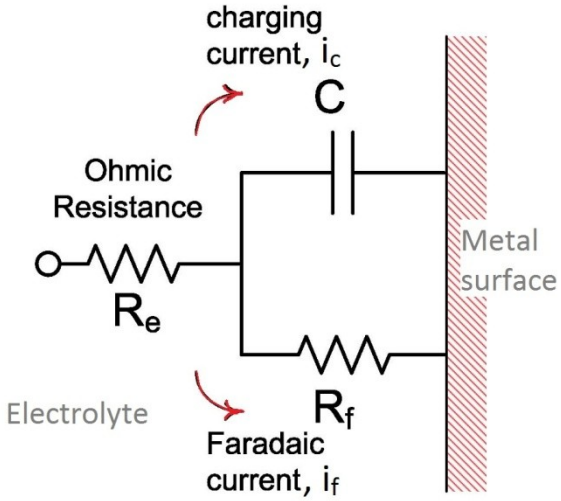

Figure 2-6. Simplified Randles circuit as a model of the metal-solution interface. The electrical double layer and oxide film is modelled as a single capacitor C, and the polarization resistance R_f represents charge transfer reactions. The two act as alternative paths for the AC to flow. Adapted from Orazem and Tribollet [46].

The two parallel-coupled components act as alternative paths for the AC signal meaning that the overall current passing through the electrode is the sum of the capacitive (i_c) and the faradaic (i_f) currents (see Figure 2-6). The distribution between the two is influenced by the frequency of the AC signal and the magnitudes of R_f and C. It can be seen from (2.16) and Figure 2-6, that at higher frequencies, the capacitive impedance vanishes relative to the faradaic impedance [47, 48]. In other words, at high frequencies there is no risk for AC corrosion.

Whenever an AC voltage is applied to an electrochemical interface, a small part of the current response will be converted to DC. As long as any electron transfer occurs across the electrode surface, the current response of an AC signal will be nonlinear and the steady-state current density will change. Orazem and Tribollet provide an understanding of the effect of AC in a DC system. Under the assumption that the faradaic reaction rate obeys Tafel kinetics,

Orazem and Tribollet[46] showed, based on a Taylor series expansion of the current response, that the DC component of the current can be expressed by

$$i_{DC} = i_0\left(1+\frac{b^2\cdot\Delta V^2}{4}\right) \tag{2.17}$$

where $i_0 = K\cdot\exp(b\cdot E_{DC})$, b is the tafel constant, and K is a constant including the exchange current density. The implication of this result is that application of a large amplitude AC introduces a DC component to the interface [49, 50], thereby causing an added risk for corrosion. The effect is apparent from Figure 2-7 where an AC perturbation (of only 40 mV and a frequency of 100 Hz) results in a non-symmetrical current response corresponding to the generated DC. This is accompanied by a phase lag, i.e. the current response lags the potential input. The phase shift reflects the distribution of current between the capacitive (i_C) and faradaic (i_f) component. In a simplified circuit as shown in Figure 2-6, the following is valid. No phase shift implies that the AC signal passes through the capacitive component only. Conversely, a phase shift of 90° implies that the current passes only through the faradaic component, and an increased phase shift therefore represents an increased risk for corrosion. Recall though that the faradaic current relates to all electrochemical processes at the metal surface. Thus, a phase shift cannot quantify AC corrosion because such a shift can be associated with other processes than metal dissolution, e.g. oxidation and reduction of hydrogen. An analogous result in regard to the current response under influence of large amplitude AC, but by another approach (i.e. by Fourier series expansion), has been provided by Hirschorn et al. [51] and Harrington [49].

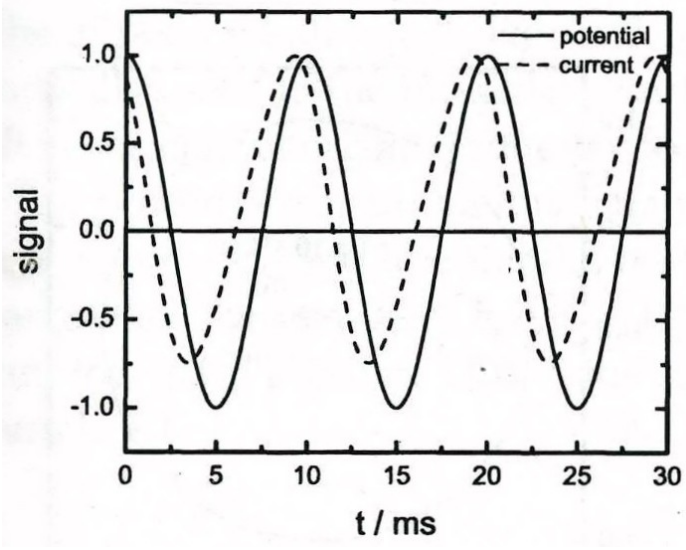

Figure 2-7. The current response (dashed line) under influence of a sinusoidal AC potential input (solid line), of amplitude ΔV = 40 mV and a frequency f = 100 Hz. Figure from Orazem and Tribollet [46].

In relation to the theory of Orazem and Tribollet, Strandheim documented experimentally in his master theses that AC corrosion is a pure DC phenomenon [4]. The results presented in the author's specialization project [2], were also in accordance with (2.17). In particular, in weight loss experiments where AlZnIn anode and carbon steel were coupled, a proportionality was found between the DC current of the system and the square of the AC amplitude, ΔV_{AC}^2 (2.18).

$$i_{DC} \propto \Delta V_{AC}^{\ 2} \tag{2.18}$$

The current response for a system under influence of AC depends on the characteristics of the system [46] and the model (Figure 2-6) and theory presented here is highly simplified as compared to an actual metal-solution interface. Of high importance for the characteristics of the electrode-solution interface, and resulting current response are geometrical factors that affect the current distribution across the surface such as electrode design and surface irregularities and heterogeneities, the distance in between electrodes, surface coverage and the conductivity of the electrolyte itself. In addition, the current response is greatly complicated by the existence of multiple and coupled reactions and adsorption of species at the electrode surface. The model of Figure 2-6 accounts for none of these aspects.

The overall impedance in the simplified circuit (of Figure 2-6) is given by

$$Z = R_e + \frac{1}{\frac{1}{R_f} + j \cdot \omega \cdot C} \tag{2.19}$$

where $j = \sqrt{-1}$ is the imaginary number. In cases where an appreciable ohmic resistance R_e is introduced, a reduced part of the applied AC will be related to the processes at the metal-solution interface (i.e. the capacitive and faradaic components). This is evident by the expression for the overall impedance (2.19). This in turn results in a lower faradaic current and thus a lower distortion of the current response of the system [46]. In conclusion, an appreciable ohmic resistance may reduce the risk for AC corrosion.

2.4 AC induced corrosion

Corrosion engineering and field studies have attempted to develop standards to guide in the assessment and management of the risk for AC corrosion of steel structures in soil. Corrosion rates are generally seen to increase in accordance with an increase in the corrosion current with applied AC [4, 48, 52]. A general statement is that there is a risk for AC corrosion on

steel if the AC density is higher than 30 A m^{-2} or when the current ratio between AC and DC values exceeds five, at which protective measures are needed [48]. The challenge of AC corrosion in marine environments has been given little attention. Even fewer studies have addressed the combined effect of AC and CP in seawater (section 2.5).

A general agreement found in the literature is that the corrosion rate due to a given AC density (with a frequency of 50-60 Hz) is below 1 % of a corresponding corrosion rate observed with a DC density of the same intensity [48]. The greater part of the applied AC is consumed for charge and discharge of the double layer and thus only a residual amount of the current is associated with faradaic processes on the metal surface of influence [32, 53, 54]. However, experimental studies on AC corrosion of aluminium are not in accordance with this general agreement.

Concerning aluminium, studies that date back to the 1960-70's have assessed the risk for, and understanding of, AC corrosion in various environments. Williams reported in 1967 of a considerable increase in corrosion of aluminium conductors in water when an alternating current was applied, the extent of which was dependent on time and applied AC level [55]. Corrosion occurred mainly during the initial test period and the corrosion rate increased with applied AC in the test range of 50 A m^{-2} to 2000 A m^{-2}. In contrast to measured corrosion rates of lead, copper and iron, which were found to be less than 1 % of that caused by a DC of the same magnitude, the corrosion rate of aluminium was found to be up to 50 % of that caused by an equivalent DC. In other words, aluminium appears to be more susceptible to AC corrosion than other materials. Williams did not provide any explanation to these findings. In accordance with the work of Williams, French proposed a highly conservative critical AC density for aluminium of 0.775 A m^{-2}, below which no corrosion was believed to occur. The low value was based on a 1000-hour test, which was part of a comprehensive study on the effect of AC on the corrosion characteristics of aluminium [56].

2.4.1 Electrochemical behaviour under influence of AC

Recall that corrosion of a metal surface is a non-linear electrochemical process, which emphasizes the importance of the magnitude of relevant Tafel constants. The potential shift caused by introduction of an AC signal alters the electrochemical behaviour of the metal structure. A theoretical study by Bosch and Bogaerts [50] provides an insight into the relation between an applied AC and the resulting changes in electrochemical kinetics. In their work a dimensionless ratio $r = \beta_a/\beta_c$ was defined, motivated by the strong influence that the given parameters have on the behaviour of the corroding system. β_a and β_c are the Tafel constants for the anodic and cathodic reactions, respectively. The two authors investigated the effect of

application of AC by a numerical analysis of two situations. The first case considered complete activation control whereas the second case accounted for a cathodic reaction under mixed (i.e. activation and mass transfer) control. The following results were derived for a corroding system.

- For $r < 1$, the corrosion potential (E_{corr}) decreased with increasing AC amplitude.
- For $r > 1$, E_{corr} increased with increasing AC amplitude.
- For $r = 1$, E_{corr} remained the same when AC was applied.

Depending on the value of the ratio r, the corrosion current (i_{corr}) increased exponentially with AC amplitude. (Note that this result, which is based on theoretical considerations, contradicts experimental studies by others.) Further, the kinetic parameters, i_{corr} and E_{corr}, were increasingly affected as the ratio r deviated from one. For a corroding system under mixed control and $r < 1$, simulated polarization curves showed that the change in the kinetic parameters was affected notably by the current ratio i_{corr} to i_{lim}. The dependency of E_{corr} and i_{corr} on the AC amplitude is shown in Figure 2-8 a) and b), respectively. A change in E_{corr} was found to be larger if $i_{lim} \approx i_{corr}$ (i.e. system under diffusion control), whereas an opposite trend was seen for the corrosion rate. The largest increase in corrosion rate was found for the case $i_{lim} >> i_{corr}$.

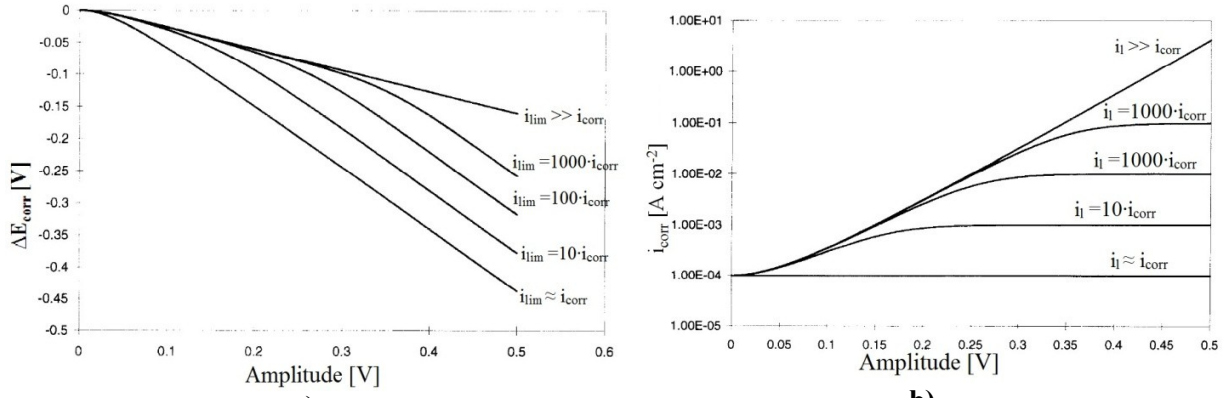

a) b)

Figure 2-8. The dependency of a) ΔE_{corr} and b) i_{corr} on the AC amplitude for different ratios of i_{corr} to i_{lim}. The cathodic reaction of the corroding system is under mixed control and the ratio $\beta_a/\beta_c < 1$. For $i_{corr} = i_{lim}$ the system is under diffusion control. Figure from Bosch and Bogaerts [50].

In accordance with the theoretical model when $\beta_a < \beta_c$, the free corrosion potential of carbon steel is reported to decrease in negative direction in several experimental studies [4, 52, 57-61], which implies that the cathodic polarization resistance is greater. However, the decrease is reported to be independent of the magnitude of the AC amplitude and moreover the decrease is with time reported to shift in noble direction, at which the potential is stabilized at a level comparable to the initial corrosion potential [2, 4, 58, 62, 63]. Note that the theoretical modelling provided by Bosch and Bogaerts assumed constant Tafel slopes. This assumption

is in general contradicted in experimental works where both the exchange current density (i_0) and the Tafel constants are reported to change under application of AC [52, 53, 58, 59].

In studies by Tan and Chin in the 1980's the electrochemical characteristics of aluminium under influence of AC was investigated [64, 65]. Application of AC (with a frequency of 60 Hz) acted as a depolarizer on a corroding system and decreased the passive regime of aluminium. Further, aluminium was reported to be susceptible to pitting corrosion in chloride containing solutions and the pit size, depth and dissolution rate of aluminium was observed to increase with increased applied AC levels. In test conditions of 3 wt % NaCl at pH 7 the passive region of aluminium was completely eliminated when applying 1 V AC (RMS), which implies surface activation.

2.4.2 Reactions and reaction kinetics under influence of AC

The fact that kinetic parameters (i_0, β_a and β_c) are changed under application of AC, demonstrates that application of AC influences the reaction kinetics at the metal surface. Drugli and Steinsmo [62] have reported the actual potential shift during AC testing of a connection of two anode and two steel specimens (i.e. identical as the SA/AS test configuration outlined in section 3.4.1). When an AC density of 240 A m^{-2} was applied and the mean potential of the steel surface was -1095 mV_{SCE}, the potential was found, by an oscilloscope, to vary between -1975 mV_{SCE} and -125 mV_{SCE}. The potential fluctuations induced by a large amplitude AC voltage clearly enable other reactions and formation of species, which are impossible or kinetically restricted at open-circuit potential.

Strandheim studied alterations in the reaction kinetics of carbon steel under application of AC in his master thesis [4]. In a test solution of 3.5 wt % NaCl, pitting corrosion of carbon steel was documented, which increased in extent with applied AC level. For $i_{AC} > 500$ A m^{-2}, Strandheim documented a change from diffusion control to complete charge transfer control for carbon steel in seawater at potentials below -1000 mV_{SCE} (i.e. at a potential level in the same range as that of a CP system). Furthermore, Strandheim observed a shift in anodic direction for the hydrogen reaction and a decrease in β_c and E_{corr} when AC was applied (Figure 2-9). The results were in accordance with changes documented earlier by Lilleby et al. [61]. When steel was polarized to -1100 mV_{SCE}, a limiting factor was introduced at the highest AC levels (i.e. $i_{AC} > 500$ A m^{-2}), explained by the formation of a "hydrogen carpet", which blocked the steel surface for any further increase in cathodic current. The depolarization of electrochemical kinetics revealed by Strandheim in relation to carbon steel was a concept initially introduced by Devay et al. [32].

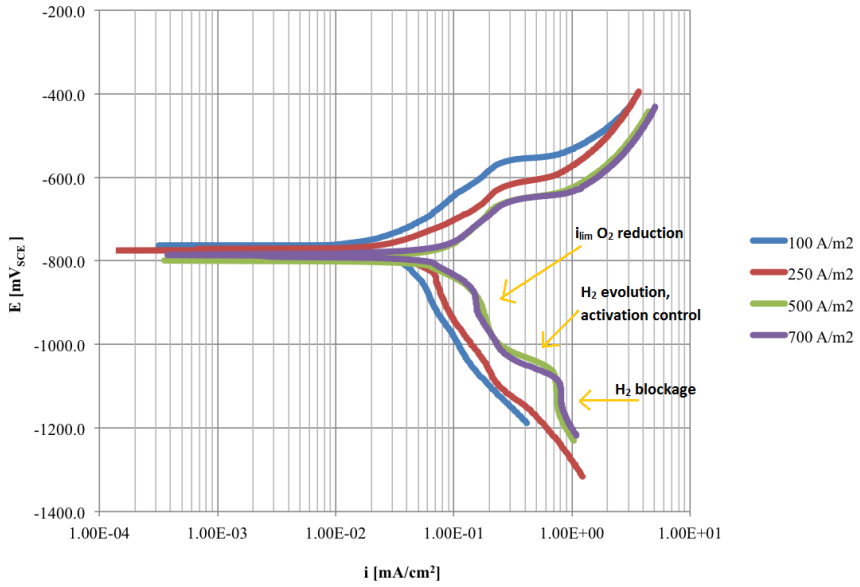

Figure 2-9. Polarization curve of carbon steel in 3.5 wt% NaCl electrolyte at various applied AC levels [A m^{-2}]. Limiting factors are evident at high AC levels. Adapted from E. Strandheim [4].

2.5 Effect of AC on cathodic protection of steel by anodes

In the author's specialization project [2], the effect of AC on a connected AlZnIn anode and steel (with an area ratio (AR) of 10) was investigated. In a test solution of synthetic seawater, weight loss testing under influence of AC was performed for one week. Although the protection current increased dramatically under application of AC, steel was found to be sufficiently protected by the anode. The AlZnIn anodes on the other hand, corroded significantly in the same experiments, both due to protection of steel and self-corrosion. Anode corrosion occurred at a rate proportional to the square of the amplitude of the applied AC (in accordance with (2.18)), an observation that challenged the expected lifetime of sacrificial anodes in seawater. It was suggested by the author that a successive alkalization (explained by gas evolution) and acidification of the anode surface destabilized the protective oxide, which in turn caused high self-corrosion rates.

Based on the dramatic increase in the protection current and observed increase in gas evolution, it was further suggested that application of AC increased the alkalization of the steel surface. The generation of a pure DC part (2.17) in the current response under application of AC and a depolarization of electrochemical kinetics (Figure 2-9 of section 2.4.1) are proposed explanations to the increased current. An alkalization of the surface of steel under CP in seawater has been documented under AC testing by Kim et al. [66].

Recall that the structure and chemical composition of the calcareous deposits depend on the pH level at the steel surface (section 2.2.3). In other words, application of AC changes the characteristics, and resulting protective properties, of the calcareous deposits. Earlier work by the author [2] and former master student Lilleby [3, 61], have demonstrated by surface analyses that application of AC inhibits the formation of $CaCO_3$, which in turn deteriorates the protectiveness of the calcareous deposits. Increased protection current and gas development at the steel surface result in an increased pH, which in turn favours the formation of $Mg(OH)_2$. At applied AC levels > 2 V RMS an eruption and persisting instability of the calcareous deposits was observed, explained by vigorous gas development at the steel surface [2]. In these cases, the current requirement for protection of steel was maintained relatively high throughout testing. The given observation questioned the importance of protective calcareous deposits for a CP system under influence of AC. In relation to this, Lilleby found corrosion to occur to a lesser degree in cases where the steel had been preconditioned to CP prior to AC testing (to form calcareous deposits), than for the case where no preconditioning had been performed [3].

In relation to application of DEH on subsea pipelines, the influence of AC on corrosion of pipelines and surrounding sacrificial anodes has been evaluated by Drugli, Steinsmo and Bjordal [62, 63, 67]. The test configuration employed by Drugli and Steinsmo was identical to the SA/AS test configuration of this thesis, which involves two pairs of parallel-coupled anode-steel (Figure 3-3). The reader is referred to section 3.4.1 for an explanation of this test setup, and its purpose. Several aspects motivated Drugli and Steinsmo to apply such a setup. Firstly, the test setup was considered more realistic. Secondly, it was of interest to estimate the distribution of AC between coupled steel and anodes, especially since aluminium is stated in the literature to be more susceptible to AC corrosion [55]. Testing (4 days) by Drugli and Steinsmo revealed no increase of weight loss on carbon steel when a 60 Hz AC density of either 240 A m^{-2} or 1000 A m^{-2} was applied. The anode corrosion rates on the other hand, were in the same tests calculated to be 8.15 mm $year^{-1}$ and 60.5 mm $year^{-1}$, respectively [62]. With an area ratio (AR) of 1, the AC signal was transferred easier through the anode sample than through steel, which implied a lower impedance associated with the anode material. Two additional findings by Drugli and Steinsmo are worth mentioning. Potential measurements during testing revealed a potential change as described in section 2.4.1 (i.e. an immediate drop followed by a positive shift back to the initial potential within 10 hours). Furthermore, the AC potential that was needed to maintain a constant AC increased during testing. The authors attributed this potential increase to the increased polarization resistance associated with corrosion products and calcareous deposits that formed on the electrode surfaces. In another report by the same authors [63], a critical current density of 20 A m^{-2} was suggested, above which AC corrosion becomes a challenge for the lifetime of sacrificial anodes. Whereas no increase in weight loss was found when AC densities up to 20 A m^{-2}

(with a frequency of 100 Hz) was applied, the application of AC levels ≤ 20 A m^{-2} was still found to promote localized corrosion and change the corrosion morphology on the sacrificial anodes.

2.6 Concluding remarks on theory and earlier work

Based on existing theory on electrochemical impedance [46, 49, 51] and experimental studies [2, 4, 48, 50, 52, 57-61] it is evident that a large amplitude AC voltage alters the reaction mechanism and kinetics of a corroding system in seawater. The potential fluctuations can enable other reactions and formation of species, which are impossible or kinetically restricted at open-circuit potential and the application of a large amplitude AC further yields a non-symmetrical current response corresponding to the generated DC. In conclusion, there is an added risk for corrosion when a large amplitude AC voltage is applied. Focus in most experimental work on AC corrosion has been on steel only, by electrochemical studies and weight loss testing in different environments. The effect of AC on the corrosion behaviour of aluminium has been given modest attention in the past.

Some studies have focused on the behaviour of steel in seawater that is cathodically polarized to a potential level similar to the galvanic couple potential of a CP system. These earlier works have been confined to the AC induced pH change associated with the alkalization mechanism at the surface and the change in reaction kinetics when AC is applied. Except for three industry related reports by SINTEF [62, 63, 67], previous studies on the effect of AC do not account for the interaction that is introduced when a sacrificial anode and steel is connected, which is the case in a CP system. This influence of AC in a CP system was the focus of earlier work by the author [2], in which sacrificial anodes were observed to corrode significantly, both due to protection of steel and due to self-corrosion. A literature review, in combination with the results of the author's specialization project, emphasizes that aluminium is perhaps more susceptible to AC corrosion as compared to steel, which appears to be under sufficient protection by AlZnIn anodes. Therefore, the focus of this thesis is put on the AlZnIn anodes. It is of interest to study further the effect of AC on corrosion of AlZnIn anodes, both in the presence and absence of connection to steel. In this regard, different test configurations will be employed that are more realistic than the earlier test setup employed by the author [2]. The lack of understanding of AC corrosion motivates for a study of the fundamental mechanism that causes AC corrosion of the anodes. The importance of calcareous deposits, which appear to be destroyed and impeded in a CP system under influence of AC [2, 3], will also be addressed in this work.

3 Experimental work

The objective with the experimental testing was to study AC corrosion of anodes that are used for cathodic protection of carbon steel in seawater. This section provides material specifications of tested materials and presents the test setups and experimental procedures. Two different materials were used for testing, low alloy carbon steel and an AlZnIn (anode) material. The experimental procedure itself consisted of one-week weight loss tests under a range of experimental conditions. The evaluation after testing involved a surface analysis of deposits and corroded surfaces.

3.1 Test materials and sample preparation

Carbon steel

The test material used in this project was machined from a sheet of carbon steel, grade X65. The steel material was not analyzed to identify its chemical composition. However, according to the supplier its composition was in compliance with the requirements set by the offshore standard provided by Det Norske Veritas (DNV) for subsea pipeline systems (DNV-OS-F101). These are shown in Table 3-1. The samples were ground through 1000 grit SiC paper.

Table 3-1. Chemical compositional requirements, wt% and carbon equivalent (CE) of carbon steel material [6].

Maximum wt%									CE
C	Si	Mn	P	S	V	Nb	Ti	Other	
0.16	0.45	1.65	0.02	0.01	0.09	0.05	0.06	[1]	0.42 *

[1] Cu ≤ 0.50%; Ni ≤ 0.50%; Cr ≤ 0.50%; Mo ≤ 0.50%; B ≤ 0.0005% and Nb+V+Ti ≤0.15%

* $CE = C + \frac{Mn}{6} + \frac{(Cr + Mo + V)}{5} + \frac{(Ni + Cu)}{15}$

AlZnIn anodes

Two different test geometries of an AlZnIn alloy were utilized for testing. Rectangular plate samples were machined from an anode material supplied by Statoil at Rotvoll and cylindrical samples were machined from anode rods supplied by Beme Corrosion International in Bergen. Milling was performed by the workshop at the Faculty of Natural Science and Technology at NTNU. The plate specimens were tested as delivered, i.e. no surface treatment other than cleaning was performed on the anode material prior to testing. A chemical analysis was performed in three ways to determine the chemical composition of the AlZnIn alloys. Energy dispersive X-ray analysis (EDS) and glow discharge mass spectrometer (GDMS) were performed at NTNU and spark-optical emission spectroscopy (spark-OES) was performed at Hydro, Karmøy. A comprehensive presentation of the analyses is contained in Appendix B . Of the three chemical analyses, the spark-OES was the most accurate. Samples were ground through 500 grit SiC paper before analysis by GDMS and spark-OES. The results of the Spark-OES are partly presented in Table 3-2. The chemical composition of the AlZnIn alloys was, by the analyses found to be in accordance with the offshore standard provided by DNV for sacrificial anodes (DNV-RP-B401).

Table 3-2. Compositional limits according to DNV-RP-B401 and chemical composition of test materials by spark-OES for AlZnIn anode materials [5].

Sample ID	Element [wt %]							
	Al	Zn	In	Cd	Si	Fe	Cu	Pb
DNV-RP-B401	rem.	2.5-5.75	0.015-0.040	≤0.002	≤0.12	≤0.09	≤0.003	na
Statoil [2]	95.287	4.540	0.025	0.00022	0.033	0.075	0.00026	0.00017
Statoil	96.110	3.744	0.015	0.00017	0.034	0.042	-0.00015	0.00007
BEME	97.155	2.650	0.026	0.00021	0.049	0.076	0.00044	0.00007

Sample preparation

The sample geometries of the various test specimens (both carbon steel and AlZnIn alloy) are given in Table 3-3. Testing was carried out on two different test geometries of AlZnIn. All test specimens, – both carbon steel and AlZnIn alloy, – were subjected to the same cleaning procedure prior to the experiments. The pre-treatment included cleaning in distilled water, acetone and ethanol followed by drying. Specimens were then weighted on an analytical balance (Ohaus AS200) and stored in a desiccator for further testing. Prior to testing, all

[2] Anode sample from a batch used in earlier experiments in the author's specialization project.

specimens were painted with “Micro-shield”, a stop-off lacquer, exposing only the desired test area.

Table 3-3. Specimen geometry of carbon steel and AlZnIn alloy.

Material	Height [mm]	Length [mm]	Width [mm]
Carbon steel	50	20	2
AlZnIn (plate)	80	30	6
	Height [mm]	**Diameter [mm]**	
AlZnIn (cylindrical)	40	38	

Figure 3-1 shows a photo of the various types of prepared specimens. A poor adhesion of the stop-of lacquer was associated with the steel specimens in the author’s specialization project [2]. The problem was addressed by application of three layers of “Micro-shield”. The supplied steel and AlZnIn materials were tested as delivered. The exposure area of the AlZnIn test specimens was set to 45 cm^2. In experiments were testing involved a galvanic coupling to steel, the exposure area of the associated steel specimens was set to 0.45 cm^2 and 4.5 cm^2, to obtain an anode-steel area ratio (AR) of hundred and ten, respectively. For both materials, a thin stainless steel rod mounted onto the upper tapped end of the samples ensured electrical connection. Galvanic effects and corrosion of the rod was avoided by the application of an isolation sock (as illustrated in Figure 3-1).

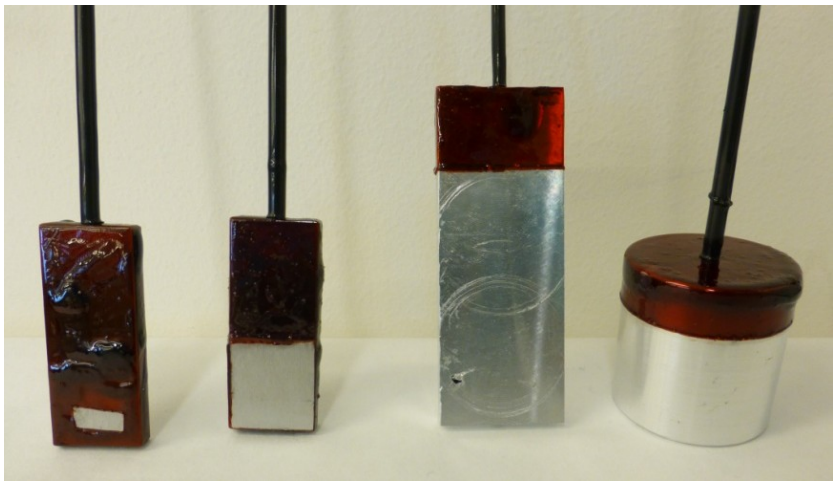

Figure 3-1. Painted test specimens with rods mounted onto the upper end for electrical connection. Carbon steel (left) with an exposure area of 0.45 cm^2 and 4.5 cm^2 and AlZnIn (right) of two different electrode designs (plate and cylinder) with an exposure area of 45 cm^2.

3.2 Test solution – synthetic seawater

Synthetic seawater was used as test solution in all experiments in this work and its preparation was in accordance with ASTM D1141 [68]. The pH of the test solution was adjusted to 8.2 by a standard pH meter (PHM210, Radiometer Copenhagen). Due to risk of development of hazardous bromides, it was decided to exclude potassium bromide (KBr) from the test solution to be in accordance with health, safety and environment (HSE) regulations. Otherwise, the composition of the synthetic seawater was in accordance with ASTM D1141, and as given in Table 3-4.

Table 3-4. Chemical composition of the synthetic seawater.

Compound	Concentration [g L^{-1}]
NaCl	24.530
$MgCl_2$	5.200
Na_2SO_4	4.090
$CaCl_2$	1.160
KCl	0.695
$NaHCO_3$	0.201
H_3BO_3	0.027
$SrCl_2$	0.025
NaF	0.003

3.3 Reference electrode

A Standard Calomel Electrode (SCE) of $Hg/HgCl_2$, immersed in a saturated KCl solution was applied throughout the entirety of the experiments as a reference electrode. Its potential is +244 mV_{SHE}. All results in this project are presented vs. SCE unless otherwise stated. Electrical connection to the test solution, i.e. artificial seawater, was established through a salt bridge of agar solution that consisted of saturated potassium chloride (KCl) and agar.

3.4 Weight loss testing under influence of AC

AC corrosion of sacrificial anodes was experimentally studied by weight loss testing under a range of experimental conditions.

3.4.1 Test setup and apparatus

The test setup involves inducing an AC signal into a DC system (i.e. an electrochemical cell). An AC supply was achieved by a Variable AC source (VariAC), which delivered a frequency of the AC signal of 50 Hz. The AC- and DC signal need to be separated in order to measure current and potential parameters of interest during testing. This aspect was the main motivation for the application and testing of different logging devices for automatic current and potential measurements. Three devices, a HP logger, a National Instuments (NI) logger and Fluke digital multimeter, were evaluated with the aim to indentify the optimal logging instrument for experiments involving AC. Application of a HP logger in combination with filters has been used in earlier projects by the author [2] and others [3, 4, 52, 57, 69]. The latter two instruments on the other hand, have the ability to separate the AC- and DC signal, making filters in the electric test circuit redundant. A comparison of the various electric circuits is given in Figure 3-2. The test setups and logging instruments are each thoroughly described in the end of this section.

Weight loss experiments are grouped in three, distinguished in the way test samples were coupled, i.e. the test configuration. The first experiments designated A/S, involved a coupled anode-steel pair, as illustrated in Figure 3-2. In A/S experiments, a constant AC potential was applied with an area ratio (AR) between anode and steel of 10 or 100. The objective with A/S experiments was to study the effect of area ratio on AC corrosion of anodes. A higher AR is thought to be more realistic, which was part of the motivation for testing with an AR of 100. In the author's specialization project, an AR of 10 was employed.

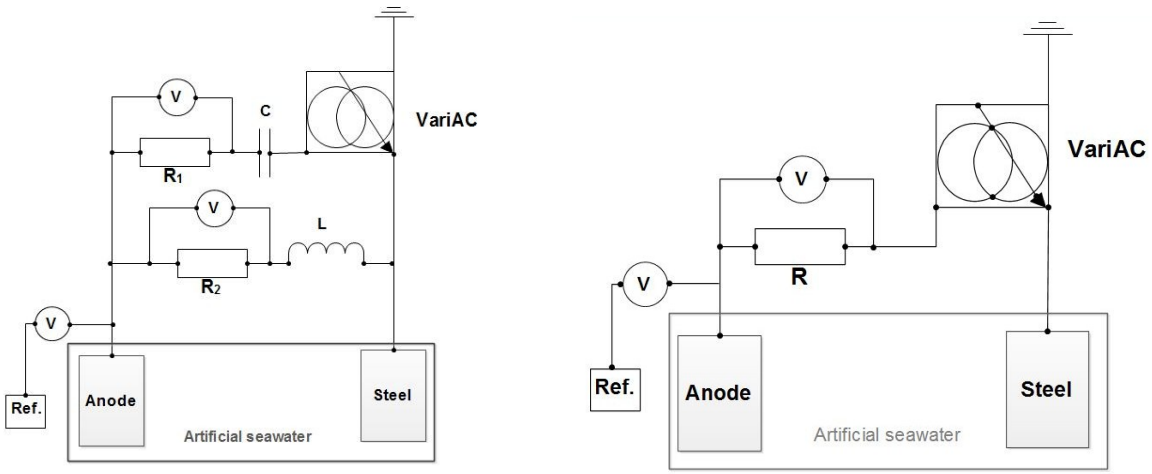

a) Test setup with filters

b) New test setup

Figure 3-2. Electric circuit for AC testing. A VariAC delivered the desired AC level. a) Old test setup with DC- and AC filtering achieved by a capacitor (C) and inductor (L). Current measurements enabled by the resistors R_1 and R_2, both of 1Ω. b) New test setup with no filters and current measurements over the same resistor, R.

The two other types of experiments aimed to investigate AC corrosion of anodes. The influence of connection to steel was evaluated, and in these experiments, a constant AC density was applied. The following test configurations were employed: an anode-anode pair (A/A experiments), and a parallel-coupled anode-steel pair, which in turn was coupled to another parallel-coupled anode-steel pair with AR of 100 (SA/AS experiments). The two test configurations, illustrated in Figure 3-3, are considered more realistic when realizing that steel is exposed only at coating defects and that multiple, larger anodes are placed along the pipeline. Note that the current measurements in A/A and SA/AS experiments at the same AC level are *not* directly comparable, as the latter test configuration involves a current transfer also between anode and steel samples. The amount of current transferred between only the anodes is not reflected in the measured current value (see Figure 3-3). The splitting of AC between the anode and a 13 Cr steel sample has been investigated in the work of Drugli and Bjordal [67]. The results of their study are of relevance for the experimental work of this thesis. The authors employed a similar test setup in their work, as shown in Figure 3-4, which enabled an estimation of the current transfer to and from each electrode by measuring the potential drop over four additional resistors of 1 Ω. In all experiments an AC density of 80 A m^{-2} was applied to each couple (of anode and steel). The splitting of AC was found strongly influenced by the area ratio (AR) between coupled anode and steel samples. At an AR of one, the total AC was split roughly 55/45 between anode and steel. Whereas the majority (i.e. 80 %) of AC was transferred to the steel sample in experiments with an AR of 0.1 (i.e. a larger steel sample), Drugli and Bjordal stated that the majority of AC will be transferred through the anodes if there is a small coating defect in the steel pipeline. No experiments were however performed to verify this proposed distribution at higher AR, e.g. of 10 or 100.

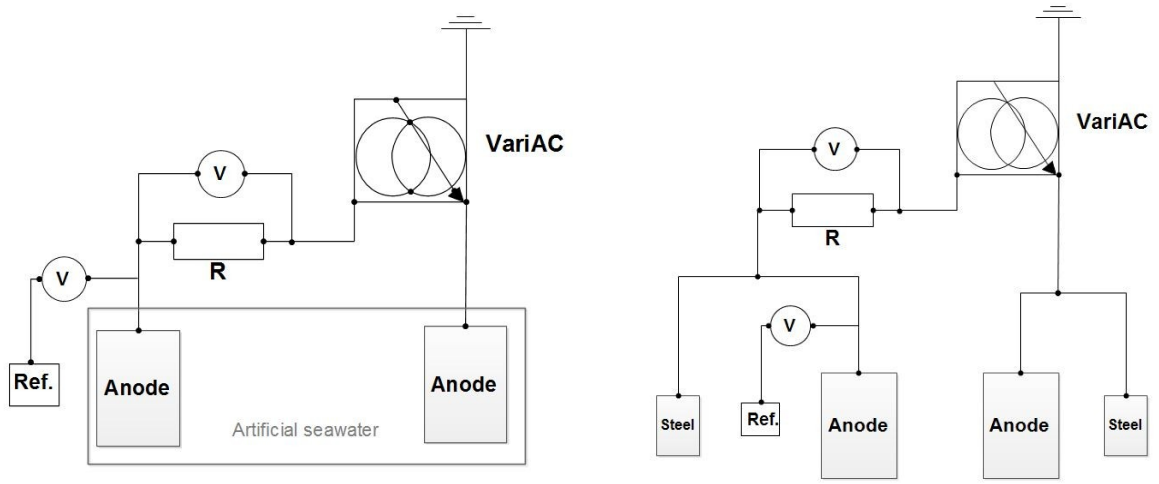

Figure 3-3. Test cell configuration for A/A experiments (left) and SA/AS experiments (right).

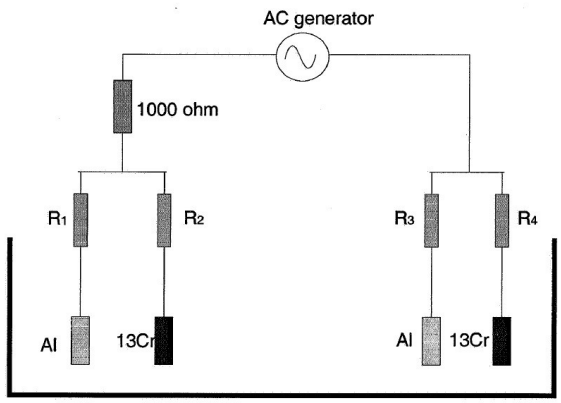

Figure 3-4. Test setup for two coupled anodes and two 13 Cr steel samples under influence of AC. From the Sintef report by Drugli and Bjordal [67].

All electrical connectors such as plugs, clamps and electric wires were checked for conductivity. For A/S experiments, the test cell consisted of 650 mL of test solution and a temperature control chamber ensured a test temperature of 25°C in the entirety of the test period. For A/A and SA/AS experiments, the test cells consisted of 1800 mL of test solution and a temperature control chamber was not utilized. Photos of the different test cells are shown in Figure 3-5 and Figure 3-7, respectively. In all experiments, a rotating glass rod immersed into the test cell itself, with a rotation speed of 100 rpm, ensured a homogeneous distribution of O_2 in the test solution.

a) Test setup with filters and HP logger

A thorough description of the test setup where a HP logger was utilized follows. The given test setup for AC corrosion testing, was developed and presented by Belzoni et al. [70] and later modified and implemented with success by Statoil [59] and former master students [3, 4, 52, 57, 69]. It was also used in the author's specialization project on AC corrosion in the autumn of 2012 [2]. An explanation to the combined AC- and DC circuit as schematized in Figure 3-2 follows. A photo of the entire test setup is shown in Figure 3-5 with an explanation to the numbered components given in Table 3-5.

A capacitor C, of 500 μF functioned as a filter for the DC signal, whereas an inductor L, of 10 H filtered out the AC signal. The given filters enabled separate automatic measurements by the HP logger of the AC density and the DC density over two different resistors, designated R_1 of 1Ω and R_2 of 1Ω, respectively. This way of preventing mutual interference from the AC- and DC signal is effective, as only 0.1% of the total AC current has been reported to circulate in the DC circuit in relevant test solutions [70]. The inductor itself introduced an inner resistance of 10Ω. In order to ensure a common ground, the electric circuit in its entirety was connected to an isolating transformer. Except for the mean potential [V_{DC}], which was recorded by a Fluke True-RMS digital multimeter, parameters of interest were monitored and logged by means of the HP 34970A logger in combination with Agilent BenchLink Data logger software.

The initial test setup with a HP logger was associated with two challenges, of which gave the motivation for an evaluation of logging alternatives. Firstly, the application of a high-impedance capacitor as a filter caused the capability of the AC source to be inadequate in that an upper limit and a large variability were associated with the applied AC potential. The second challenge was related to the logging system itself (HP 34970A logger), as it appeared to be disturbed by signal interference, which introduced unreliability and errors in any measurements associated with especially the high-impedance system of the reference electrode. The two challenges were initially addressed during the master project with the aim to implement or develop a new logging instrument capable of separating the AC- and DC signal and log automatically all current and potential values of interest. As a result, a new test setup and apparatus for AC corrosion testing was developed. A presentation of this follows.

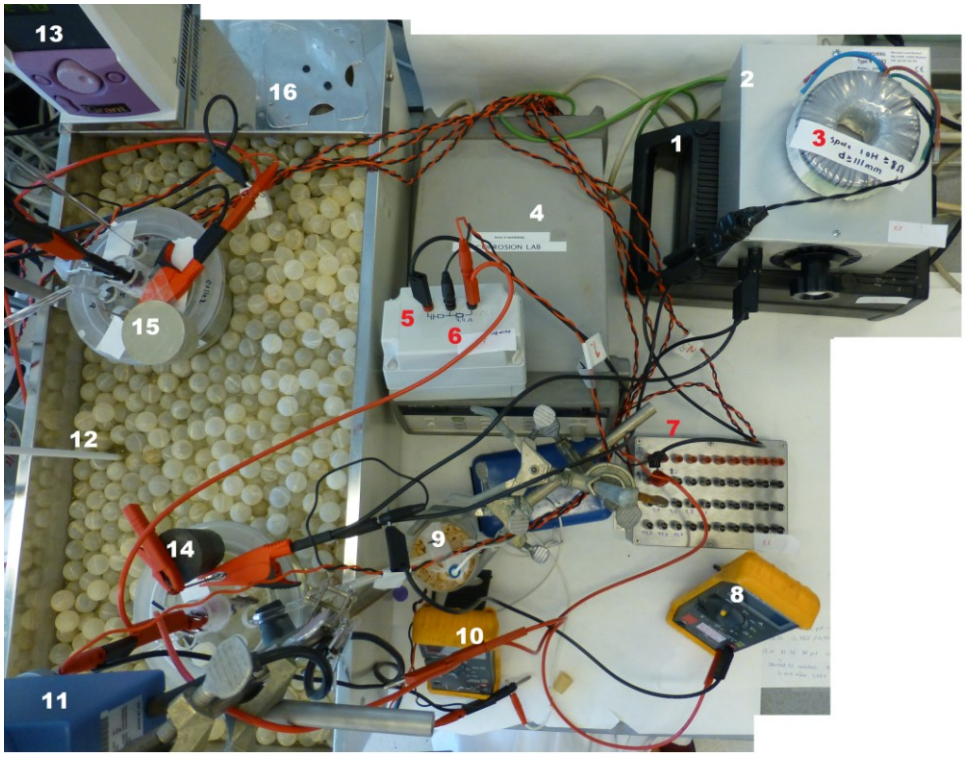

Figure 3-5. Overview of old test setup for inducing AC into a CP system. Note that two test cells are shown in the picture, with electrical circuit components for only one of the test cells. Numbered elements are clarified in the table below.

Table 3-5. Numbered components in test setup of Figure 3-5.

Item #	Explanation
1	Isolating Transformer
2	VariAC
3	Inductor
4	HP 34970A logger
5	Capacitor
6	Resistance R_1
7	Resistance R_2
8	Multimeter (to control the AC potential on steel)
9	SCE Reference electrode
10	Multimeter (to measure mean potential on anode)
11	Stirrer in test cell driven by electrical motor
12	Stirrer in test chamber driven by electrical motor
13	Temperature controller / Heater
14, 15	Test cell 1 and test cell 2
16	Temperature control chamber

b) New test setup with no filters

New logging instruments enabled the application of a new test setup with no filters. As a result, the electric circuit as given in Figure 3-2 b) was simplified and its total resistance was reduced. Two alternatives were tried and evaluated. A National Instruments logger (NI 6259) and modified true-RMS digital multimeters (Fluke 289), which both have the ability to separate an AC- and DC signal and log data. The challenge of signal disturbance was not fully managed in relation to the NI logger. Initially, the instrument was evaluated thoroughly in terms of signal interference from surrounding electrical apparatus and devices. Bias errors were addressed by a trial-and-error approach and measures were taken to avoid these.

An overview of the new test setup with NI logger is shown in Figure 3-6 with an explanation to the numbered components given in Table 3-6. AC and DC density was measured separately over the same resistor, R. A new resistor with an effect of 10 W and a resistance of 10 Ω was applied to obtain a better resolution (i.e. improved signal-to-noise ratio) of the current measurements. In order to prevent signal interference, shielded cables and shielded boxes, which contained the resistor and signal inputs, were utilized,.

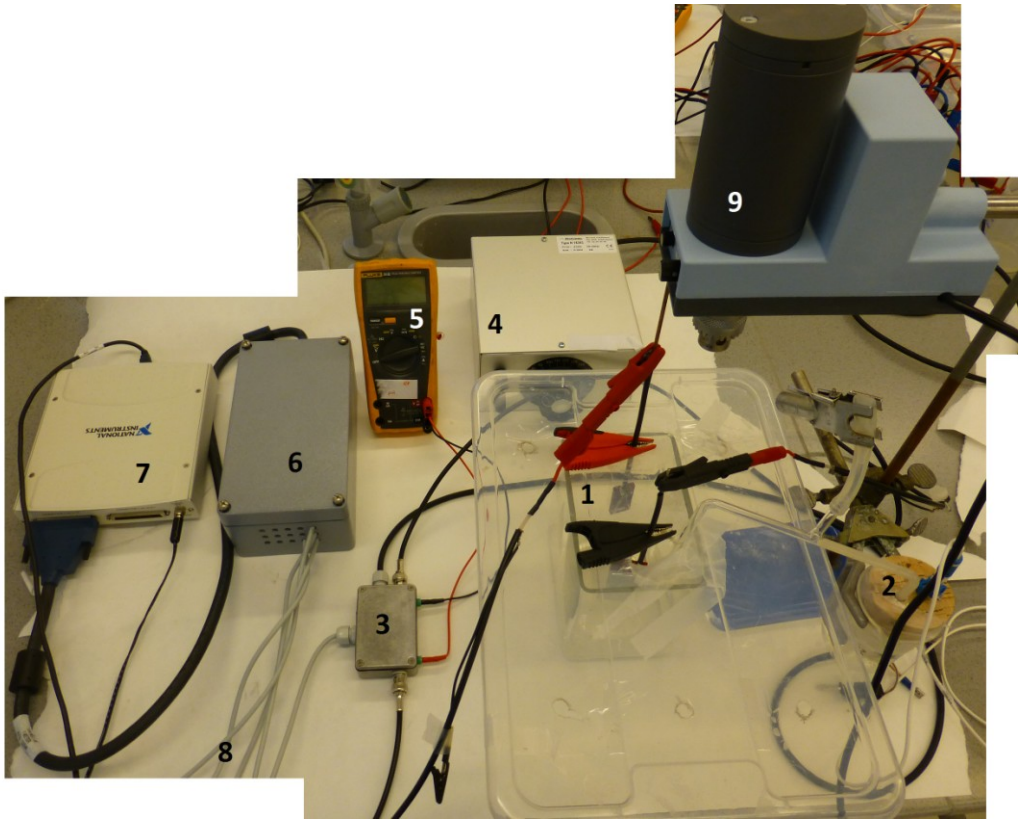

Figure 3-6. Overview of new test setup with the application of the NI logger. Numbered elements are clarified in the table below.

Table 3-6. Numbered components in test setup of Figure 3-6.

Item #	Explanation
1	Test cell with samples in synthetic seawater.
2	SCE Reference electrode with salt bridge to test cell
3	Shielding box with input of all signals and resistor R of 10 Ω
4	VariAC
5	Multimeter (to measure AC density over resistor R for adjustments of the AC signal input by VariAC)
6	Signal connection box of NI logger
7	NI logger device (connected to PC)
8	Wires connected to other experiments
9	Stirrer in test cell driven by electrical motor

New software in LabView was developed and used in combination with the NI logger. In addition to recording data of interest, both the software in Labview and the digital multimeters enabled in-situ monitoring of all current and potential parameters of interest. The NI logger has an analogue input with 16 differential channels, i.e. the signal input is the difference measured between a positive and a negative input. Its specifications are further an input range of ±10 V (amplitude) and an input impedance of 10 GΩ in parallel with a capacitor of 100 pF. The higher internal impedance provided an improved logging sensitivity as compared to the HP logger.

Similarly, the test setup with application of Fluke digital multimeters is shown in Figure 3-7 with an explanation to the numbered components given in Table 3-7. The multimeters were modified by connecting them to a current supply instead of using batteries.

Each multimeter was capable of measuring only one potential parameter. A resistor R, of 10 Ω was applied for both AC- and DC density measurements. In cases where the DC density was higher than the range at which the multimeter was able to measure (e.g. above 500 mV DC for testing at high levels of applied AC), an extra resistor R (of 1 Ω) was coupled in series to enable DC measurements. The lower resistance however resulted in a lower accuracy of the current measurements.

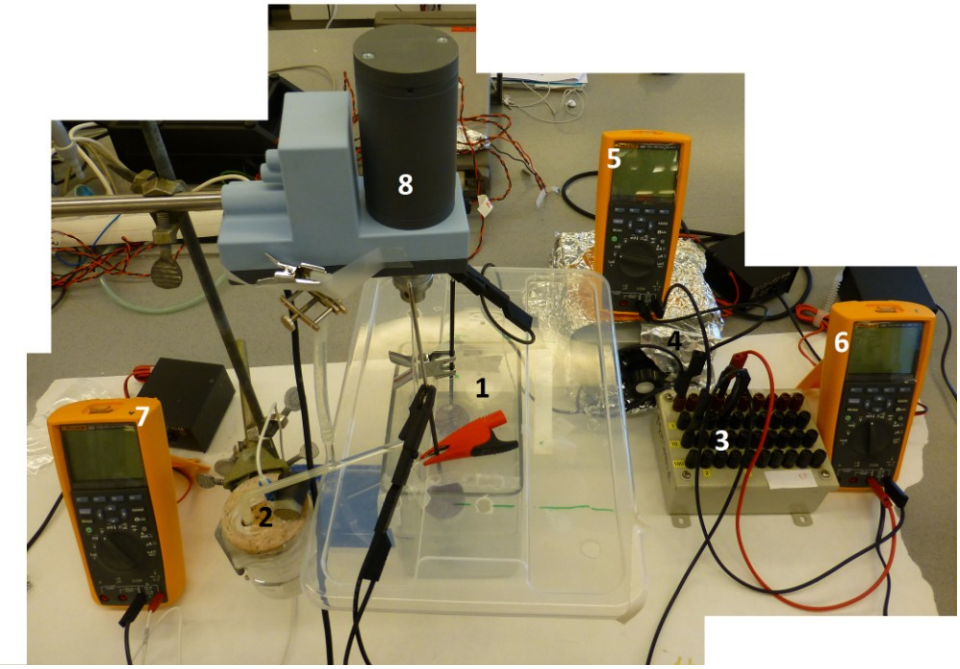

Figure 3-7. Overview of new test setup with the application of Fluke digital multimeters. Numbered elements are clarified in the table below.

Table 3-7. Numbered components in test setup in Figure 3-7.

Item #	Explanation
1	Test cell with samples in synthetic seawater.
2	SCE Reference electrode with salt bridge to test cell
3	Resistor R, 10 (and 1) Ω
4	VariAC
5	Multimeter (to measure AC density over resistor R)
6	Multimeter (to measure DC density over resistor R)
7	Multimeter (to measure the mean potential)
8	Stirrer in test cell driven by electrical motor

Current and potential measurements

Regardless type of test configuration and logging equipment, four parameters of interest were measured and recorded during the test period of one week. 1) the AC component of the current (i_{AC}), 2) the DC component of the current (i_{DC}), 3) the mean potential (V_{DC}) of the anode sample (i.e. the couple potential), and 4) the AC potential between the anode and steel (V_{AC}). Data were for the experiments recorded with a two-minute interval. A SCE reference

electrode enabled measurement of the mean DC potential of the anode. The AC level supplied by the VariAC was unsteady and showed significant variation. It was desirable to perform testing at a constant AC potential or constant AC density level. Therefore, the AC level was checked manually by a multimeter to enable adjustments to the output from the VariAC.

3.4.2 Test procedure

All experiments were performed in a test cell of synthetic seawater for one week, at which the test was ended and specimens were removed from the test cell. Weight loss experiments were performed under various experimental conditions (see Table 3-8), with the objective to study the influence of connection to steel and the resultant influence of area ratio (AR) between anode and steel on AC corrosion behaviour of AlZnIn anodes. Replicates were run to verify test results. Weight loss experiments are grouped in three (i.e. SA/AS, A/A, A/S), distinguished in the way test samples were coupled (section 3.4.1). Note also that either a constant AC density or a constant AC potential was applied. The AC density is presented relative the area of one anode sample. A/S experiments were compared to test results from an earlier specialization project by the author [2], where an AR of 10 were used in the range of 0 to 3 V RMS. Testing was at that time carried out with a HP logger and filters, and the comparison thus functioned as to provide a validation of the new test setup and logging instrument. The previous A/S experiments also involved preconditioning of the steel to CP to form calcareous deposits. As a result, the comparison moreover enabled an evaluation of the importance of calcareous deposits on steel for the corrosion of sacrificial anodes under influence by AC.

Table 3-8. Test matrix for one-week weight loss testing under various experimental conditions. Replicates were run at several AC levels.

A/S experiments Study influence of area ratio (AR)		**SA/AS and A/A experiments** Study influence of connection to steel	
AR	V_{AC} [V RMS]	**Test config.**	i_{AC} [A m^{-2}]
100	0.5 1 1.5 2 2.5 3.5 4.5	**SA/AS**	10 40 80 100
10	1.5 2 2.5 3	**A/A**	10 30 40 55 60 80 90 100

The test solution was refilled with distilled water whenever the level dropped. After testing, samples were cleaned gently in distilled water, air-dried and photographed macroscopically.

Thereafter, samples were given a treatment as outlined in section 3.4.3 for weight loss measurements. In the event of surface analysis, samples were stored separately in a desiccator.

3.4.3 Weight loss measurements

AC corrosion testing at a given AC potential or AC density was followed by weight loss measurements, and these were carried out on all anode samples, but only for the steel samples in cases where corrosion was apparent by the naked eye. Weight loss measurements and cleaning was performed according to ASTM G1-03 [71], where the corrosion product was removed by a cycled chemical treatment, as outlined in Table 3-9.

Table 3-9. Chemical treatment for removal of corrosion products according to ASTM G1-03 [71].

Material	Cleaning solution	Temp. [°C]	Time of each cycle [min]	# of cycles
AlZnIn	Diluted H_3PO_4 (sp. gr. 1.19) and 20 g l^{-1} CrO_3	90-100	5	2-4
C-steel	Diluted HCl (sp. gr. 1.69) and 3.5 g l^{-1} hexamethylene tetramine	20-25	10	1

Note that every experiment was performed for one week and calculated corrosion rates are thus comparable. The corrosion rates were calculated based on the weight loss between initial and final weight of the test specimens. Equations are given in Appendix A. A significant uncertainty is related to the cleaning procedure and resulting weight loss measurements of the steel samples. These aspects are reported and discussed elsewhere by the author [2]. For each cycle, specimens were cleaned and then weighted. The cleaning was performed with distilled water, acetone and ethanol followed by drying with a heat gun at 60 °C. The number of necessary cycles to obtain a cleaned sample increased with the severity of corrosion attack. The removal of base material in the chemical treatment of the steel samples was inevitable and needed to be adjusted for. In order to consider this, an untested steel sample underwent the exact same chemical treatment for which the weight loss of this was accounted for in calculations. During an earlier specialization project by the author [2], an untested anode sample underwent the exact same chemical treatment in order to account for any weight loss of base material during cleaning. It showed that the chemical cleaning outlined in Table 3-9 did not attack the anode material itself.

3.4.4 Impedance measurements

The impedance of both steel and anode samples in SA/AS experiments was analyzed using a potentiostat (Gill AC Serial no 776, ACM instruments). The objective with the measurements was to obtain information about any changes in the reaction kinetics at the anode and steel surface after AC testing. Impedance measurements were performed in a three electrode cell at open circuit potential (Figure 3-8), before and after one-week AC testing. In-situ measurements were inapplicable by the Gill AC potentiostat, and the measurements therefore provided no information about the reaction kinetics *during* AC influenced corrosion. A Standard Calomel Electrode (SCE) was used as reference electrode whereas a platinum (Pt) electrode functioned as a counter electrode. In total 100 readings was performed in the frequency range from 10 kHz to 0.5 Hz, with AC amplitude of 100 mV.

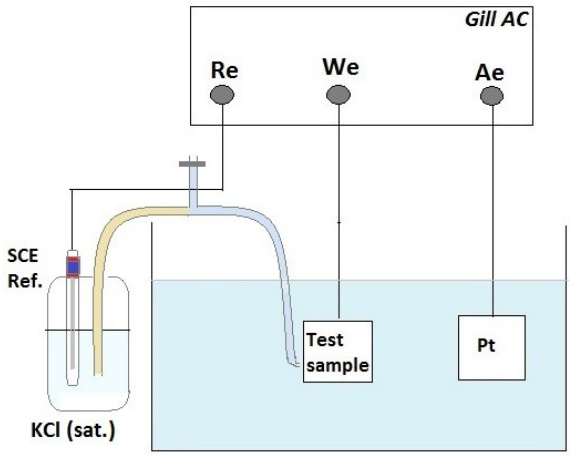

Figure 3-8. Three electrode cell for impedance measurements.

3.4.5 pH measurements

A standard pH meter (PHM210, Radiometer Copenhagen) was used for a pH measurement of the test solution after ending three SA/AS experiments. The pH-measuring electrode was calibrated with reference solutions prior to use.

3.5 Surface characterization

Test materials underwent a surface analysis after AC corrosion testing. Characterization of the deposits on both the steel and anode samples was performed by means of X-ray Diffraction (XRD) analysis. Corroded anode (and steel) surfaces were characterized by SEM.

3.5.1 Characterization of deposits

The deposits that remained on the steel and AlZnIn surfaces after testing were investigated by XRD analysis to identify its composition and crystal structure. Prior to analysis, calcareous deposits on the steel surface and corrosion products on the anode samples were stripped off, crushed and dispersed onto a silicon low-background specimen holder with ethanol. Powder XRD was performed using a Bruker AXS, D8 Focus Diffractometer with a step time of 2.0 s, a step size of 0.019997° and a fixed divergence slit of 0.2°. The data was collected in the 2θ range of 10° to 80°. An evaluation of possible crystal structures was obtained using the Bruker AXC Diffrac.EVA software.

3.5.2 Characterization of corroded specimen surfaces

After AC corrosion testing, the corroded specimen surfaces (both anode and steel samples) were studied by low vacuum scanning electron microscopy (LVSEM), (Hitachi S-3400N) to observe the surface morphology. An accelerating voltage of 10kV, a working distance (WD) of (around) 7 mm and a secondary electron (SE) detector was used. Because of the geometry of cylindrical anode specimens, only rectangular plate anode specimens were SEM analyzed.

4 Results

The objective with the weight loss testing was to investigate AC corrosion of sacrificial AlZnIn anodes. This section presents test results, which are designated in accordance with the test matrix of Table 3-8 (in section 3.4.2). Three different test configurations were employed and they are distinguished by how test samples were coupled. The results from testing at constant AC density levels are presented first. Two different test configurations were employed in these experiments, i.e. a pair of coupled anodes (A/A experiments) and steel coupled to anode, which in turn was coupled to another identical pair of parallel-coupled anode and steel sample (SA/AS experiments). Then, a presentation of the results from testing at constant applied AC potential involving an anode-steel couple (A/S experiments) with varying area ratio (AR) is given. Results from impedance measurements of a few anode samples and macroscopic and microscopic surface analysis of all test samples are presented in the end to support the findings from the weight loss testing.

4.1 AC corrosion of anodes and influence of connection to steel

The influence of steel on the AC corrosion of sacrificial anodes was investigated by comparing results of two test configurations, i.e. A/A and SA/AS experiments. In both cases, a constant AC density was applied and experiments are designated by the current density level that was applied (relative the area of one anode sample, and assuming the overall current was transferred only between anode samples). An AR of 100 was employed in experiments that involved coupling to steel. In most figures, results from the SA/AS and A/A experiments are distinguished by designating the experiments with steel as “w/S”.

4.1.1 Key parameters

Figure 4-1 to Figure 4-5 shows the general development of key parameters throughout the entire test period. Time and current scales are logarithmic and current parameters relates to the area of one anode sample. Note that the measured current values from SA/AS experiments do not reflect the true current density experienced by one anode, as the test circuit (Figure 3-3) allow for current transfer also between steel and anode samples. The reader is referred to section 3.4.1 for a clarification of this aspect. Figure 4-1 shows the occurrence of variability in the applied AC density, which increased in extent with increasing levels of AC.

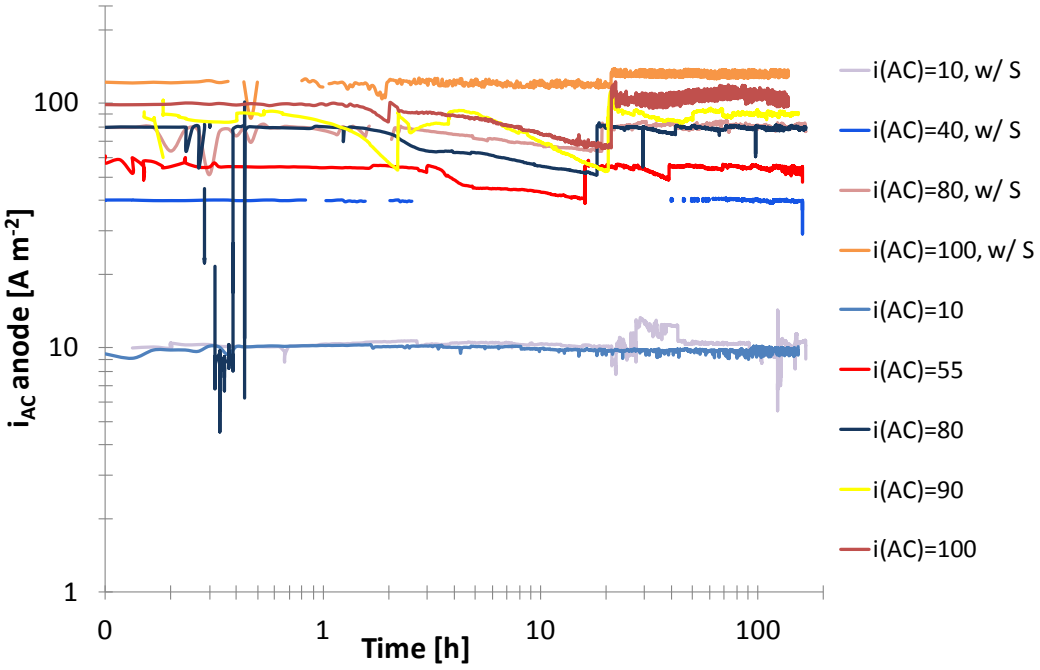

Figure 4-1. Applied AC density [A m^{-2}] between anodes (A/A experiments) and between two pairs of anode and steel (SA/AS experiments designated "w/ S"), as a function of time.

Figure 4-2 shows the mean potential (V_{DC}) measured on one of the anode samples throughout the test period. The general trend was an immediate reduction in the mean potential, i.e. a negative polarization under influence of AC. The mean potential was more negative the higher level of applied AC. Contrary to A/S experiments (section 4.2.1), the mean potential remained low throughout the test period. Under removal of induced AC (in the end of the test), a significant negative polarization was observed at AC levels > 40 A m^{-2} in experiments with no connection to steel. The drop is more clearly presented in Figure 4-3 showing only the final 30 minutes of the test period. The extremely low potential remained low throughout the rest of the period of logging. However, logging was ended already about 5 min after the removal of induced AC.

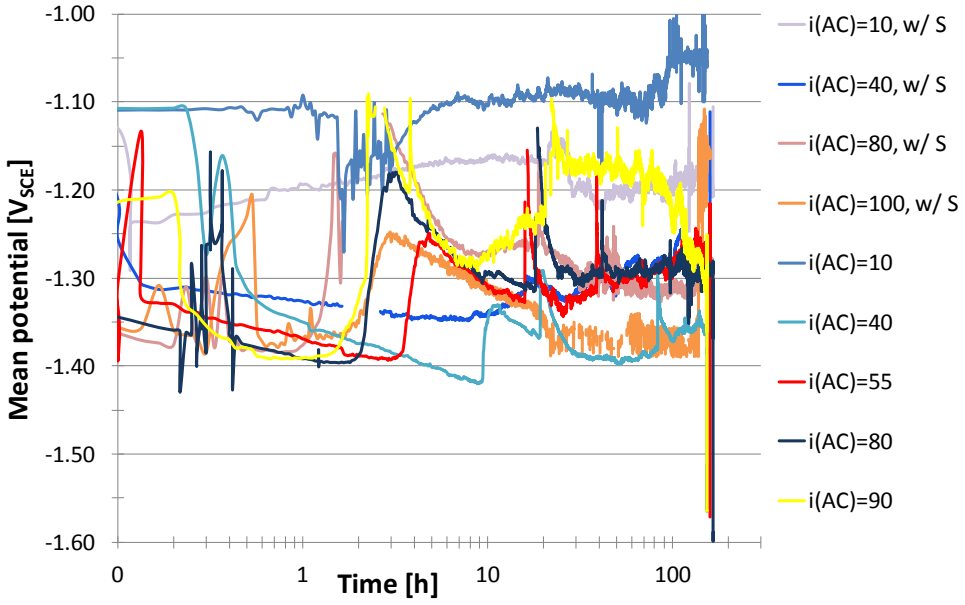

Figure 4-2. Mean potential of anode with time at various AC levels [A m^{-2}] for SA/AS ("w/ S") and A/A experiments.

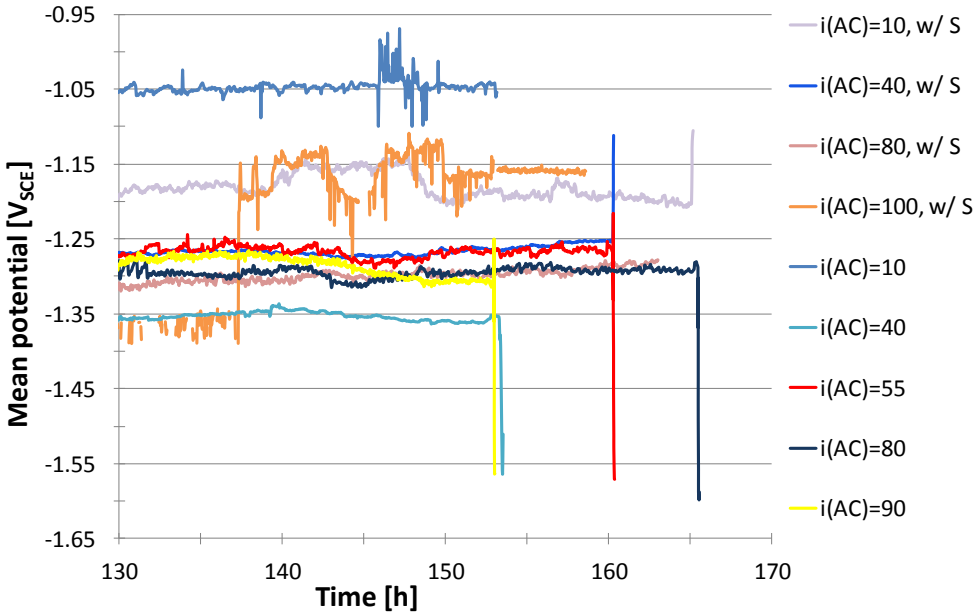

Figure 4-3. Mean potential of the anode at the end of the test period at various AC levels [A m^{-2}] applied in SA/AS ("w/ S") and A/A experiments. Under removal of AC, a significant drop was observed for A/A experiments at $i_{AC} \geq 40$ A m^{-2}.

Figure 4-4 shows the measured DC density with time. For most experiments, i_{DC} was small throughout the entire test period. Figure 4-5 shows the measured AC potential (between anode samples) with time for four experiments at two different applied AC levels.

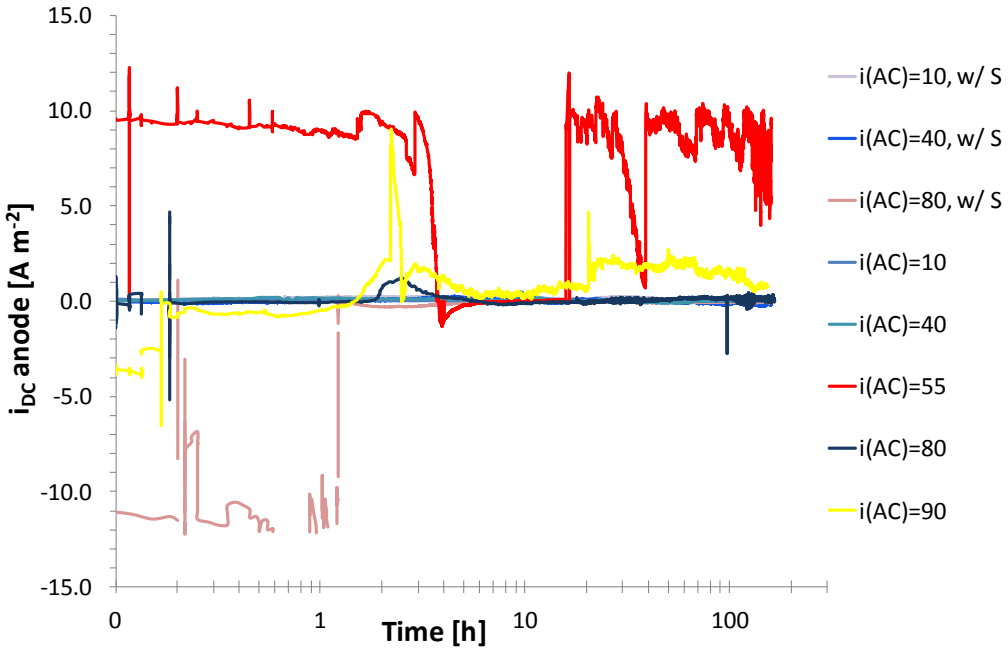

Figure 4-4. DC density measured between anode samples at various applied AC levels [A m^{-2}] in SA/AS ("w/ S") and A/A experiments.

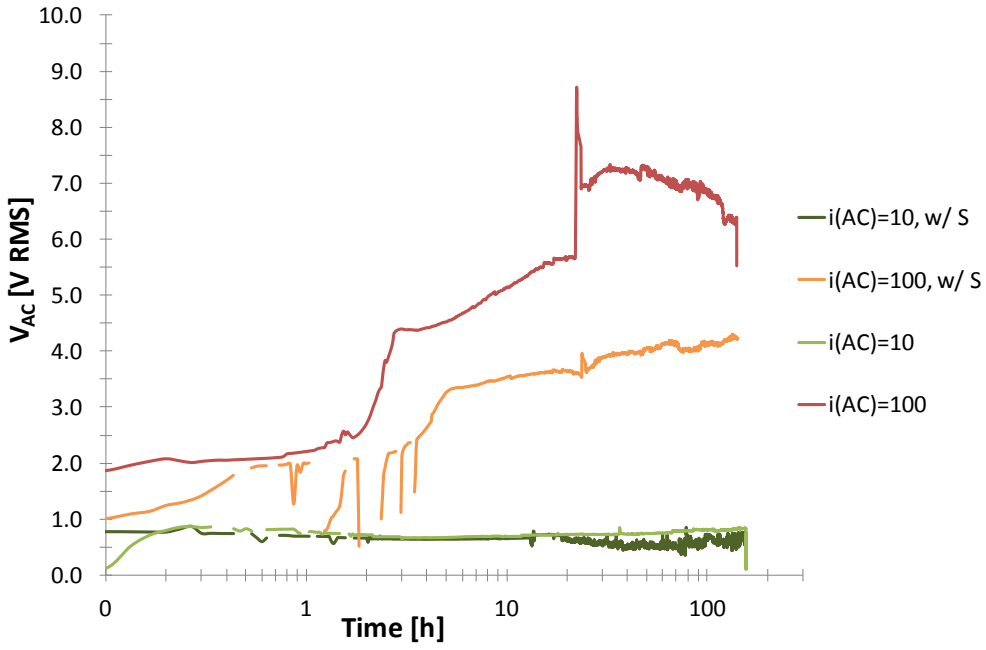

Figure 4-5. Measured AC potential as a function of time for SA/AS and A/A experiments at i_{AC} = 10 A m^{-2} and at i_{AC} = 100 A m^{-2}.

The AC potential increased clearly with applied AC level. For AC testing at 100 A m^{-2}, the potential also increased with time, and at this AC level, the potential difference was higher for the experiment with no connection to, and thus no influence of, steel.

4.1.2 Anode corrosion rates

Testing involved coupling of two anodes and calculated corrosion rates of these are presented in Figure 4-6, as a function of applied AC level. A clear increase in anode corrosion rates with applied AC level was found for both A/A and SA/AS experiments up to $i_{AC} \approx$ 80-90 A m^{-2}, at which the corrosion rates decreased with any further increase in the applied AC level. It is evident by Figure 4-6 that connection to steel had no clear influence on the anode corrosion rates. Experimental observations in relation to testing at high AC levels revealed heat development and increased viscosity in the test solution caused by the formation of extreme amounts of corrosion product (section 4.4.1). Replicates were run at 10 A m^{-2} and in SA/AS experiments at this AC level, only one of the anodes were found to corrode, the amount of corrosion being comparable to the total corrosion rate of both anodes in the A/A experiments.

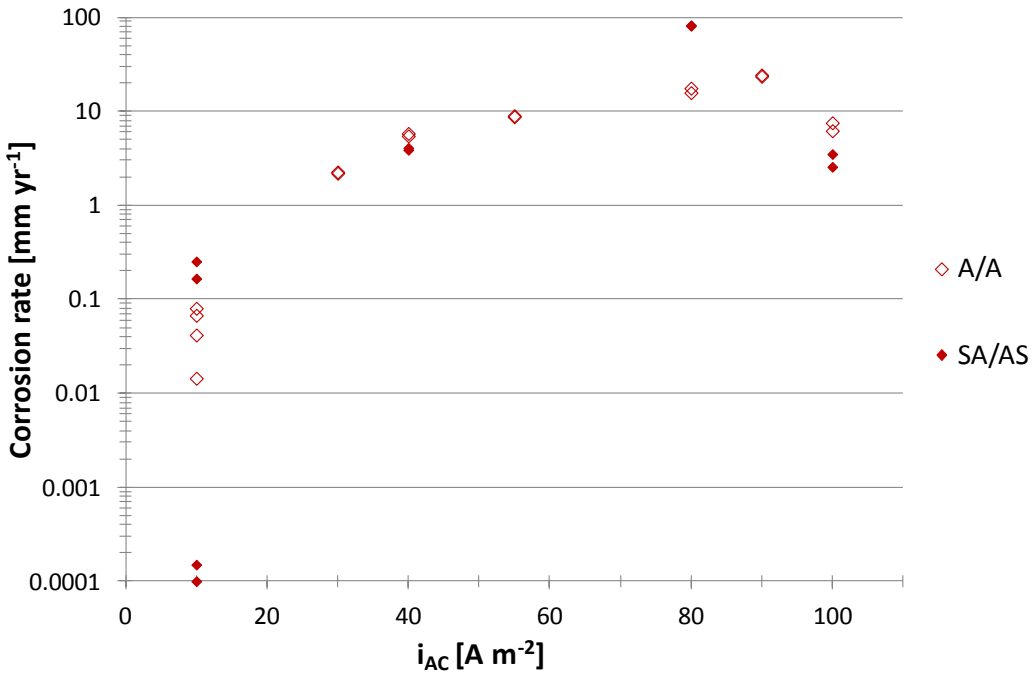

Figure 4-6. Anode corrosion rates of each anode in SA/AS and A/A experiments as a function of applied AC level [A m^{-2}].

4.1.3 Steel corrosion rates

Earlier work has shown that a high uncertainty is related to the weight loss measurements of steel [2]. Therefore, except for three steel samples where experimental observations revealed corrosion, weight loss measurements were not performed. The corrosion rates of the three clearly corroded steel samples were calculated to be 2.6 and 3.6 mm $year^{-1}$ (tested at 80 A m^{-}

^{2}) and 1.3 mm year^{-1} (tested at 100 A m^{-2}). Note that the applied current density relates to one of the anode samples, with a corresponding AR between anode and steel of 100. The steel samples thus experienced extreme values for i_{AC} during these experiments, even though most of the AC is believed to be transferred between the anode samples. The reader is referred to section 3.4.1 for a discussion of the aspect of current transfer to steel samples from anode samples under AC testing in SA/AS experiments. The removal of base material in the chemical cleaning of the steel samples was inevitable and accordingly adjusted for by performing the same cleaning procedure on an untested reference sample.

4.1.4 Impedance measurements

Impedance measurements were performed on anode samples before and after AC testing to characterize properties on the anode surface and possible changes caused by weight loss testing. Note that the measurements provided no information about the influence of AC on the reaction mechanism and surface characteristics, as in-situ measurements were inapplicable. Impedance measurements were of low reproducibility and only the measurements of two anode samples at 10 A m^{-2} is reported. Figure 4-7 shows Nyquist representations of the two anode samples prior to AC experiments. The Nyquist plot of one of the two anode samples after AC testing at 10 A m^{-2} is given in Figure 4-8.

The following main results were obtained from impedance measurements. Activation of the anode surface is evident by a general decrease in the overall impedance after AC testing. The impedance response before and after AC testing resembles in shape. In both cases, the impedance response deviated from that of a simplified Randles cell, indicating that the electrode kinetics of the AlZnIn surface is complicated, possibly involving surface coverage and multiple time-dependent reactions.

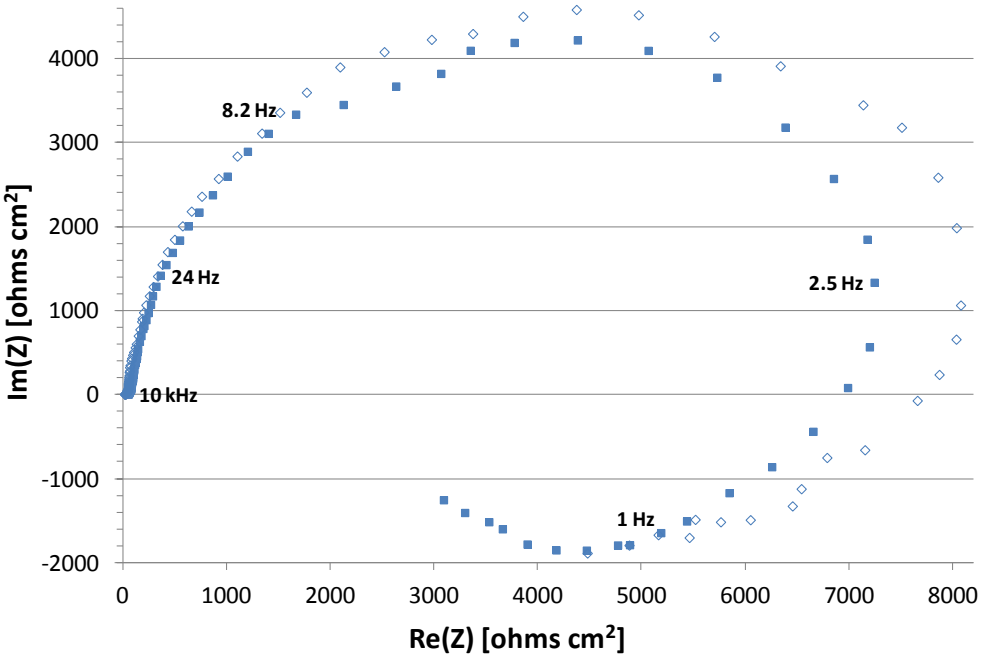

Figure 4-7. Nyquist plot of two anode samples prior to AC testing at i_{AC}=10 A m^{-2}.

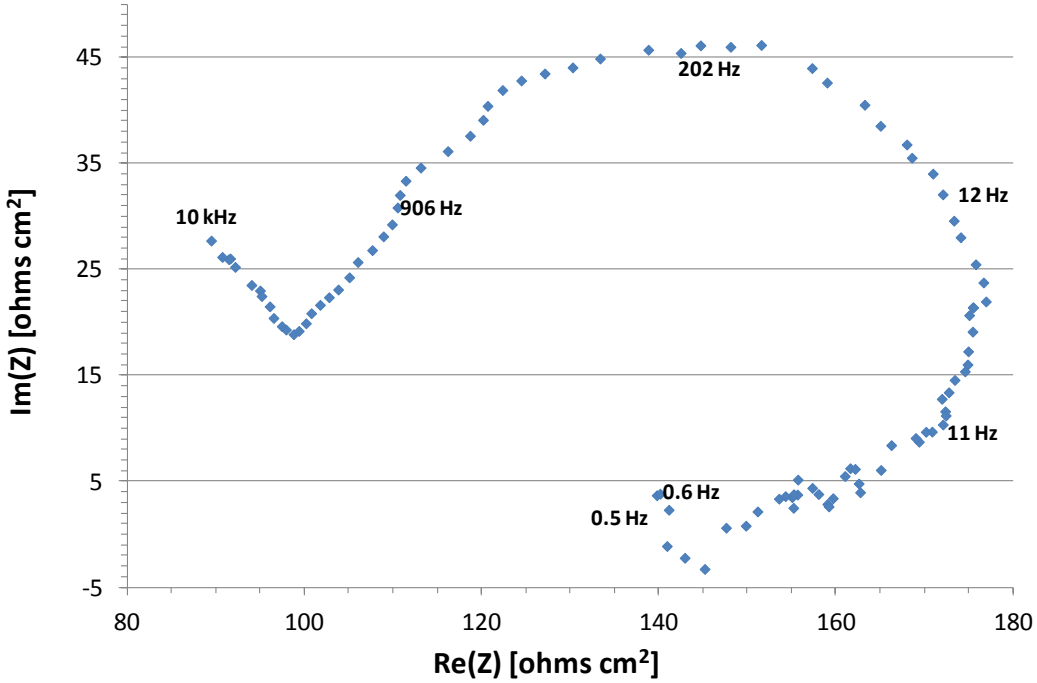

Figure 4-8. Nyquist plot of one anode sample after AC testing at i_{AC}=10 A m^{-2}.

Figure 4-9 shows corresponding bode plots of anode samples obtained before and after AC testing. When considering a frequency of 50 Hz, the phase angle (and overall impedance) was lower after AC testing. It is evident by Figure 4-9 that the decrease was only modest for one anode sample and significant for the other. In accordance with this observation, the ratio

between the imaginary and real impedance, Im(Z)/Re(Z), increased for one anode sample and remained the same for the other anode sample.

Under the assumption that the electrochemical system can be modelled as a simplified Randle circuit (see Figure 2-6), the following results are valid (for the anode sample presented in Figure 4-7 and Figure 4-8). The characteristic frequency of the electrochemical system, estimated by the peak of Im(Z) in the Nyquist plots, increased from $f_{1/RC}$ = 4.5 Hz to $f_{1/RC}$ = 202 Hz by one week of AC testing. Analogous, the polarization resistance R_f of the electrochemical system, estimated by the diameter of the semicircle, decreased around hundred times.

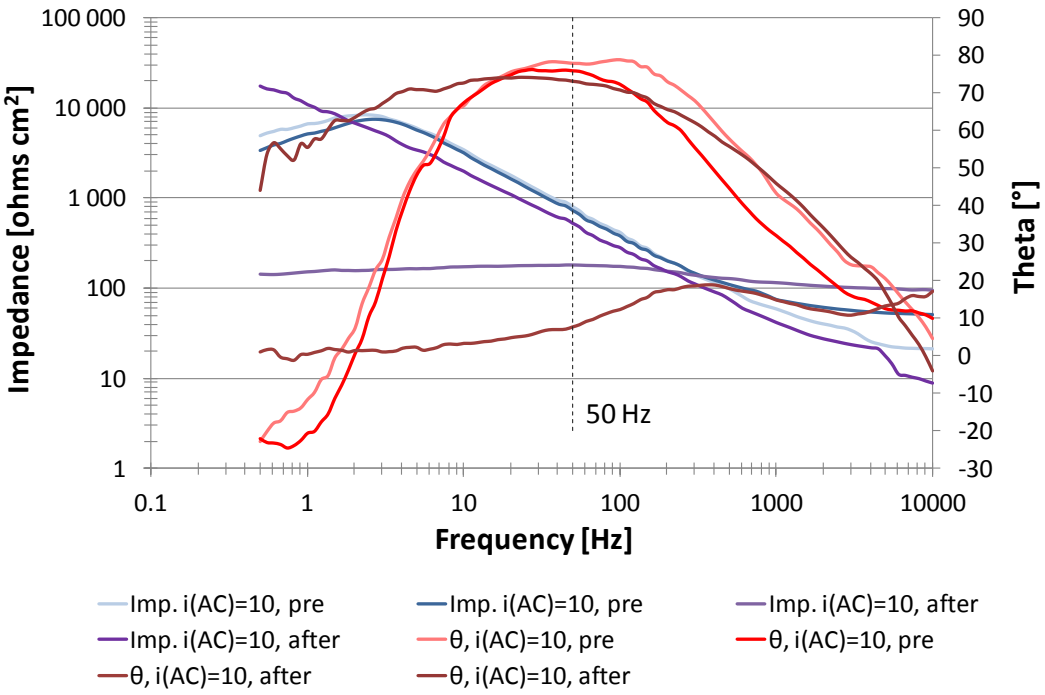

Figure 4-9. Bode plots of the two anode samples, showing the impedance (Imp.) and the phase angle (θ), before and after AC testing at 10 A m^{-2}. Vertical line at a frequency of 50 Hz.

4.1.5 pH measurements

Prior to AC testing, the pH of the synthetic seawater was adjusted to 8.2. In three experiments, a pH measurement was performed after AC testing. It revealed a decrease in pH level (Table 4-1), the decrease being stronger for higher levels of applied AC level.

Table 4-1. pH measurements of test solution after AC testing.

Test config.	i_{AC} [A m^{-2}]	pH
SA/AS	10	6.8
	40	4.6
A/A	55	5.3

4.2 AC corrosion of anodes in a CP system – influence of Area Ratio (AR)

The effect of AC on the corrosion behaviour of sacrificial AlZnIn anodes was further investigated by applying a constant AC potential in an A/S test configuration. Two different area ratios (AR), i.e. 100:1 and 10:1, were used to evaluate its influence on AC corrosion. Experiments are designated by the applied AC level and the set AR. Experiments with an AR of 10 are compared to results from earlier work by the author [2]. The reader is referred to section 3.4.2 for an explanation of the similarities and differences between experiments from the two different projects.

4.2.1 Key parameters

Key parameters, which were logged during testing for every A/S experiment are summarized in Table 4-2 (i.e. AC and DC component of the cell current (i_{AC} and i_{DC}), the mean DC (couple) potential of the anode (V_{DC}) and the average AC potential measured in between the steel and anode sample (V_{AC})). All experiments in this work were performed under constant AC potential, in the potential range of 0.5 to 4.5 V AC RMS. Figure 4-10 - Figure 4-13 shows the general development of the key parameters throughout the entire test period. Note that the time scale in figures is logarithmic and that current parameters relate to the area of one anode sample.

The increased variability in the applied AC potential with increasing levels of applied AC, see Figure 4-10, is in accordance with the variability in AC density in relation to A/A and SA/AS experiments (Figure 4-1), and was experienced regardless type of test circuit and apparatus used. Hence, the variation was related to effects in the electrochemical cell.

Table 4-2. Key parameters for AC testing with an A/S test configuration and two different area ratios (AR).

AR	ID	Avg. V_{AC} [V RMS]	i_{AC} [A m^{-2}]			i_{DC} [A m^{-2}]			Mean
			Start	End	Avg.	Start	End	Avg.	DC pot. [V]
100	0.5	0.5	3.0	0.6	1.4	0.4	0.02	0.06	-1.15
	1.0	1.0	5.0	1.7	2.5	0.6	0.05	0.11	-1.14
	1.5	1.5	12	10	11	1.8	0.15	0.4	-1.13
	2.0	2.0	19	15	17	2.4	0.6	0.9	-1.14
	2.5	2.3	26	19	20	2.9	1.3	1.2	-1.15
	3.5	3.5	37	25	30	3.5	1.1	1.4	-1.14
	4.5	4.6	53	20	38	4.0	0.4	1.2	-1.13
10	1.5	1.5	47	22	33	4.5	0.3	0.7	-1.15
	2.0	2.1	72	39	55	5.8	0.5	3.3	-1.18
	2.5	-	90	54	72	6.0	0.5	2.0	-1.08
	3.0	3.1	144	64	76	20	5.1	6.5	-1.47

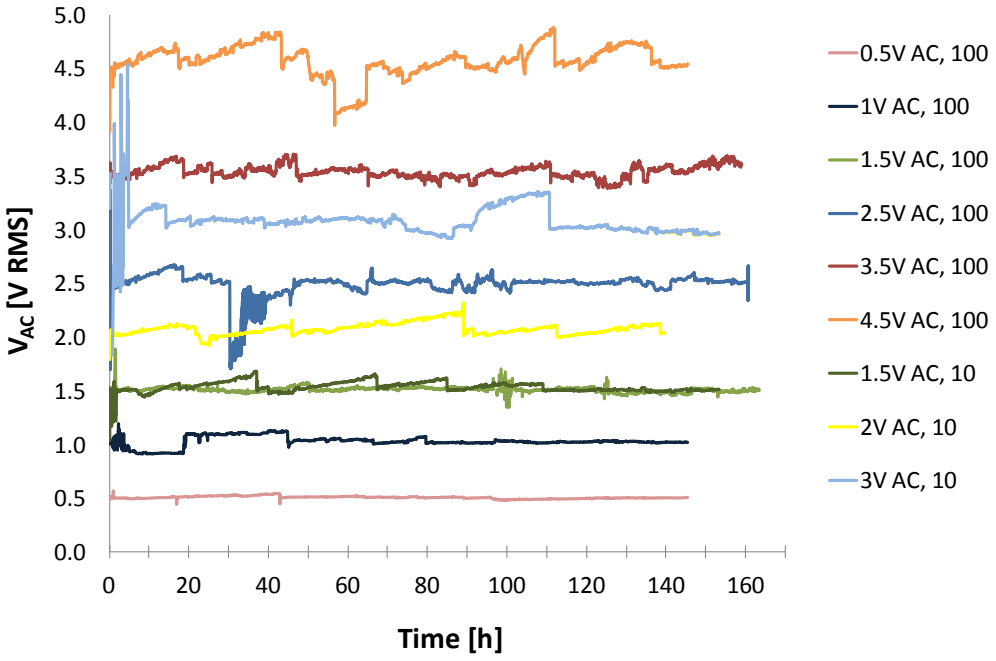

Figure 4-10. Applied AC potential (measured between steel and anode) as a function of time in A/S experiments with area ratio (AR) of 10 or 100.

The mean DC (couple) potential was influenced strongly by application of AC and by the set AR, see Figure 4-11. In accordance with A/A and SA/AS experiments, an immediate negative polarization was observed when AC was applied, the decrease increased with the level of applied AC potential. Whereas the potential remained low in A/A and SA/AS experiments (Figure 4-2 of section 4.1.1), a subsequent positive potential shift followed within 20 hours in all but one of the A/S experiments (Figure 4-11). The couple potential stabilized at a level lower than the DC operation potential of the AlZnIn anode (-1.05 V_{SCE}). To some extent, the time until the positive shift increased with applied AC level and with decreased AR. However, in the experiment with the lowest AR (of 10) and the highest applied AC level (i.e. 3 V AC), the negative polarization remained throughout the entire test period.

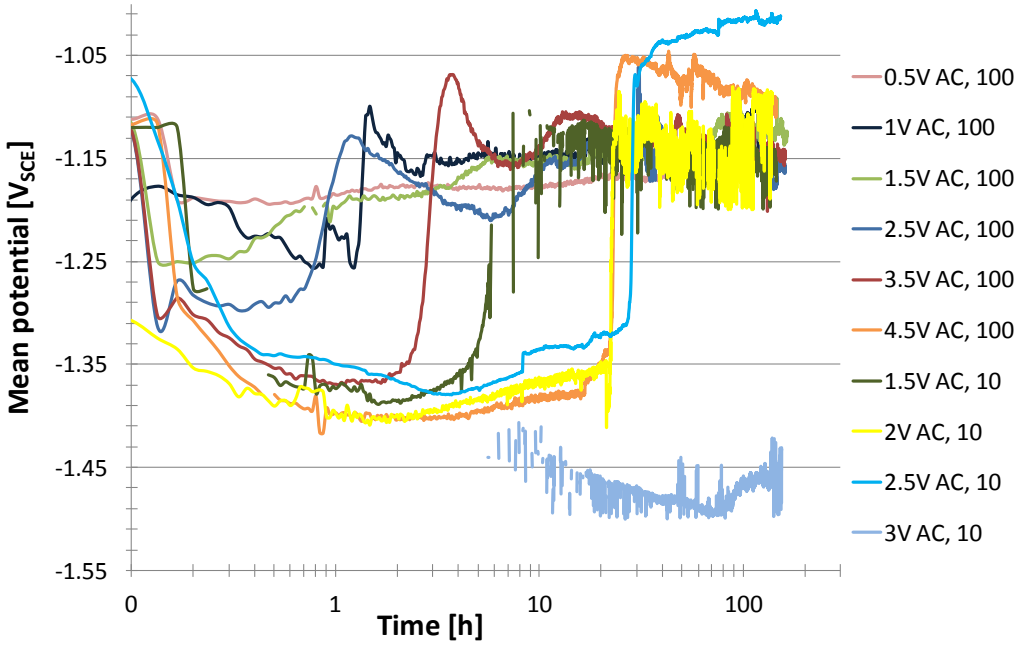

Figure 4-11. Mean DC (couple) potential [V_{SCE}] measured on the anode sample in A/S experiments with area ratio (AR) of 100 and 10 and at various levels of applied AC potential.

Both current density parameters were found to increase clearly with increasing levels of applied AC, see Figure 4-12 and Figure 4-13. Clear differences were observed in experiments with different AR, in accordance with the higher current requirements of a larger steel sample. The increase in both i_{DC} and i_{AC} was of a dramatic character for AC potential ≥ 2V AC. Current parameters from earlier A/S experiments by the author with the same test conditions are directly comparable to the results of this work. The reader is referred to Appendix D for a comparison.

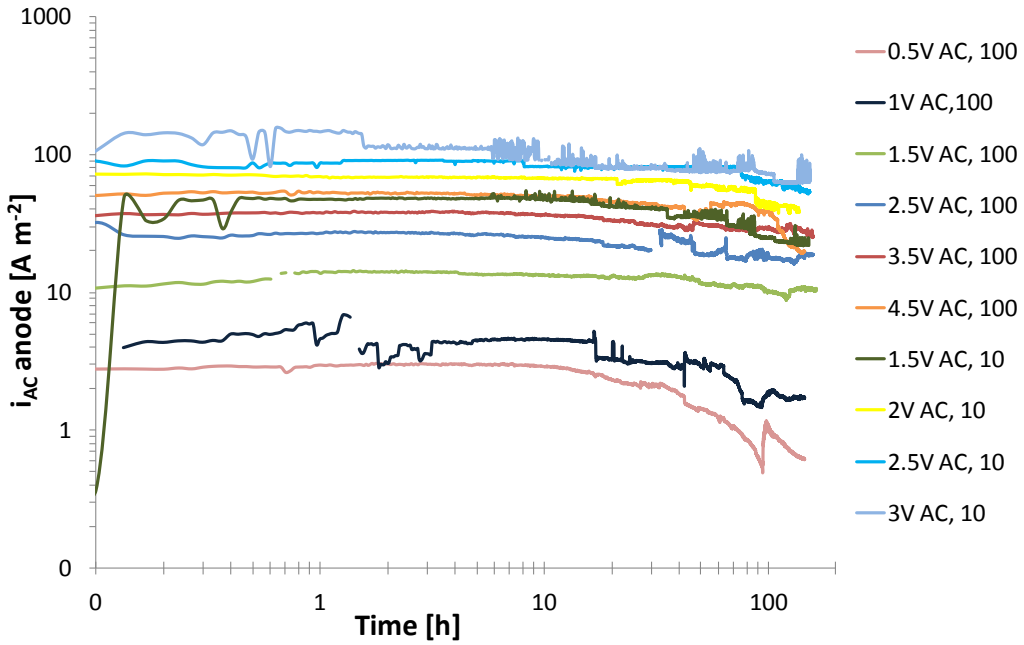

Figure 4-12. AC density for anode specimens in A/S experiments with area ratio (AR) of 100 and 10 and at various applied AC levels.

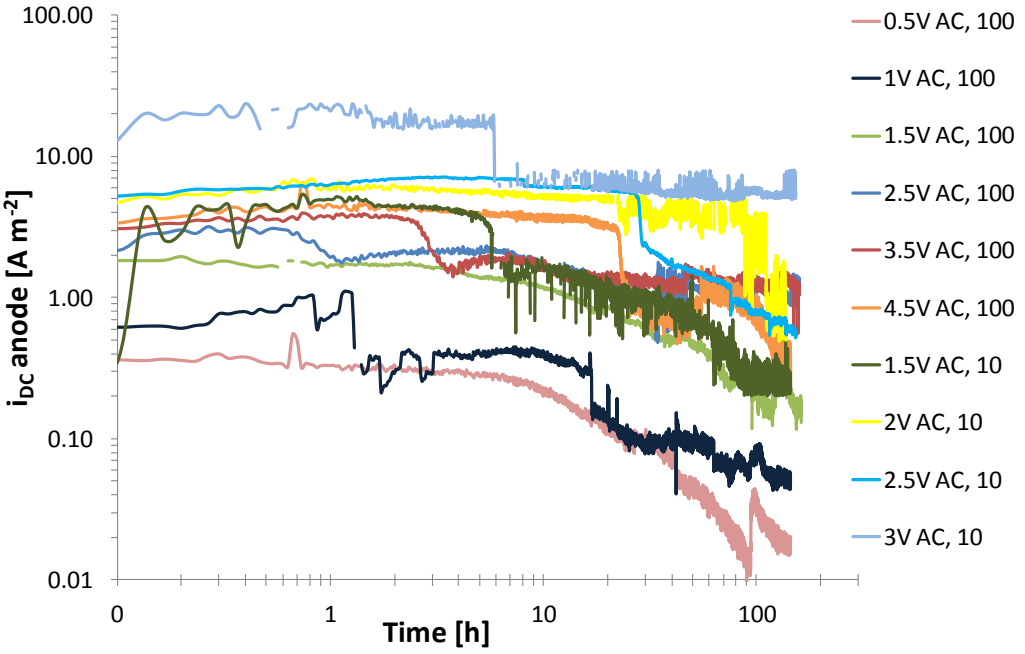

Figure 4-13. DC density for anode specimens in A/S experiments with area ratio (AR) of 100 and 10 and at various applied AC levels.

There was a similar trend in both current densities with time in that both parameters decreased

in a stepwise manner. The relative decrease in the DC density was of a more pronounced character. For experiments with AR of 100 and applied AC level ≤ 1 V AC, i_{DC} decreased and approached a level in accordance with a CP system where no AC voltage was applied (see Figure D. 2 of Appendix D). With regard to earlier experiments where a calcareous scale was allowed to deposit prior to AC testing (by CP under DC conditions), the protection current was lower, see Figure D. 4 for comparison. However, the impact of pre-developed calcareous deposits on CP under influence of AC was only apparent in the initial test period, as i_{DC} values decreased and eventually reached a similar steady-state value with time. In relation to i_{AC} values, no clear difference was found between experiments with and without preconditioning of the steel surface by CP (see Figure D. 3).

4.2.2 Anode corrosion rates

Corrosion amounted to self-corrosion and corrosion resulting from current provided for protection of the steel was estimated by numerical integration. The reader is referred to Appendix A for additional information regarding calculation of corrosion rates. In compliance with the results of A/A and SA/AS experiments (section 4.1.2), the anode corrosion rate increased with applied AC level in A/S experiments, see Figure 4-14.

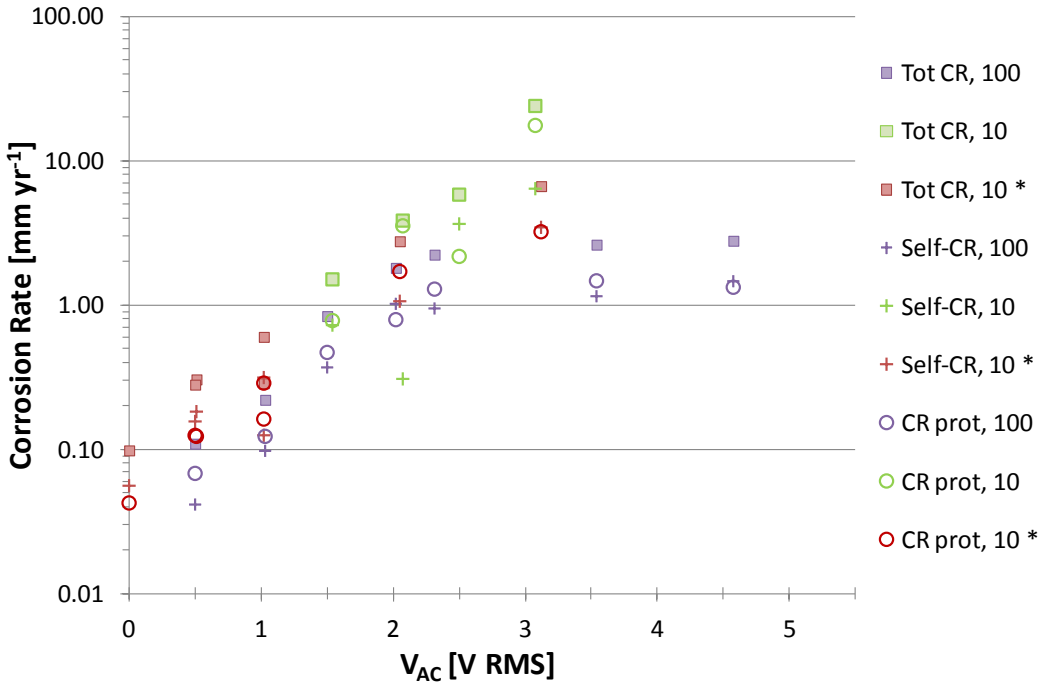

Figure 4-14. AC corrosion rate of anode samples (total, self-corrosion and due to protection) as a function of applied AC potential in A/S experiments, with an area ratio (AR) of 100 and 10. Results designated * from earlier work by the author [2], involved a preconditioning of the steel samples by CP to form calcareous deposits.

Results from earlier work (designated by *), in which a calcareous scale was deposited on steel prior to AC testing by cathodic conditioning under DC, corresponded well with the new test results. A comparison with earlier work, see Figure 4-15 with no logarithmic scale, demonstrated that the calcareous scale on the steel surface had no clear influence on the AC corrosion of the anodes. Note that the extremely high corrosion rate at 3 V AC is omitted in the graph of Figure 4-15.

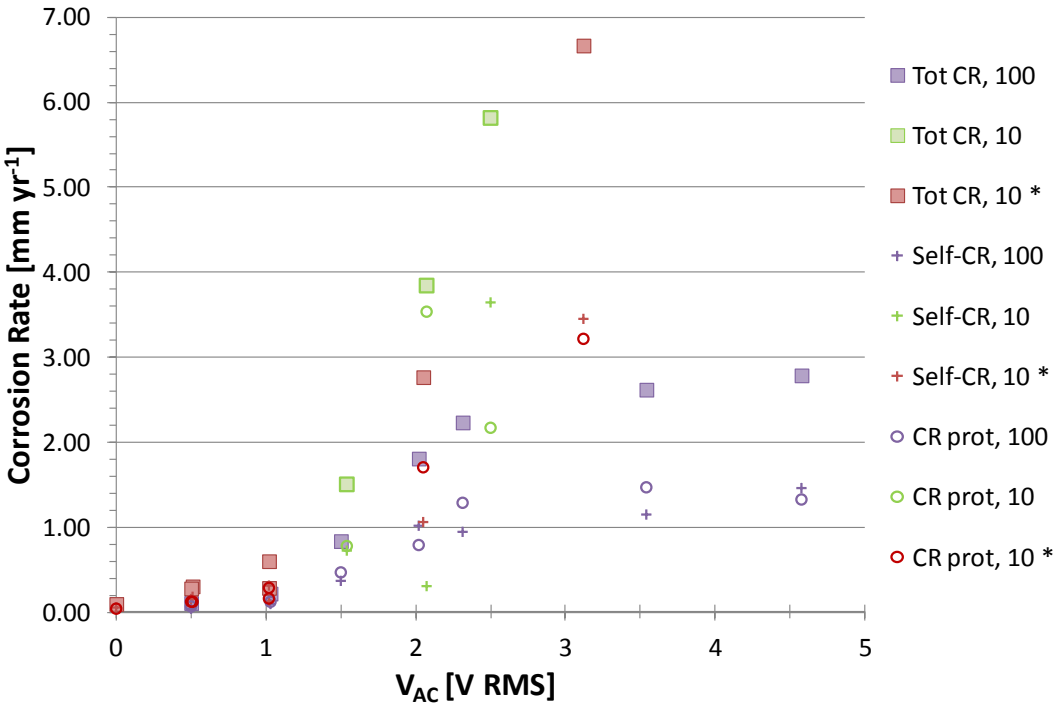

Figure 4-15. AC corrosion rate of anode samples (total, self-corrosion and due to protection) as a function of applied AC potential in A/S experiments, with an area ratio (AR) of 100 and 10. Results designated * from earlier work by the author [2], involved a preconditioning of the steel samples by CP to form calcareous deposits.

Higher anode corrosion rates were observed with a decrease in area ratio, explained by the increased current requirements by a larger steel area. Whereas the increase in corrosion rate with applied AC level was of a modest character, and further limited at high AC levels with an AR of 100, the same increase in corrosion rate showed a dramatic character when the AR was 10, accelerating at applied AC potential > 1 V AC. This was the case for both the anode corrosion rate related to protection of steel and the self-corrosion rate. No clear trend was observed as to whether any of the two types of anode corrosion (i.e. self-corrosion or due to protection of steel) dominated.

4.2.3 Anode efficiency

Application of AC had no clear influence on the resulting anode efficiencies, see Figure 4-16. Except for one experiment at 2 V AC, the anode capacity (and resulting current efficiency) was found to be lower than the acceptance criteria provided by DNV when testing the anode capacity of Al based anodes (i.e. 2500 Ah kg^{-1}) [5]. Note that the test configuration and test procedure in this work is different from the test method specified by DNV to evaluate anode capacity. A direct comparison is therefore infeasible. The reader is referred to Appendix A.4 for relevant equations in relation to calculation of the anode efficiency.

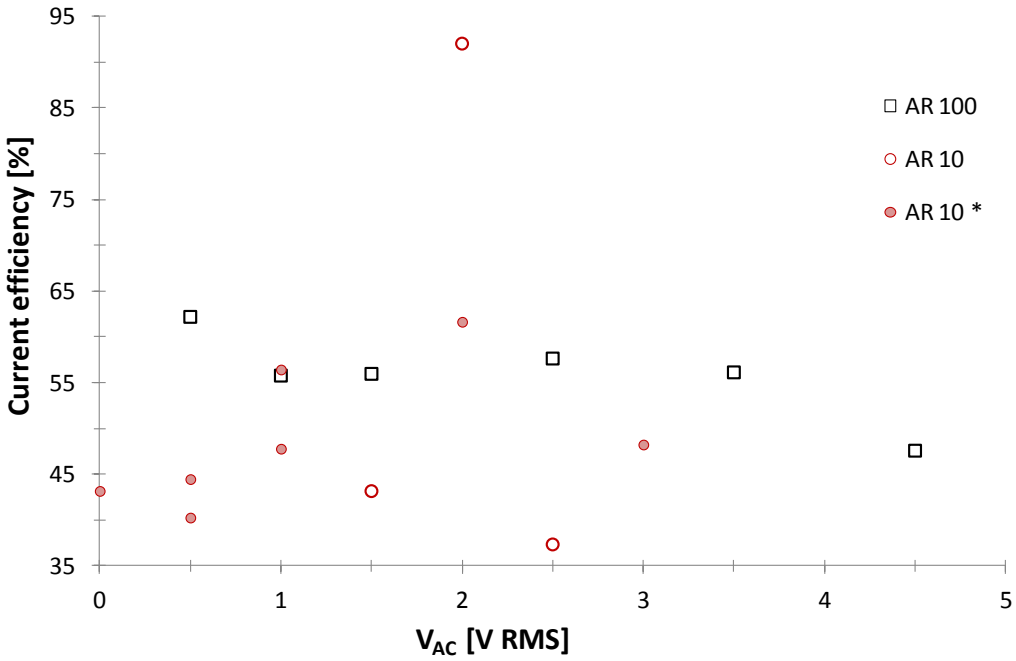

Figure 4-16. Calculated anode efficiency [%] as a function of applied AC potential in A/S experiments at two area ratios (AR). Results designated * are from earlier work by the author[2], and involved preconditioning of the steel by CP to form calcareous deposits.

4.2.4 Reduction reaction on the sacrificial anode

In compliance with increased self-corrosion rates, the charge related to the reduction rate on the anode surface (Q_{red}), was found to increase with applied AC level, see Figure 4-17. However, especially in experiments with lower steel area (i.e. AR of 100), a limitation in the increase of Q_{red} occurred at high AC levels. Relevant equations for calculation of Q_{red} are presented in Appendix A.

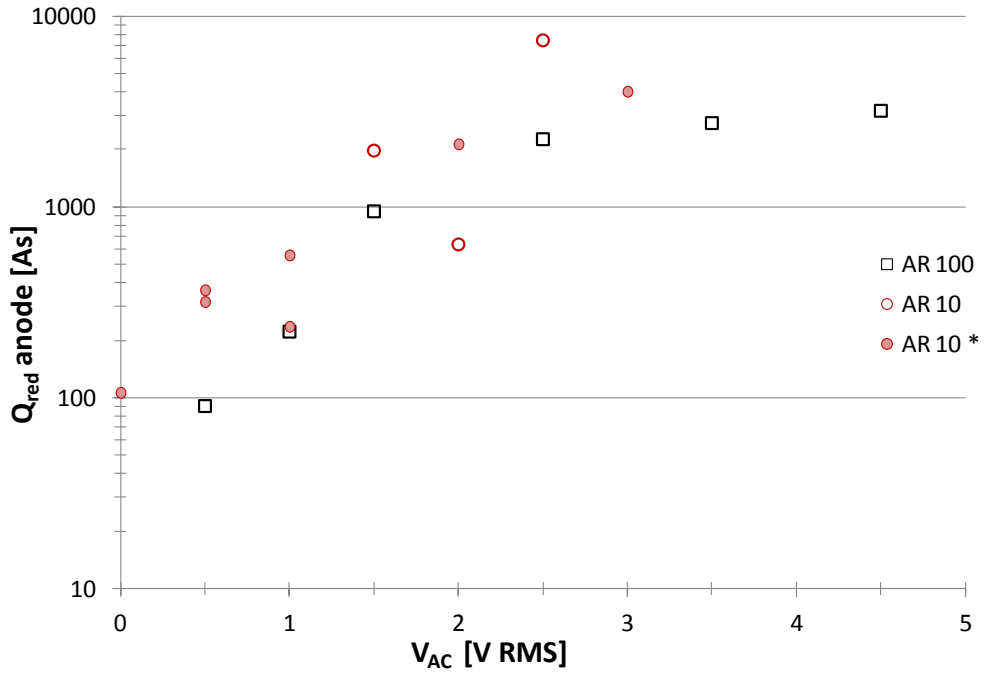

Figure 4-17. Calculated charge related to the reduction reaction on the anode surface (Q_{red}) as a function of the applied AC potential in A/S experiments at two area ratios (AR). Results designated * are from earlier work by the author [2], and involved preconditioning of the steel by CP to form calcareous deposits.

4.3 Signal interference in logging measurements

A new test setup was developed based on the application of National Instruments (NI) logging apparatus and Fluke True-RMS digital multimeters. The development was motivated by logging errors experienced during application of a HP logger in earlier work by the author [2]. However, clear logging errors were experienced during application of the new NI logging device, most likely caused by signal interference from the surroundings. Examples of this are displayed in Figure 4-18, where manual measurements by Fluke multimeters confirmed the logging errors. Application of Fluke 289 True-RMS digital multimeters on the other hand, was successful in that no signal interference and resulting logging errors were experienced using this instrument.

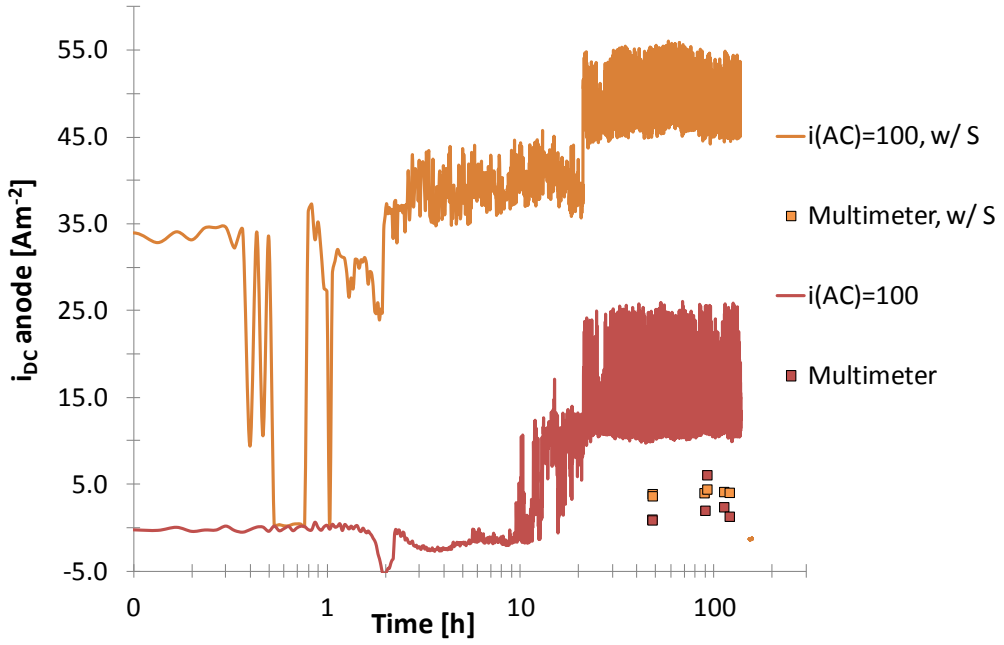

Figure 4-18. Signal interference and resulting errors in logging parameters during application of NI logging device.

4.4 Surface characterization

A surface analysis follows that aimed to clarify the effect application of AC have in a CP system. The analysis involved a macroscopic and microscopic study of both surface deposits and corroded surfaces of steel and anode samples. Test samples at the start and end of the experiments are shown in Figure 4-19. A drastic increase in surface activity was seen when AC was applied (at start), which increased in extent with the applied AC level. Gas evolution was present on both the anode and steel surfaces. At low AC levels, only minor activity was seen at both test samples (Figure 4-19 a). Vigorous gas evolution was observed on both surfaces at the highest applied AC levels (Figure 4-19 e, g) in combination with a test solution that turned cloudy white and in time, formation of extreme amounts of corrosion products (Figure 4-19 d, e, f, h). Corrosion product detached from the test samples during testing at high AC levels, at which the viscosity of the grey test solution increased. In A/A and SA/AS experiments where no temperature control chamber was utilized, the temperature of the test solution was observed to increase at high AC levels. The electrochemical system appeared to stabilize with time (especially at low and intermediate AC levels), shown by a clear decrease in surface activity. No clear differences were observed between A/A and SA/AS experiments.

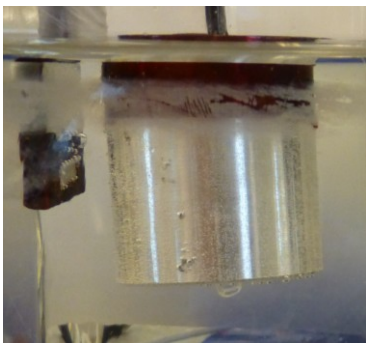

a) i_{AC} = 10, at start

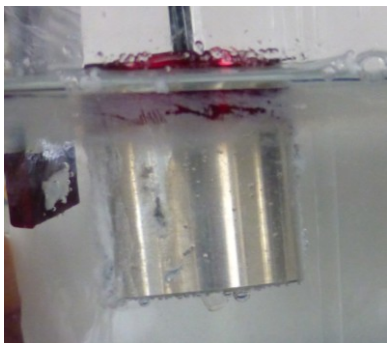

b) i_{AC} = 10, at end

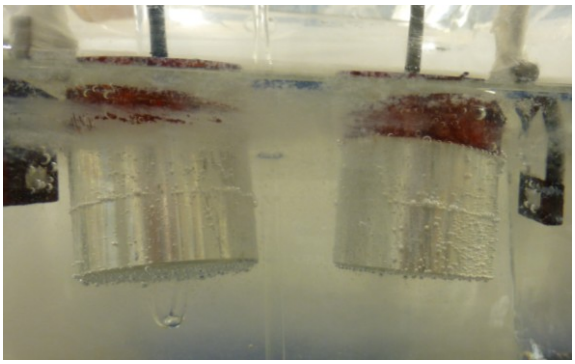

c) i_{AC} = 40, at start

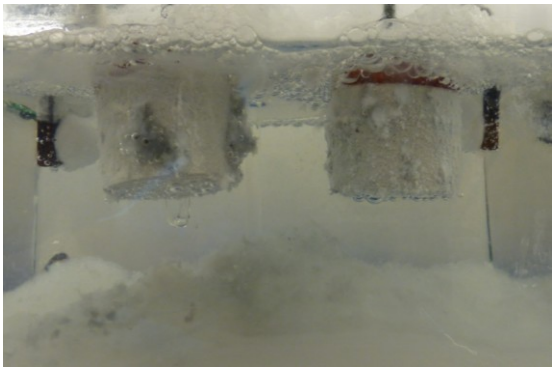

d) i_{AC} = 40, at end

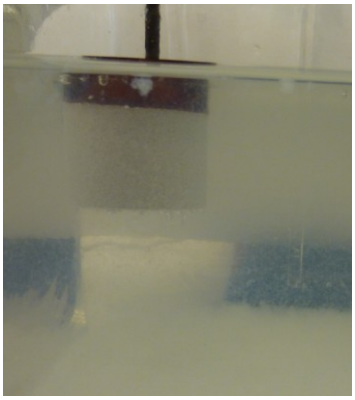

e) i_{AC} = 90, at start

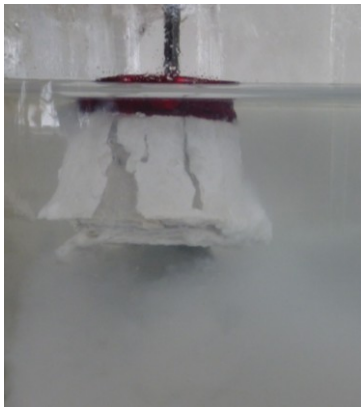

f) i_{AC} = 90, at end

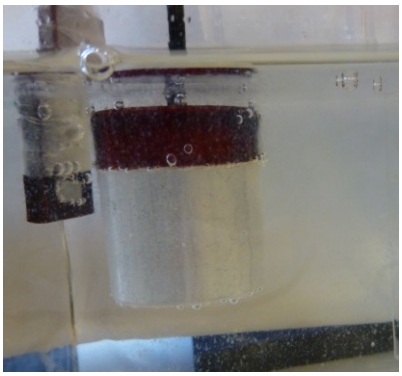

g) i_{AC}= 100, at start

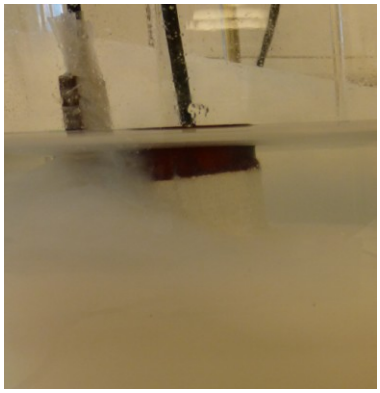

h) i_{AC} = 100, at end

Figure 4-19. Test samples at various applied AC levels [A m^{-2}]. Clear differences observed in surface activity, indicated by gas evolution and appearance of the test solution.

Experimental observations of calcareous deposits were complicated by the appearance of the test solution in experiments at high AC levels (as exemplified in Figure 4-19 h). The thickness of calcareous deposits on steel increased with applied AC levels (Figure 4-19 b,d), but were prevented from being deposited at high AC levels (Figure 4-20), because of vigorous gas development.

4.4.1 Macroscopic characterization of surface deposits

A/A and SA/AS experiments

Macroscopic characterization of surface deposits in A/A, SA/AS experiments revealed the same main result in terms of appearance of corrosion products, and calcareous deposits as for the A/S experiments (see below). In compliance with calculated anode corrosion rates (section 4.1.2), one anode sample (of two) appeared to corrode more in the SA/AS experiments at 10 A m-2 (Figure 4-20 a). Otherwise, no differences in appearance were observed for coupled anode samples or when comparing test samples from A/A and SA/AS experiments. Corrosion products were of a non-uniform character on the originally uniform anode surface, which indicated localized corrosion (Figure 4-20 a).

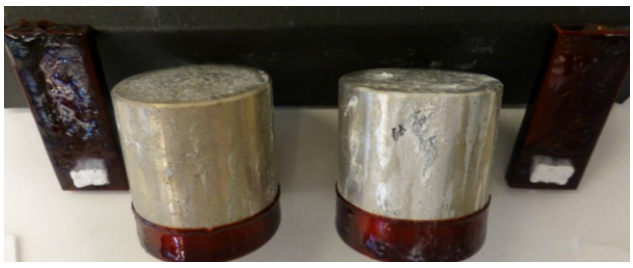

a) i_{AC} = 10

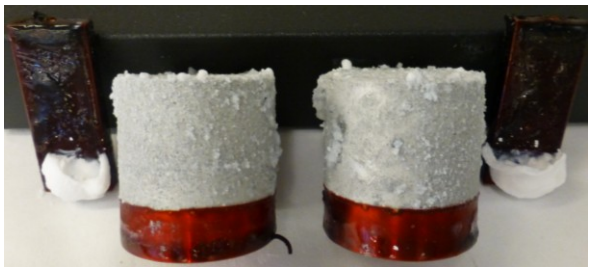

b) i_{AC} = 40

c) i_{AC} = 80

d) i_{AC} = 90 (A/A)

Figure 4-20. Clear variations in surface appearance of anode and steel samples with increasing applied AC levels [A m^{-2}].

The following drastic changes in the appearance of surface deposits occurred in tests with applied AC levels ≥ 80 A m^{-2}. The calcareous deposits were unstable and the bare steel

surface was accordingly exposed to the test solution. In some cases, rust formation was observed (Figure 4-20 c). A dramatic corrosion of anode samples was evident by corrosion products of a flaky character (Figure 4-20 c, d).

In earlier work by the author, adhesion problems were experienced in relation to the painted steel samples [2]. Whereas the steel samples in this work were sufficiently protected at painted areas, blister formation and flare-up of painting was observed on a few anode samples. The reduced paint adhesion was observed to a varying extent in relation to only cylindrical anode samples in experiments with $i_{AC} \geq 55$ A m^{-2} (Figure 4-21). The adhesion of the paint was clearly destroyed because of vigorous gas evolution, causing blister formation.

i_{AC} = 55 A m^{-2} (A/A) i_{AC} = 80 A m^{-2} (A/A) i_{AC} = 80 A m^{-2} (SA/AS)

Figure 4-21. Blister formation and flear-up of painting on anode samples caused by gas evolution in A/A and SA/AS experiments at applied AC levels > 40 A m^{-2}.

A/S experiments

Macroscopic characterization of surface deposits in A/S experiments with an AR of 10 and 100, revealed the following main results. The amount of corrosion products on anode samples and the instability of calcareous deposits on steel samples increased with applied AC level and with decreased AR.

Figure 4-22 shows the appearance of the steel and anode surface after one week of testing at various applied AC levels and two different area ratios (AR). As regards the anode samples, corrosion was evident by the formation of a white layer, believed to be aluminium hydroxide. The layer was of a modest and non-uniform character, increasing in extent and thickness with applied AC potential and with decreased AR. The presence of dark spots (Figure 4-22 e, f) indicated local areas of higher corrosion rates, an observation that was expected due to the many pores initially contained on the anode surface.

In most cases, a complete coverage of calcareous deposits on the steel surfaces was present after testing. At increasing AC levels, the calcareous deposits were seen to go from being

evenly distributed (Figure 4-22 d) to becoming of a non-uniform character (Figure 4-22 a, b, f). At still higher AC levels, the formation of calcareous deposits were erupted and impeded by vigorous gas evolution and the persisting instability of the calcareous deposits was evident by steel surfaces being exposed after testing (Figure 4-22 c, e).

AR 10

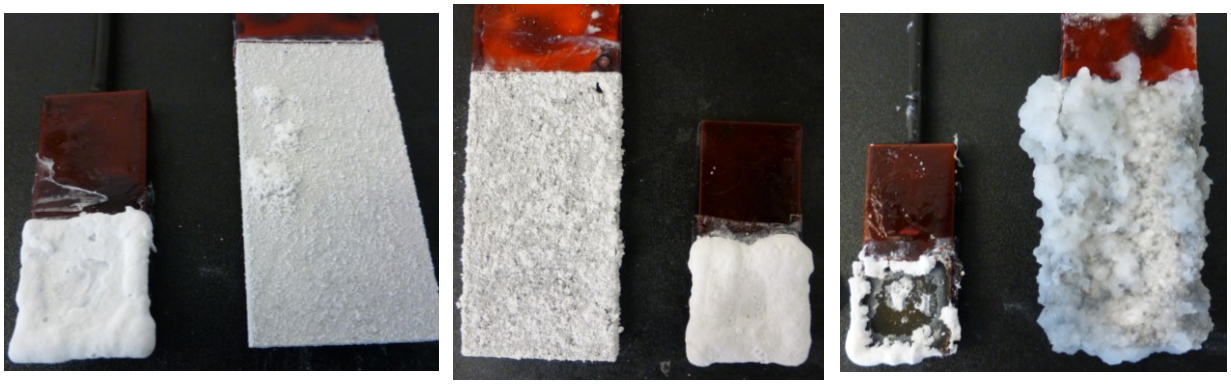

a) 1.5 V AC b) 2 V AC c) 3 V AC

AR 100

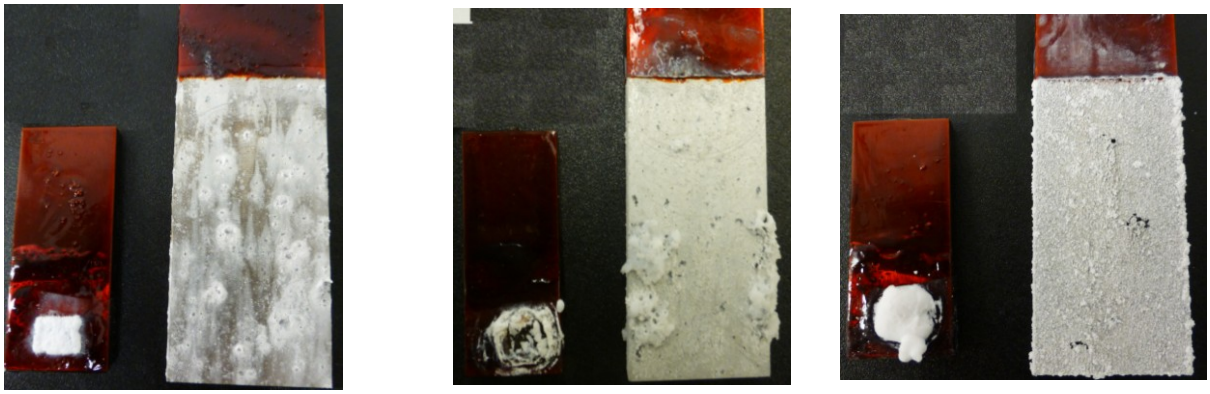

d) 0.5 V AC e) 2.5 V AC f) 4.5 V AC

Figure 4-22. Clear variations in surface appearance of anode (large) and steel sample (small) after one week of testing at various AC levels [V_{AC}]. AR of 10 or 100.

4.4.2 Microscopic characterization of surface deposits by XRD analysis

An XRD analysis was performed in an attempt to identify the composition of the deposits on the steel and anode samples. A presentation of the main results follows. The reader is referred to Appendix C for a comprehensive presentation of X-ray diffractograms.

Analysis of anode samples

XRD analysis of surface deposits removed from tested anode samples revealed a deposit consisting mainly of bayerite ($Al(OH)_3$), but also halite (NaCl) and sodium aluminium chloride oxide ($Na_{0.5}Al_{0.5}ClO_{0.5}$). Additional X-ray diffractograms of the surface deposits are presented in Appendix C. The corrosion product of aluminium is however believed to consist of mainly amorphous aluminium hydroxide (section 2.1.1), which cannot be revealed by XRD analysis. Therefore, an analysis of the corrosion products from each tested anode sample was considered redundant.

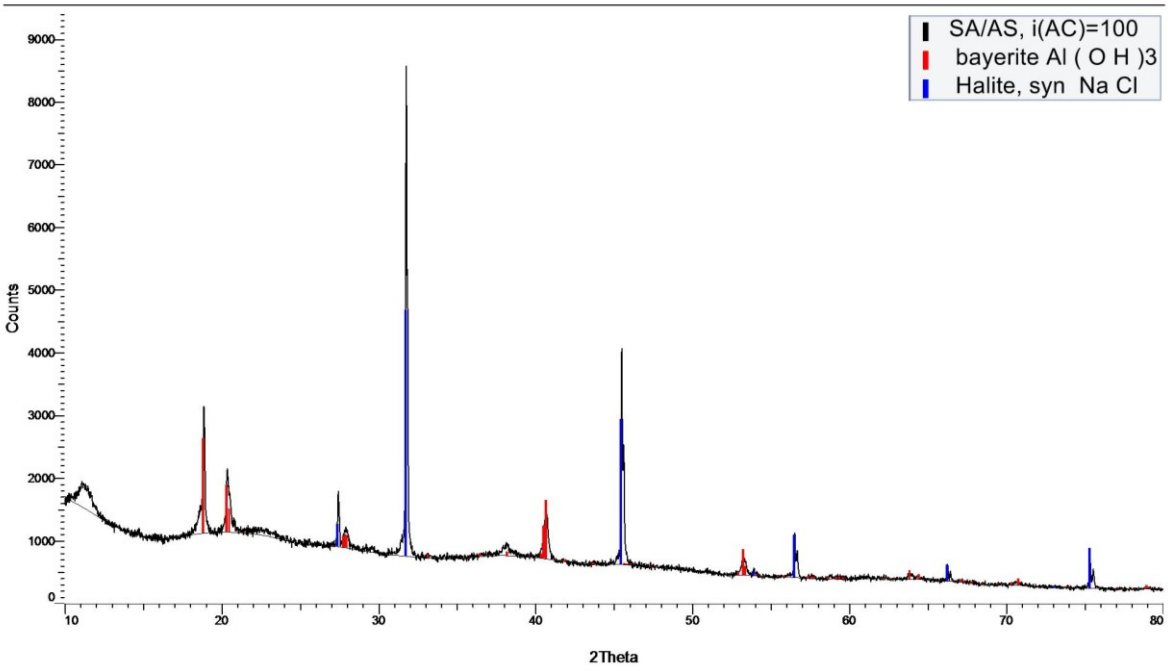

Figure 4-23. X-ray diffractogram of the corrosion product removed from an anode sample tested at i_{AC} = 100 A m^{-2}. Peaks match mainly halite (NaCl), but also bayerite $Al(OH)_3$.

Analysis of steel samples

XRD analysis of calcareous deposits removed from tested steel samples revealed a deposit consisting mainly of $Mg(OH)_2$ (brucite), and also $CaCO_3$ (aragonite), but to a decreasing extent as an increasing AC voltage was applied. The reduced amount of $CaCO_3$ with increased AC level is demonstrated by comparing the X-ray diffractograms in Figure 4-24 and Figure 4-25. The results were in accordance with earlier results by the author [2]. Additional results are given in Appendix C. The analyses also revealed a minor amount of NaCl (halite) and different corrosion products in the surface deposits. In one case, the X-ray diffractogram also indicated a small amount of calcite (polymorph of $CaCO_3$) (Figure C. 9).

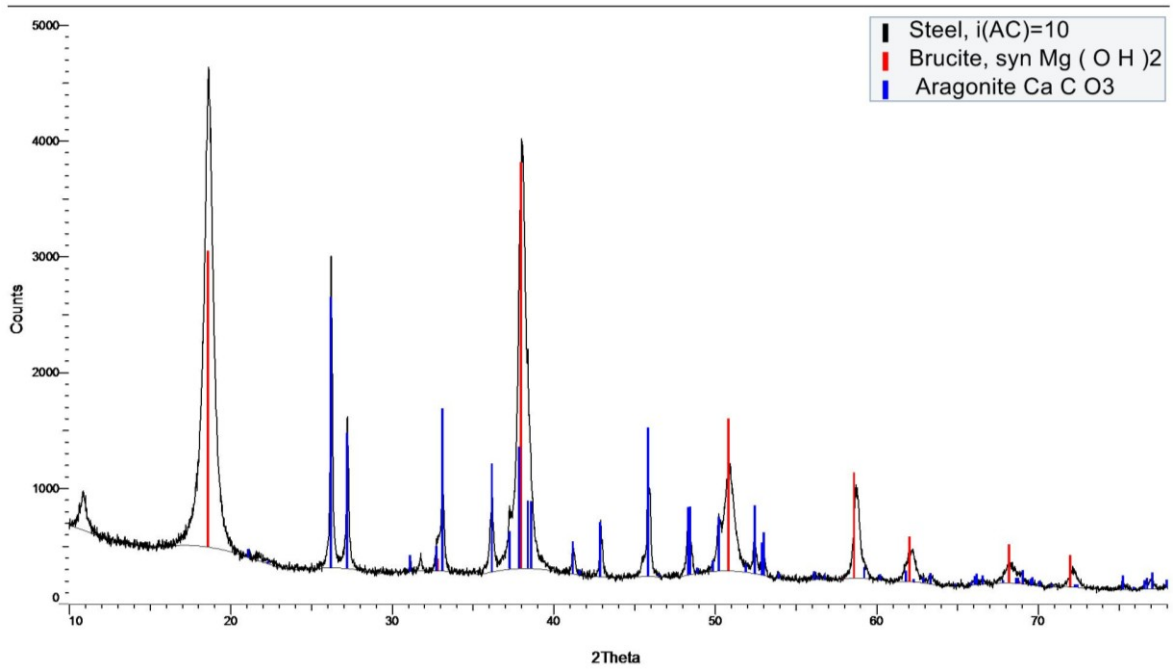

Figure 4-24. X-ray diffractogram of calcareous deposits from a steel sample tested for one week at i_{AC}=10 A m^{-2}. Peaks match the crystal structure of $Mg(OH)_2$ (brucite) and $CaCO_3$ (aragonite).

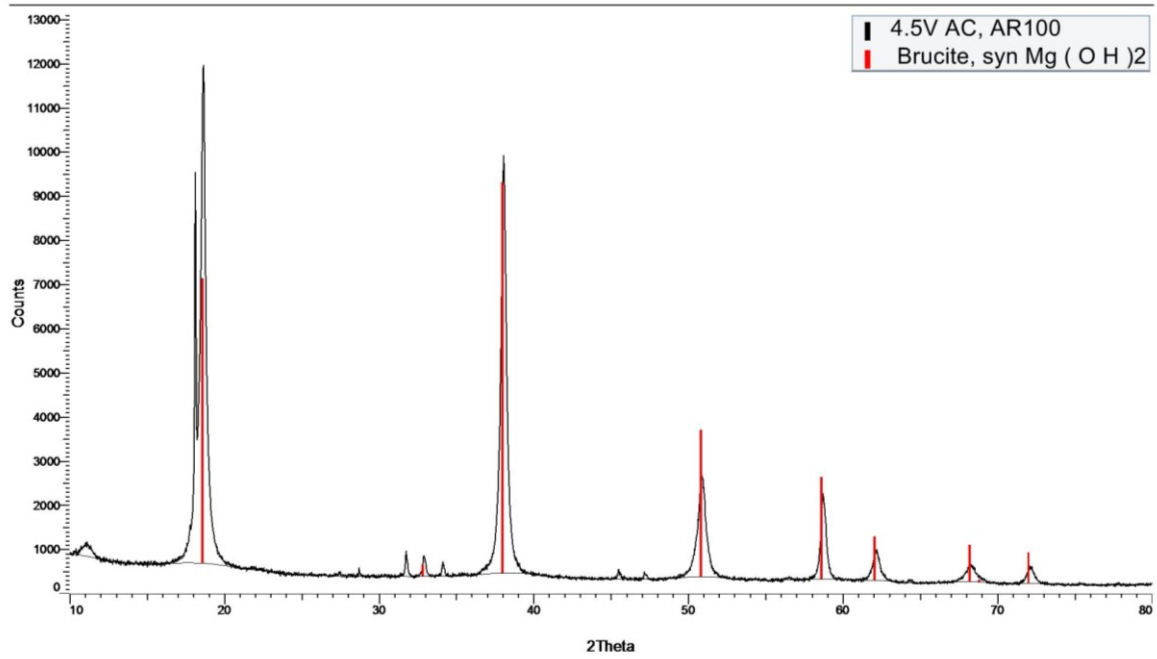

Figure 4-25. X-ray diffractogram of calcareous deposits from a steel sample tested for one week at 4.5 V AC. Peaks match the crystal structure of $Mg(OH)_2$ (brucite).

4.4.3 Macroscopic characterization of corroded surfaces

Test samples were cleaned in accordance with ASTM G1-03 (as described in section 3.4.3) to remove corrosion products. Firstly, an analysis of corroded anode samples is presented and then, an analysis of corroded steel samples is given. No corrosion was detected at the samples' connections to the external circuit (i.e. in the upper end of the samples).

Macroscopic analysis of anode samples

A macroscopic analysis of the anode sample surfaces revealed the following main results. For anodes tested at high AC levels, the corrosion attack was extreme. The side of the sample facing the sample it was connected to was in all cases seen to be corroded to a higher degree than the remaining surface.

The appearance of the anode surfaces after A/S experiments and chemical cleaning is shown in Figure 4-26. In general, a clear increase was seen in corrosion with increasing levels of applied AC potential. Anode samples coupled to steel with an AR of 10 clearly corroded more than corresponding anode samples tested at the same AC level, but with an AR of 100. Note that surface pores are believed to be favourable sites for corrosion, and the initial presence of these in the rectangular anode samples complicated the evaluation of corrosion characteristics based on a surface analysis.

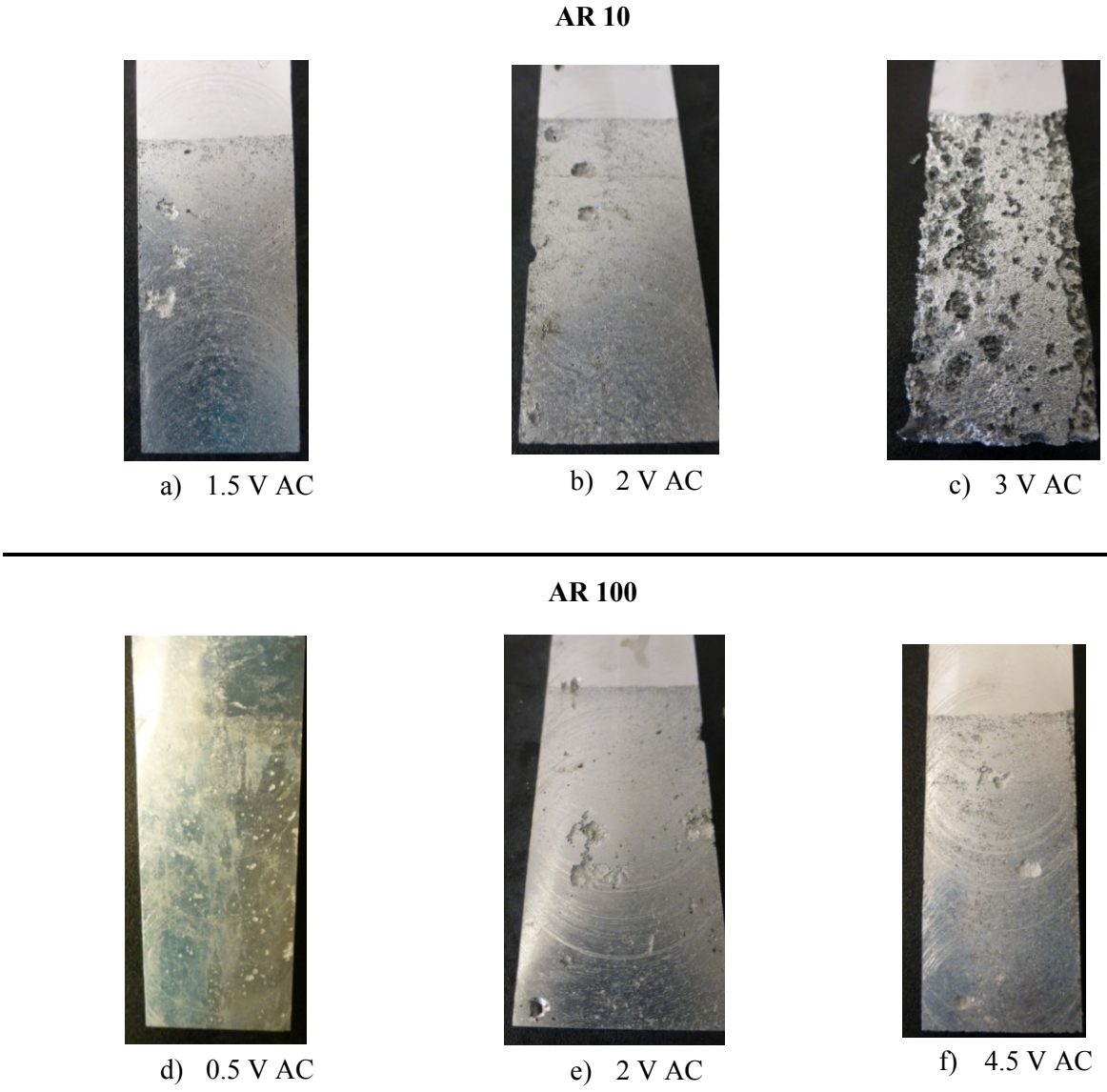

Figure 4-26. Clear variations in surface attack of anode after AC testing at various AC levels [V_{AC}] with area ratio (AR) of 10 and 100 in A/S experiments.

The surface appearance of cylindrical anode samples from SA/AS and A/A experiments after chemical cleaning is shown in Figure 4-27. When considering tests at the same AC level, no clear differences were observed between anodes from A/A and SA/AS experiments, i.e. no clear influence on appearance of the anodes was observed by connection to steel. The corroded surfaces were characterized by unevenly distributed attack. Pit formation increased in extent, size and further coalesced at high AC levels. Poor adhesion of the stop-off lacquer to the anode sample, resulting in formation of blisters and corrosion products underneath the stop-off lacquer, was in some cases seen after testing at high AC levels (Figure 4-21). Successive cleaning of these anode samples revealed corrosion by the naked eye in the interface between painted and exposed area (Figure 4-27 c, f).

SA/AS experiments

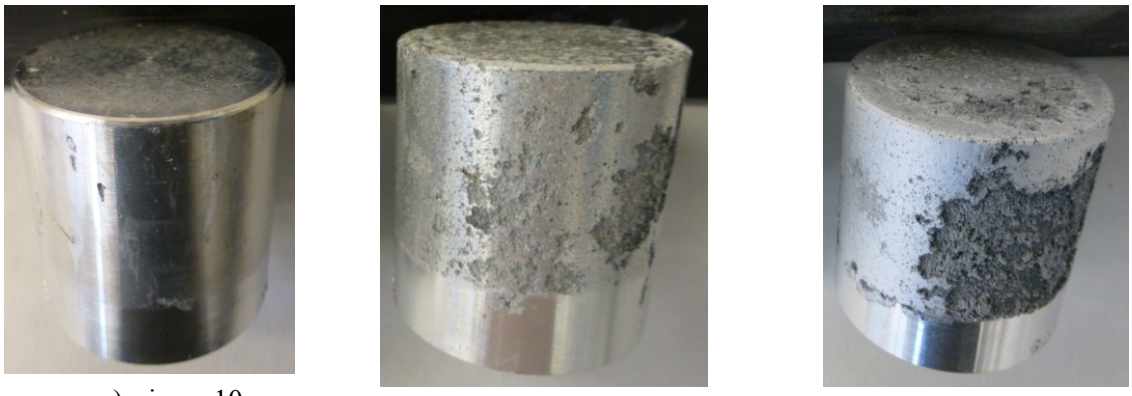

a) i_{AC} = 10 b) i_{AC} = 40 c) i_{AC} = 100

A/A experiments

d) i_{AC} = 10 e) i_{AC} = 40 f) i_{AC} = 100

Figure 4-27. Clear variations in surface attack of anode samples after one week of AC testing at various AC levels [A m^{-2}] in SA/AS and A/A experiments.

Macroscopic analysis of steel samples

Most steel samples appeared unaffected by AC testing, but for testing at the highest AC levels, rust formation indicated corrosion of steel samples to a minor degree (Figure 4-20 c). Successive chemical cleaning of three steel samples revealed clearly corroded steel surfaces (Figure 4-28). The corrosion attack was however of a superficial character.

a) b)

Figure 4-28. Corrosion of steel samples after testing for one week at a) 80 A m^{-2} and b) 100 A m^{-2}.

4.4.4 Microscopic characterization of corroded surfaces by SEM analysis

Analysis of anode samples

Figure 4-29 shows SEM pictures of anode samples after testing and chemical cleaning.

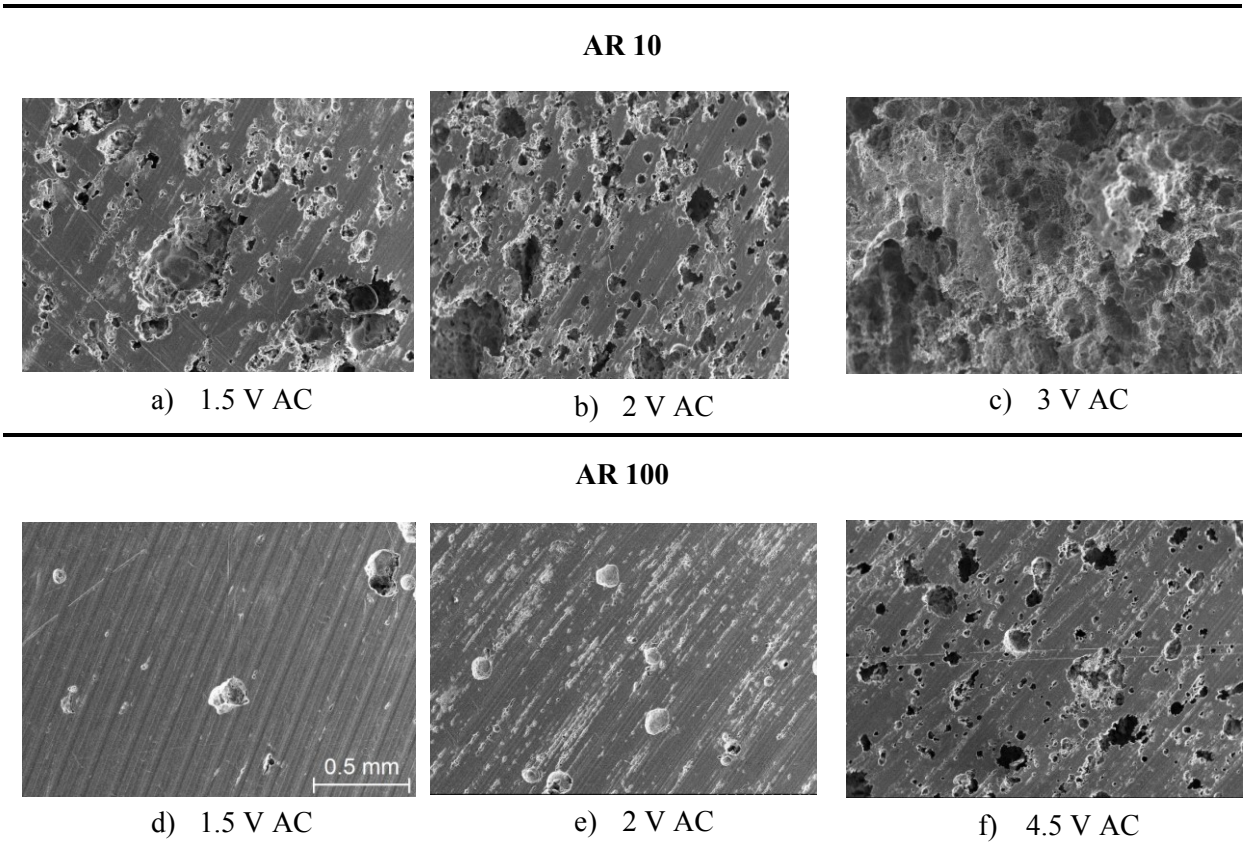

Figure 4-29. SEM pictures of anode samples after A/S experiments at two area ratios (AR) and at various AC levels. Identical magnification in all pictures as displayed in d).

Images are displayed with identical magnification (as designated in Figure 4-29 d). A clear increase was seen in the extent of corrosion on the anode surfaces with applied AC level and with decreased AR. Note that the rectangular anode samples contained pores prior to testing. Pits increased in quantity, size and depth with applied AC level. At higher levels of applied AC, corrosion of the anode in experiments with AR of 10 was extreme.

The appearance of attack and the overall surface morphology after testing is not believed to be related to the original surface morphology, as the surface appearance of rectangular and cylindrical samples observed by a macroscopic characterization (section 4.4.3) were similar. Contrary to the rectangular anode samples, cylindrical samples were free of pores prior to AC testing (Figure 3-1). A SEM analysis of cylindrical anode samples was for this reason considered redundant.

Analysis of steel samples

The majority of tested steel samples appeared to be protected by sacrificial anodes, and a SEM analysis of every steel sample was thus considered redundant. Figure 4-30 shows an example of the smooth surface of an unaffected steel sample where surface grooves from grinding are apparent. In comparison, SEM pictures of two steel samples that was corroded after testing are shown in Figure 4-31, at two different magnifications. The SEM analysis revealed a dimpled surface and possibly the presence of surface deposits.

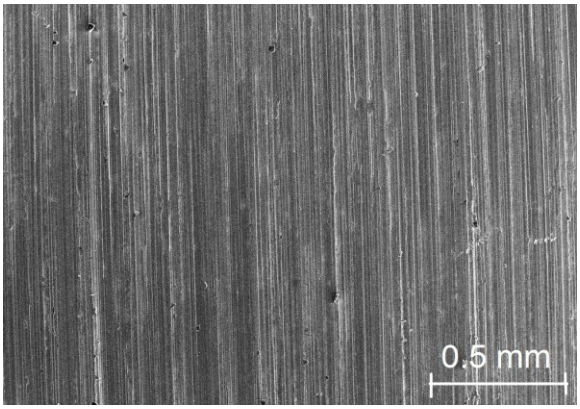

Figure 4-30. Unaffected steel surface with clear surface grooves from grinding.

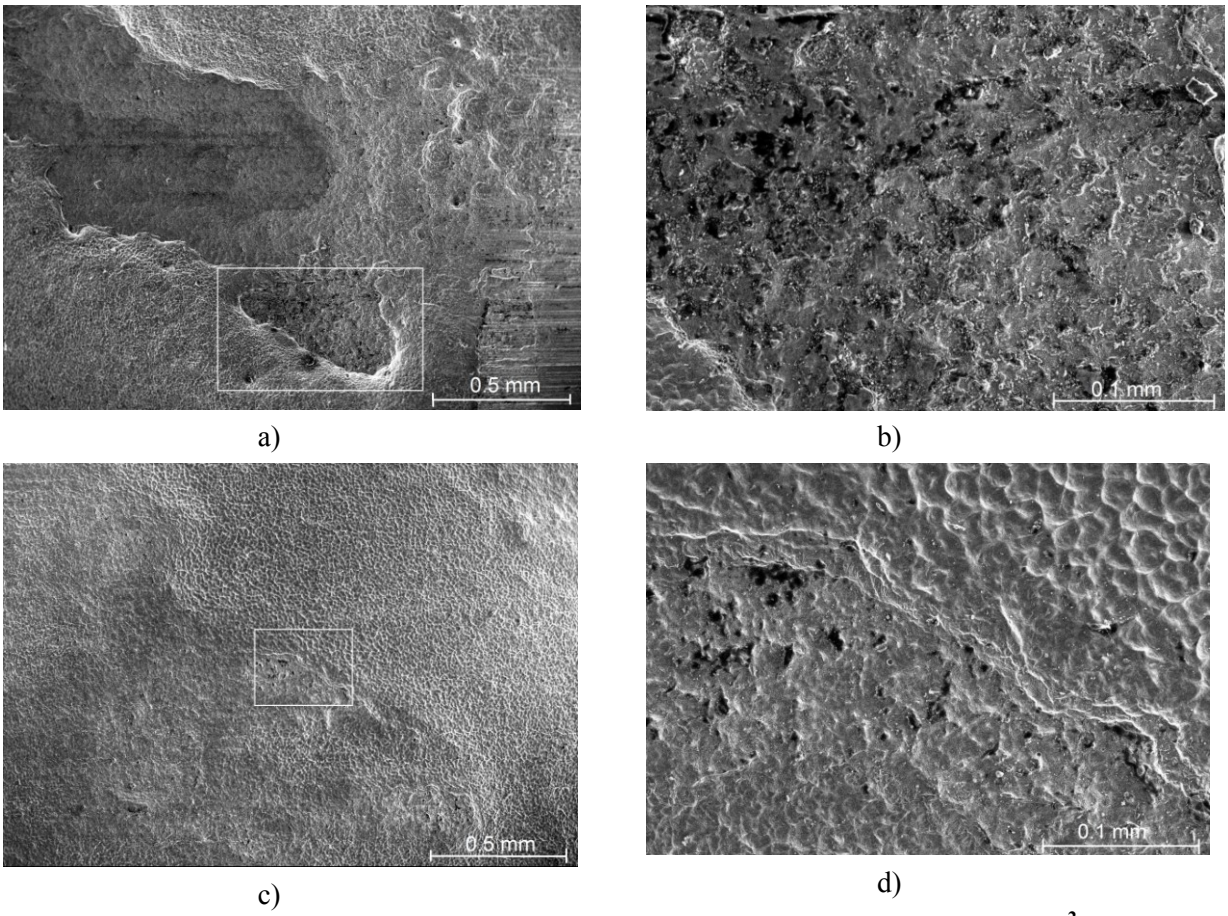

Figure 4-31. SEM pictures of two corroded steel samples tested at i_{AC} = 80 A m^{-2}. Magnification of marked area in a) and c) are shown in b) and d), respectively.

4.5 Summary of results

A summary of the most important results from the experimental work is given. The corrosion of anodes under influence by AC, resulting from both current provided for protection of steel and self-corrosion was significant and increased with applied AC level, and this challenges the lifetime of the sacrificial anodes. However, AC corrosion of anodes was limited at high AC levels. Connection to steel had no clear influence on the anode corrosion rates in SA/AS experiments. In A/S experiments, the influence of connection to steel was dependent on the area ratio. At a lower AR (of 10) anode corrosion rates were extreme at high AC levels, while an area ratio of 100 resulted in the same limitation in anode corrosion rates at high AC levels, as observed in SA/AS and A/A experiments. In comparison with earlier experiments, preconditioning of the steel surface by CP to allow formation of calcareous deposits appeared to have no clear influence on AC corrosion of the AlZnIn anodes. Although the initial

protection current was lower in the experiments involving preconditioning of the steel, this difference decreased in time.

Both the AC and DC components of the cell current (i_{AC} and i_{DC}) increased with applied AC and decreased in a stepwise manner as a function of time. At low levels of applied AC [V_{AC}], i_{DC} stabilized and approached levels similar to the case where no AC voltage was applied. Once AC was applied, an immediate negative polarization of the mean DC (couple) potential was observed. A subsequent positive polarization within 20 hours to a level slightly lower than the DC operation potential of the AlZnIn anode was observed in A/S experiments and the time until the given positive shift increased with applied AC level and decreased AR. No such potential increase was recorded for tests involving anode pairs (i.e. A/A and SA/AS experiments) and the mean potential of the anodes thus remained low. Under removal of applied AC, a further (and significant) negative polarization was observed in experiments involving only an anode pair, at applied AC levels > 40 A m^{-2}. The pH of the test solution decreased during AC testing.

The results of the surface analysis of corroded surfaces conformed well to the increase in anode corrosion rate with applied AC level and decreased area ratio. Whereas corrosion of the steel samples was of little significance, corrosion of the anode samples was clear by the naked eye, characterized by formation of pits, and coalescence of these at high levels of applied AC. Connection to steel during AC testing appeared to have no influence on the appearance of corroded anode surfaces. Corrosion products formed on the anode samples, and the amount increased with applied AC level. Vigorous gas evolution was seen to occur increasingly with applied AC level at all electrode surfaces. A persisting instability of the calcareous deposits on the steel surfaces was observed at the highest applied AC levels. XRD analyses revealed calcareous deposits on the steel surfaces consisting mainly of brucite ($Mg(OH)_2$) and in addition, aragonite ($CaCO_3$), which decreased in content as the applied AC level was increased. Analogous analyses of surface deposits in relation to anode samples revealed surface deposits consisting mainly of bayerite ($Al(OH)_3$), halite (NaCl) and sodium aluminium chloride oxide ($Na_{0.5}Al_{0.5}ClO_{0.5}$). No calcareous deposits were detected on any of the anode surfaces, and the surface deposits are further believed to consist of mainly amorphous $Al(OH)_3$.

Clear logging errors were after a while experienced in relation to application of the new NI logging device. Fluke 289 True-RMS digital multimeters were utilized with success.

5 Discussion

This section contains a discussion of the results and experimental work. Aspects are discussed in an order that reflects its importance in relation to the project aim and results. Focus is put on the AC influenced changes in anode corrosion rates and the influence of connection to steel and resultant area ratio (AR) for AC corrosion of AlZnIn anodes. This section also contains a discussion of logging equipment and methodology.

5.1 AC corrosion of anodes

One of the most important results from this project is the very high anode corrosion rates found at increasing AC level. This result is valid in all experiments, and also in accordance with earlier work by the author [2] and theory of electrochemical impedance [46, 49, 51]. The latter explains the generation of a pure DC part during application of AC by the non-linear nature of an electrochemical cell (section 2.3). In earlier work, proportionality was found between the amplitude of the applied AC squared (ΔV_{AC}^2) and the found anode corrosion rates [2], in compliance with the deduction (2.17) provided by Orazem and Tribollet [46]. Even though a similar increase in anode corrosion rates was obtained in this work, the results do not comply with the proportionality. In accordance with the critical current density of 20 A m^{-2} presented by Drugli and Steinsmo [63], (above which AC corrosion introduced a challenge for the lifetime of sacrificial anodes), the self-corrosion of AlZnIn anodes was found to be significant at AC levels $\geq$ 30 A m^{-2}. The results from the study of AC influenced corrosion of carbon steel and sacrificial anodes by Drugli, Steinsmo and Bjordal [62, 63, 67] are in general comparable to the results from the experimental work and results in this thesis. The authors reported of no weight loss of cathodically protected carbon steel, but increased anode corrosion rates under influence of AC (section 2.5). Conversely, the results of this project are in general *not* in accordance with analogous work by Torstensen [69]. For tests that appear to be identical to the A/S experiments in this thesis, the former master student found no clear increase in either anode or steel corrosion rates with applied AC and the reported corrosion rates were in general significantly lower.

An understanding of AC corrosion of sacrificial AlZnIn anodes remains yet to be established. In relation to this aspect, it was of interest to investigate the possible influence by steel on corrosion of anodes when AC is applied to a CP system. From the results of Figure 4-6, it appears that connection to steel have no clear influence on AC corrosion of connected AlZnIn anodes (with AR of 100). In other words, the protection current requirements from

surrounding steel structures appear to have no impact on AC corrosion of AlZnIn anodes, which implies that current transfer between anodes dominates and the system in reality acts as an anode-anode galvanic couple. However, further testing is required in order to conclude, especially considering the fact that connection to steel clearly affects the polarization of the system during application of AC. The reader is referred to section 5.3 for a discussion of these aspects.

It was of interest to evaluate whether the anode-steel area ratio (AR) has an influence on corrosion behaviour under application of AC. Weight loss measurements in A/S experiments where a constant AC potential was applied, revealed a clear influence of AR on corrosion of AlZnIn anodes (Figure 4-14). In contrast to tests with an AR of 10 where the corrosion rate increased dramatically at high levels of AC, the increase in anode corrosion rate with applied AC level was modest and reached a steady value in experiments with an AR of 100 (shown clearly in Figure 4-15). The latter limitation in increased anode corrosion at high AC levels complies with the findings presented in Figure 4-6 from A/A and SA/AS experiments. Here, the increase in anode consumption is not only observed to cease at high levels, but also to reach a maximum at i_{AC} = 80-90 A m^{-2}, followed by a decrease in corrosion rate at even higher AC levels. Even though no such cease in anode corrosion rate is obtained in experiments of larger steel area (i.e. AR of 10), it cannot be excluded that such an effect will take place at AC levels still higher than the applied test range of this project [i.e. $V_{AC} > 4.5$ V AC RMS].

The limitation in increase of anode weight loss at high AC levels when the steel area is small (AR of 100) or not present at all is thought to be due to poor ability of the anode surface to act as a cathode. Two explanations for the observed limitation in anode consumption at high AC levels (Figure 4-6 and Figure 4-14) are proposed. Firstly, a vigorous gas evolution was observed at all electrode surfaces under application of high AC levels. In consequence, a "hydrogen blanket" can possibly form at the surfaces, restricting a further increase in reaction rates. Secondly, an ohmic resistance is introduced by the formation of a porous hydroxide layer on the anode surface where hydrogen further can become trapped in the pores of the hydroxide film. This introduces an additional restriction in reaction rates. It is worth mentioning that, according to Orazem and Tribollet [46], a non-negligible ohmic resistance reduces the faradaic current and thus the distortion in the current response under influence of AC (2.19). In other words, an ohmic resistance can restrict the corrosion of the AlZnIn anode. An alternative explanation to the limitation in weight loss increase relates to the role of alloying elements in AlZnIn anodes. Indium is enriched at the anode surface and thus activates the surface, but function at the same time poorly as a cathodic site (section 2.1.2). The resulting increase in anodic dissolution due to surface activation, but at the same time restriction in water/oxygen reduction may contribute to a restriction in further increase of

anode corrosion rates at high levels of AC. The alloying element zinc is also associated with an inhibition of hydrogen evolution (section 2.1.2). However, it is not known whether zinc is preferentially dissolved during the corrosion process or is enriched at the surface, as indium is.

Conversely, when the exposed steel area is larger (i.e. AR of 10), it naturally causes higher current requirements for protection (Figure 4-13) resulting in higher anode corrosion rates (Figure 4-14 and Figure 4-15). In addition, the ability of steel to act as a cathode can possibly promote further anode activation by indium enrichment, thereby resulting in increased anode self-corrosion rates. In this regard, the calculated current efficiency, which is an important parameter in CP design, were found to be low in all cases but one, and generally lower for the anodes coupled to steel of larger area (i.e. AR of 10), as seen in Figure 4-16. However, the important result of calculation of anode efficiencies is the observation that application of AC has no clear effect on this parameter. Note that the calculation of anode efficiencies is not believed to be representative to the actual performance of the anodes due to a relatively short test period and a test procedure different from that specified by DNV for testing anode capacity [5]. Nevertheless, the results pose a challenge to the use of anode capacity specifications in designing CP system where an AC voltage is applied.

5.1.1 Role of calcareous deposits on anode consumption

Understanding how calcareous deposits on steel affect the AC corrosion of sacrificial AlZnIn anodes is important to manage DEH applied to subsea pipelines under CP in seawater. In earlier work by the author [2] and by Lilleby [3], eruption of calcareous deposits on steel were observed when AC was induced, an observation that questioned the importance of calcareous deposits in an AC influenced CP system. The experimental work of this thesis, where steel samples were directly AC tested, were compared to earlier work by the author, which included preconditioning of steel samples to form calcareous deposits [2]. In comparison with this work, no clear difference was found in terms of anode corrosion rates (Figure 4-15), current efficiencies (Figure 4-16) or charge related to the reduction reaction (Q_{red}) on the anode sample (Figure 4-17). In other words, the pre-developed calcareous scale on steel had no influence on the anode consumption under influence of AC. In addition, even though the initial protection current was higher in experiments of this project compared to earlier work (Figure D. 4), i_{DC} appeared to approach and stabilize at the same level regardless preconditioning of steel. It is therefore possible that the role of calcareous deposits for the lifetime of AlZnIn anodes is only relevant in the initial period when AC is applied. Note that no calcareous deposits were found to deposit on the anode samples, as discussed in section 5.6. In conclusion, the importance of calcareous deposits for a CP system under influence of

AC is possibly exaggerated because of the clear eruption of this deposit under vigorous gas evolution, its reduced protectiveness (section 5.6) and the very high water reduction rates in which a calcareous deposit is incapable of impeding (section 2.2.1). Even though the results obtained in this thesis question the importance of calcareous deposits for AC corrosion of sacrificial AlZnIn anodes, further studies are needed to conclude. Suggestions are given in section 5.10. Earlier work on this aspect has not been found.

5.2 AC corrosion of cathodically protected steel

Earlier work by the author demonstrated that, although the corrosion rate increased with applied AC level, steel was sufficiently protected by AlZnIn anodes under application of AC potential in the range of 0 to 3.5 V RMS (Figure D. 5 in appendix D). Surface analysis further revealed no steel corrosion of significance. In this work, alkaline corrosion occurred on at least three steel samples (section 4.1.3) in SA/AS experiments where high AC levels were applied (i.e. 80-100 A m^{-2} relative area of one anode sample). Note that an evaluation of AC corrosion of steel based on weight loss measurements is associated with high uncertainty due to the cleaning procedure and the size of the steel samples, as discussed in section 5.7.1. Based on the following observations, it is thought that alkaline corrosion is relevant for the three steel samples. A superficial character of the attack (Figure 4-28 and Figure 4-31), a net reduction rate on the steel samples, and a pH decrease in the test solution (Table 4-1) was observed. The latter implied a strong alkalization of the electrode surfaces to maintain mass balance. Alkaline corrosion occurs if steel enters the corrosive region at high pH, as shown by the Pourbaix diagram in Figure 2-4. This type of corrosion was also reported by Strandheim at AC levels > 250 A m^{-2} for steel samples polarized to -1200 mV_{SCE} [4]. The alkalization of the steel surface is believed to be enhanced at high AC levels by the instability of the calcareous deposits in combination with increased gas evolution.

Note that the AC density levels on the steel samples are of unknown magnitude in SA/AS experiments, which complicates the evaluation of how AC affects the corrosion behaviour of steel. Drugli and Bjordal have investigated the amount of current transfer to steel and to anodes when AC is applied to a test setup identical to an SA/AS test configuration (section 3.4.1). Even though their work indicated that the current transfer to steel from anodes is minor when the AR is large, (i.e. current transfer between anodes dominate,) the current transfer is still extreme when considering the small area of the steel samples in SA/AS experiments. As an example, application of 100 A m^{-2} is equivalent to a current of 450 mA transferred between the two parallel-coupled anode-steel pairs in the electric circuit (see

Figure 3-3). Assuming that only 10 % of the current is transferred to the steel sample, it will still result in an AC density on the steel samples of 1000 A m^{-2}. The equivalent AC density to the anodes will be 90 A m^{-2}. Such high AC densities explain the steel corrosion rates found at high AC levels (up to 3.6 mm $year^{-1}$), explained by the strong alkalization at the steel surface.

5.3 Mechanism and reaction kinetics under influence of AC

5.3.1 Mechanism

Theory of electrochemical impedance [46, 49, 51] demonstrates that application of a large amplitude AC voltage generates a pure DC in the metal-solution interface (section 2.3). The corrosion mechanisms that occur according to DC theory are possibly also valid for AC corrosion. A net corrosion of the anode implies that there will be a net acidification associated with the anode surface. At the same time, the observation of vigorous gas evolution on the anode surface at high AC levels implies that an alkalization is also present to a certain extent on the anode surfaces. This is further supported by the measured decrease in pH of the test solution (Table 4-1), which implies a local alkalization at the electrode surfaces in order to maintain mass balance. A repeated alteration between both mechanisms can arise on the anode surface because of the cyclic nature of an AC signal. The successive acidification and alkalization at the anode surface destabilizes the oxide and activates the surface, and probably thus contributes to an increased self-corrosion rate of the anode. Corrosion of aluminium and its alloys is in general characterized by the presence of (local) cathodic and anodic sites (section 2.1.1), and alkalization and acidification therefore take place at different areas of the anode surface. Activation of AlZnIn occurs by indium enrichment (section 2.1.2), but whether this is relevant for AC corrosion is unknown.

The potential fluctuations under application of a large amplitude AC voltage enable alternative reactions and formation of species, which are not possible or kinetically restricted at open-circuit potential (section 2.4.2). As a result, alterations in reaction kinetics and possibly the corrosion mechanism are expected. Based on the work of Perrault [10], an alternative mechanism for dissolution of aluminium has been documented during cathodic polarization and/or high pH levels [14, 15]. It involves the formation of aluminium hydride in an intermediate step (section 2.1.1), which is enabled by favourable kinetics as compared to the kinetics for recombination of hydrogen. For two reasons, this mechanism is suggested to be of relevance for AC corrosion of AlZnIn anodes. Based on observations of vigorous gas evolution and pH measurements of the test solution (Table 4-1), it is known that a strong

alkalization of the anode surface takes place under application of AC, and thus reaction kinetics are altered at the anode surface. Secondly, it is known that application of AC causes an actual potential shift that enables formation of hydrides. Under influence of an AC density of 240 A m^{-2}, the potential shift was documented by Drugli and Steinsmo [62] to vary between -1975 mV_{SCE} and -125 mV_{SCE} in a cycle (section 2.4.2), which comply partly with the region of thermodynamic stability of aluminium hydride (see Figure 2-1 b). Even though the potential shift reported by Drugli and Steinsmo relates to steel, the potential shift on the coupled anode samples is thought to be similar, based on results from the author's specialization project [2], where the difference between the mean potential of connected anode and steel was found to be in the range of 5 to 20 mV. The increased anode corrosion rates under application of AC can thus be attributed to a change in the corrosion mechanism as presented in section 2.1.1, where adsorbed hydrogen react with aluminium. Concerning the increased corrosion rates, Adhikari and Hebert [15] reported of a significantly higher dissolution rate, influenced by both mass transport and ohmic resistance, at test conditions where they thought this alternative mechanism was valid (section 2.1.1).

Other reactions that are enabled by the potential fluctuations under application of a large amplitude AC voltage are reduction of ferrous ions in relation to the steel surface [63] and hydration of the aluminium oxide layer [72], which results in a porous surface film of lower resistivity. During the cathodic cycle of an applied AC voltage, species can possibly accumulate or adsorb at the electrode surface in combination with excessive hydrogen evolution. The cathodic shift further promotes water reduction of which the calcareous deposits on the steel surface are incapable of impeding (section 2.2.3). In the anodic cycle on the other hand, oxidation of adsorbed species and formed hydrogen can possibly take place. The oxidation of hydrogen is explained by the frequency of the AC signal and limited reaction kinetics associated with both recombination of hydrogen atoms and diffusion of hydrogen into the material. It is evident that the faradaic current introduced by application of AC can possibly relate to multiple charge transfer reactions at the metal surfaces. Note that the mechanism of AC corrosion remains yet to be clarified and the reactions discussed here are therefore merely suggestions to illustrate the complexity associated with a metal-solution interface under influence of AC. The kinetics and time constants associated with the above-mentioned reactions are not taken into consideration, and may be too slow for the reactions to occur when applying an AC signal with a frequency of 50 Hz.

5.3.2 The reduction reaction on the anode surface

The total charge related to the reduction rate on the anode surface (Q_{red}) increased with applied AC level, and this was expected when bearing in mind the observed increase in gas

evolution at the anode surface (Figure 4-17). However, at high AC levels a limiting plateau is reached, which resembles the limiting trend observed for the anode corrosion rates (Figure 4-6). The given trends are, as discussed elsewhere (section 5.1), thought to be due to the formation of a hydrogen carpet and possibly the hydrogen trapping within the pores of the hydroxide film, both effects of which increase the ohmic resistance. The occurrence of a limiting factor at high AC levels was also observed in the author's specialization project [2] and by Strandheim concerning steel samples polarized to -1100 mV_{SCE} at applied AC levels > 500 A m^{-2}[4].

5.3.3 Polarization of mean DC potential

An important result from the experimental work of this thesis is the AC influenced changes in the mean potential (measured on the anode), which implies alterations in the reaction kinetics at the anode surface. Upon application of AC, the mean DC potential was suppressed significantly in the negative direction, increasingly in extent with applied AC level (from about -1.10 V_{SCE} to a potential level in the range of -1.20 V_{SCE} to -1.40 V_{SCE} as shown in Figure 4-2 and Figure 4-11). A proposed explanation in the literature relates to the nonlinear relation between current and potential of a system under corrosion, quantified by the ratio $r = \beta_a/\beta_c$ (section 2.4.1). A negative shift in the mean DC potential during an AC perturbation is in accordance with $r < 1$, i.e. the cathodic Tafel slope is higher than the anodic Tafel slope. The fact that the potential remained low during the entire test period in A/A experiments (and SA/AS experiments at intermediate and high AC levels) implies that the anode corrosion rate is limited by the cathodic reaction rate (i.e. the system is under "cathodic control"). The idea of, and possible reasons for, this shift was introduced in relation to the observation of a limitation in weight loss increase for the anode at high AC levels (Figure 4-6), discussed in section 5.1. It is further supported by the same limiting plateau observed in relation to Q_{red} at high AC levels (Figure 4-17). It is believed that the immediate drop in mean DC potential under influence of AC is attributed to the same effects as explained previously. That is, restricted gas evolution and increased resistance at the anode surface due to formation of a hydrogen blanket and the possible trapping of hydrogen within the porous hydroxide film and possibly indium enrichment at the anode surface.

In experiments involving anode pairs, connection to steel appeared to have no influence on either anode corrosion rates (as discussed in section 5.1) or the mean DC potential under influence of AC (Figure 4-2). These observations indicate that current transfer between anodes dominates, and that steel of moderate size (i.e. AR of 100) appears to be shorted out under influence of AC. In other words, the system acts as an anode-anode galvanic couple. Note however that the anodes still protect the steel samples. In experiments involving only

one anode-steel galvanic couple (i.e. A/S experiments), connection to steel has a clear influence on the mean DC potential of the anode. Following the initial potential drop, a positive shift within 20 hours was observed, at which the potential stabilized at a level slightly lower than the DC operation potential of the AlZnIn anode (-1.05 V_{SCE}). The shift is explained by the ability of steel to act as a cathode, resulting in water reduction and hydrogen evolution at this surface. The potential drop and subsequent positive shift is well documented when addressing the steel at its corrosion potential [4, 52, 57, 59, 60] and also AC testing of sacrificial anodes [2, 62, 63].

The change in potential at a steel surface under influence of AC has been reported in earlier work by Strandheim [4] and Lilleby [61], where the shift in time was explained by a change in reaction kinetics from diffusion control to complete charge transfer control (Figure 2-9 of section 2.4.2). However, if there is a change in reaction kinetics resulting in a positive potential shift, as discussed by Strandheim and Lilleby, the proposed alterations in reaction kinetics are incapable of explaining the time-dependency of this positive potential shift (i.e. potential shift appeared after 1 to 20 hours). This can be related to the very high initial current requirements by steel in combination with a vigorous gas evolution at the steel surface, which restricts further increase in the cathodic reaction rate at this surface. When the current requirements decrease with time however, the cathodic reaction rate is reduced at which the potential hydrogen blankets on the electrode surfaces are removed. The time until the mean potential moved in positive direction increased with applied AC level and increased area of steel (Figure 4-11). These relations are in accordance with a corresponding increase in current requirements due to larger steel specimens and longer time required for protective deposits to develop. This in turn, results in higher anodic and cathodic reaction rates. Note that the mean DC potential reported here, relates to measurements on the anode sample. Identical measurements were not obtained on the connected steel sample. However, in the author's specialization project [2], the mean potential of the steel sample in one experiment was found to be in the range of 2 to 20 mV higher than the mean potential of the anode sample. The anode is thus associated with the most negative potential.

Under removal of AC, a drastic drop in the mean DC potential was observed in A/A experiments at intermediate and high AC levels (Figure 4-3), which implies an anode surface under further "cathodic control". No earlier works by others or by the author have reported of the same potential drop. The potential drop maintained for about five minutes, at which the logging was ended and the stability in time of the mean DC potential is therefore not known. However, it is clear by Figure 4-3 that application of AC has a strong influence on the reaction kinetics of AlZnIn. When the applied AC is removed, reaction kinetics is slowed down. The potential drop can possibly relate to the accumulation of adsorbed species at the anode surface, i.e. aluminium hydrides and hydrogen, which no longer can oxidise fast

enough. Note that no such potential drop was experienced in experiments involving connection to steel.

5.4 Effect of AC on current response

The effect of AC on the protection current (i_{DC}) is substantial. Even though the protection current clearly increased with applied AC, as presented in Figure 4-13, the results are not in agreement with the theory of Bosch and Bogaerts [50], where i_{corr} was stated to increase exponentially with the AC amplitude. The increase in protection current can be attributed to an increased susceptibility of carbon steel to pitting corrosion when under influence of AC [4]. In accordance with earlier work by the author [2] and reports by others [3, 62], the protection current decreased in a stepwise manner with time. The time-dependent decrease in i_{DC} is attributed to the formation of a more protective calcareous deposit with time, a well-known feature of in relation to CP of steel [43, 44]. This implies that the oxygen reduction rate is significant, wherein the protective calcareous scale is able to restrict. Note that calcareous scales were found by surface analyses (section 4.4.2) to deposit on steel samples only, but not on anode samples. The rather high level of i_{DC} that persists after one week testing at high AC levels ($V_{AC} \geq 2$ V AC) (Figure 4-13) is explained by the instability and destruction of the calcareous deposits during testing, caused by vigorous gas evolution. An alternative explanation to the persisting levels of i_{DC} at high AC levels is related to AC influenced alterations in reaction kinetics (as discussed in section 5.3). Calcareous deposits are unable to impede water reduction [37]. In other words, it is possible that the calcareous deposits do not play an important role for the lifetime of a CP system at high levels of applied AC, as already discussed in section 5.1.1. The decrease in i_{DC} and i_{AC} with time can also be attributed to the increased resistance associated with formation of corrosion products on the anode surface, and an increase in surface area of test samples because of localized corrosion and formation of a porous surface film.

In most experiments, i_{DC} decreased significantly during about 10 h of testing. In combination with the observation of a decrease in surface activity at the anode surface with time, there appears to be a time-dependent stabilization of the steel-anode galvanic couple when an AC voltage is applied. This aspect has already been documented and discussed in earlier work on AC corrosion of aluminium by Williams (section 2.4) [55]. The anode weight loss in association with AC testing is thought to occur mostly in the initial test period and longer durations of testing would most likely allow all experiments to reach a steady and low protection current, at which the anode consumption is low. Testing for longer or shorter

periods would possibly provide further insight into these aspects.

In experiments where a constant AC density was applied (i.e. A/A and SA/AS experiments), the measured AC potential increased clearly with applied AC level (Figure 4-5). The measured increase in AC potential with time, needed to maintain a constant AC density of 100 A m^{-2}, is thought to be due to the increased resistance associated with the formation of a porous hydroxide film, where hydrogen also can become trapped. Note that signal interference in the logging instrument was experienced in relation to the experiments involving an AC density of 100 A m^{-2} (section 4.3). As a result, an uncertainty is associated with the potential measurements in these experiments. However, the increase in AC potential with time has also been documented in similar experimental work by Drugli and Steinsmo [62], although of a smaller magnitude. In SA/AS experiments (4 days) with an AR of 1 where an AC density of 240 A m^{-2} was applied, the authors reported of an increase in the AC voltage from 0.88 V to 1.56 V. The authors explained the increase by the formation of corrosion products and possibly calcareous deposits on the test samples.

5.5 Effect of AC on surface activity and surface characteristics

The significant effect application of AC has on the corrosion behaviour of the anodes, was clear from the surface analysis of tested anode samples. Corrosion was characterized by pit formation and coalescence of these at high AC levels. The corrosion morphology is in accordance with earlier work by Steinsmo and Drugli [63], of which anodes was found to be more susceptible to localized corrosion under application of AC. Yet another study, by Tan and Chin [64, 65], reported of similar results in a test solution of 3 wt % NaCl. The authors documented an increase in pit size, depth and dissolution rate of aluminium with increasing levels of applied AC (section 2.4.1). The increase in surface activity (Figure 4-19), amount of corrosion products (Figure 4-20) and the amount, size and depth of corrosion pits (Figure 4-26, Figure 4-27 and Figure 4-29) found by surface analysis, supports the increase in anode corrosion rate found with increasing level of applied AC and increased area of steel (i.e decreased AR).

It is worth noting that increased solution temperature was in some cases observed during AC testing. Aluminium is more susceptible to corrosion at increasing solution temperature [9]. During testing at high AC levels, extreme amounts of corrosion product were formed (Figure 4-19 h)), which increased the viscosity of the test solution. A corresponding increased solution resistivity caused the solution temperature to increase, and this may have contributed

to an excessive increase in anode corrosion rate in experiments where no temperature control chamber was utilized (i.e. A/A and SA/AS experiments). On the other hand, Orazem and Tribollet have emphasized that a non-negligible ohmic resistance reduces the AC part related to processes at the metal-solution interface. This in turn results in a reduced current distortion (section 2.3).

5.6 Effect of AC on deposit properties

In accordance with an increase in both surface activity and corrosion rates with increased AC levels, clear variations were observed with the naked eye of surface deposits on both test samples after AC testing (Figure 4-20 and Figure 4-22). Variations in the amount and characteristics of calcareous deposits on steel were therefore expected. A comparison between X-ray diffractograms of the deposits from steel samples indicates that the formation of $CaCO_3$ is inhibited by application of intermediate and high AC levels ($\geq$ 1 V AC) (Figure 4-24 and Figure 4-25). In other words, the protectiveness of the calcareous deposits is deteriorated by application of AC (section 2.2.3), a result that is in accordance with earlier work by the author [2] and Lilleby [3]. The reduced amount of $CaCO_3$ is explained by the increased protection current and gas evolution with increasing AC level, both effects of which are associated with increased pH level, which in turn favours the formation of $Mg(OH)_2$ [44]. In one case, the X-ray diffractogram indicated that the calcareous deposits contained a small amount of calcite ($CaCO_3$). It is stated in the literature that presence of Mg(II) ions inhibit the formation of this compound (section 2.2.2), and this result was therefore unexpected. The reader is referred to section 5.1.1 for a discussion of the importance of calcareous deposits in relation to anode corrosion rates and resulting lifetime of sacrificial anodes.

In relation to the anode samples, a complete coverage of a thick and gray layer of corrosion product with a flaky character was observed at intermediate and high AC levels ($i_{AC} \geq 40$ A m^{-2}) (Figure 4-20). The determination of the main component in the surface deposits was associated with large variation. Several compounds were found by XRD analyses to dominate in the deposits (e.g. NaCl, crystalline $Al(OH)_3$ and $Na_{0.5}Al_{0.5}ClO_{0.5}$) and the large variation in the results of the analyses implies that the deposits consisted mainly of amorphous $Al(OH)_3$. Even though the results of the XRD analyses revealed no formation of calcareous deposits on the anode surfaces, further studies are needed to conclude about the composition of any surface deposits. In this regard, alternative analysis techniques are recommended in section 5.10.

The inability of the XRD analysis to detect any amorphous compounds is a drawback, in view of the fact that the corrosion product on the anode is believed to be, in fact, amorphous. On the other hand, the strength of the XRD analysis lies in the fact that it identifies the composition of the deposits over a larger area, as compared to e.g. an Energy-dispersive X-ray spectroscopy (EDS). The latter analysis may suffer from local variations and thus be of a qualitatively lower accuracy.

5.7 Evaluation of the experimental work

5.7.1 Evaluation of weight loss testing

In earlier work by the author, measures were suggested to prevent poor adhesion of paint and corrosion of steel samples at the connections to the external circuit. Therefore, the preparation procedure in this work was successfully changed. On the other hand, corrosion in the interface of exposed and painted area of cylindrical anode samples was experienced in experiments involving high AC levels (Figure 4-21). Even though the extreme gas development caused blister formation and tear-off of painting, the amount of corrosion in the interface was modest as compared to the overall corrosion attack in the exposed area (Figure 4-27). Hence, the undesirable corrosion is not believed to represent a significant error in the weight loss measurements.

The cleaning solution (section 3.4.3) was not seen to attack the anode specimens and replicate runs revealed similar corrosion rates. Based on this, the evaluation of AC corrosion of anode samples by weight loss testing is considered a reliable test method. Conversely, the cleaning procedure of steel samples is known to introduce a significant uncertainty in calculation of steel corrosion rates. In earlier work it was observed that corrosion occurred during chemical cleaning on a level comparable to the amount of corrosion during an entire week of AC testing [2]. Even though measures are taken to correct for this after cleaning (section 3.4.3), the uncertainty in relation to calculated corrosion rates are still significant and thus questions the reliability of using weight loss testing to study AC corrosion of steel.

5.7.2 Evaluation of apparatus

Variations in the applied AC were experienced in an increasing manner as the AC level was increased (either constant i_{AC} as in Figure 4-1 or constant V_{AC} as in Figure 4-10). It clearly demonstrated the need for control and manual adjustments of the signal output from the

VariAC. The given variations were experienced in application of any logging device and test setup, which indicate that the alterations are due to resistances in the electrochemical test cell.

In this work, three logging devices were used and evaluated for investigation of AC corrosion. Two of them were new, the Fluke True-RMS digital multimeter and the NI logger, of which both have the ability to separate AC- and DC signals. A development and optimization of software was needed to implement the NI logger. The main motivation for application of new logging devices was the realization that application of filters introduced a restriction in the level of AC that could be applied in the electrochemical system to be studied. In addition, logging errors were experienced with the HP logger. A thorough discussion of challenges and advantages in association with the new instruments follows.

NI logger

In relation to the NI logger (NI 6259), new software was developed in LabView that allowed for in-situ monitoring of all current and potential parameters. Differential input connections were used to measure current and potential parameters of interest. Preliminary testing, both by a dummy cell and with a test setup involving an electrochemical cell, demonstrated that the NI logger was capable of separating the DC signal from the higher AC signal. Initially, significant signal interference was experienced when using the NI logger. The challenge of bias errors was addressed by a trial-and-error approach. Connecting the VariAC's to the same isolating transformer or electrical circuit was identified as a root cause for mutual interference and resulting bias errors. The reason for the mutual interference between VariAC's is however unknown. The VariAC's are floating signal sources, which ensures an isolated ground-reference point. In order to eliminate this error, every VariAC was directly connected to a *separate* circuit in the electrical network, after which the NI logger was used with success. External devices emanate electric fields that cause noise in a system. This was most easily apparent in the high-impedance system of the reference electrode where the mean DC potential was measured. Any noise signal was mitigated by measures explained in section 3.4.1. After some time however, large signal errors were experienced in relation to application of the NI logger (Figure 4-18). The reason for a sudden bias error in some of the current measurements is unknown. Considering the fact that the NI logger uses differential input connections, a large bias error indicates noise that couples electrostatically either to the positive or the negative line. Such an effect can arise by accidental ground. It was suggested that this effect was attributed to noise transferred through the USB cable from the desktop computer in which the NI logger was connected to. The desktop computer was, like other electrical devices, coupled to an isolating transformer. However, the signal noise remained when using a laptop instead of a desktop computer. Because a laptop has a battery as power

supply and thus contains a galvanic isolator, the signal interference cannot be related noise transferred from the computer and the electrical network. A further evaluation of signal interference from surroundings and a further development of signal filters in the NI logger is needed in order to optimize the given test setup. Considering the fact that the NI logger at first functioned adequately, it is believed that the large bias error is related to the logging instrument itself.

True-RMS Fluke multimeters

True-RMS digital multimeters (Fluke 289) with the ability to separate the AC and DC signal and log data were applied with success. The multimeters, initially powered by batteries, were modified to receive power directly from the electrical network. No signal interference was experienced in relation to application of Fluke multimeters. However, other challenges related to the application of Fluke's are in the following addressed. Each multimeter is capable of logging only one parameter. Thus, four multimeters were needed in each experiment, which strictly limited the amount of experiment that could be performed. In relation to the measurement of the protection current (i_{DC}) over a resistor, measurements by digital multimeters were applicable in the range of -500 to 500 mV. At high AC levels, the resistor was changed from 10 Ω to 1 Ω, to avoid saturation of the multimeters because of high values of i_{DC} (i.e. values exceeded 500 mV). Application of a lower resistance caused an undesirable decrease in the signal-to-noise ratio.

Concluding remarks

Of all three logging devices, only the application of digital multimeters from Fluke was free from signal interference, and thus superior in terms of reliability. Nevertheless, the need for a large number of expensive multimeters restricts the amount of experiments and furthermore, the processing of logged data from each Fluke multimeter after testing is time consuming. The application of NI logger is preferred as it allows for in-situ monitoring of up to eight parallel experiments. The setup is further simplified by the application of accustomed shielding boxes containing a resistor of 10 Ω and signal inputs/outputs. Contrary to the application of Fluke multimeters, all logged data is directly saved into the computer by the software. Any future testing by application of NI logger requires an identification of the root cause for signal errors and a further optimization of the software to improve the signal to noise ratio.

5.8 Impedance measurements

The Gill AC serial instrument enabled a study of the characteristics of the electrode-solution interface by measuring the impedance response of the test samples. Note that in-situ impedance measurements were inapplicable by the instrument utilized in this thesis and the measurements thus provided no information about the current response or reaction kinetics of test samples under influence of AC. The reduction in overall impedance found after AC testing at 10 A m^{-2} for one week (section 4.1.4), indicates that the anode surface was activated. The activation was only modest for one anode sample, but significant for the other. This result is in compliance with the result of weight loss measurements (section 4.1.2), where it was found that only one of two anode samples corroded during testing at 10 A m^{-2}.

The similarity in shape of the impedance response before and after AC testing (Figure 4-7 and Figure 4-8) indicates that the same processes were valid at the anode surface. Recall that this comparison provides no information about any processes on the anode surface while under influence of AC. Based on the presence of two overlapping semicircles (Figure 4-7), two different time-dependent processes at the AlZnIn electrode is suggested to take place. In addition, a low-frequency loop is observed in the Nyquist plots, which can be attributed to the formation of adsorbed intermediate species in association with a faradaic process at the electrode [46]. Adsorbed species can be hydroxide, chloride ions, hydrides or other species that form in intermediate steps at the electrode surface (section 2.1.1). It is emphasized that the discussion and interpretation of the impedance response given here include merely suggestions.

The physical meaning of the impedance response is not straightforward for several reasons. Firstly, measurements are complicated by the fact that the impedance test itself introduces a change in the characteristics of the electrode surface as a function of time. The given dependency is clear in the Nyquist plots (e.g. Figure 4-8), where a curving is apparent in the low-frequency range. Secondly, the geometry of the test samples further allow non-uniform current distribution, an effect which is enlarged after AC testing when irregularities are introduced in the surface due to localized corrosion and also formation of corrosion products.

In many cases, an interpretation of impedance measurements was found infeasible, as results were clearly incorrect. It is believed that the non-uniform current distribution caused by the geometry and surface morphology of the test samples introduced a distortion in the impedance measurements. It is further thought that the accuracy of the instrument used for impedance measurements (i.e. Gill AC Serial no 776) is inadequate. An instrument of higher accuracy that allow for a higher range of frequency measurements should be utilized in future

impedance testing. In any case, the incorrect measurements obtained by this technique, question the reliability of the results presented in section 4.1.4. Moreover, the main result obtained from the impedance measurements (i.e. activation of anode surface) was apparent from other experimental work such as the surface analyses. Therefore, the impedance measurements of this thesis are considered redundant. However, impedance measurements by another approach are suggested for future work in section 5.10.

5.9 Significance of work

The motivation behind the project for Statoil is to be able to understand and manage the risk that application of DEH has for corrosion of steel and anodes in a CP system. DEH of subsea pipelines involves application of AC potentials in the range of 1 to 3 V AC. Several test configurations were employed in the experimental work of this project. It is believed that the results from test configurations involving an anode pair, i.e. A/A and SA/AS, are more realistic when realizing that steel is exposed only at coating defects and that multiple, larger anodes are placed along the pipeline in an actual combined DEH and CP system. In any case, an unexpected and significant influence was found for the corrosion behaviour of sacrificial AlZnIn anodes under application of AC and the effect of DEH on the anode performance should be given higher emphasis in future studies. The steel pipelines are coated, which means in practice that the risk for AC corrosion is only relevant at coating defects. Nevertheless, the experimental work in this thesis has shown that steel is under sufficient protection by sacrificial anodes under application of AC. Even though the results from this project challenge the lifetime of the sacrificial anodes under influence of AC, the relevance of these results in relation to CP systems where DEH is applied, is uncertain.

5.10 Suggestions for further work

This work has established that the AlZnIn anodes are susceptible to AC corrosion in seawater in connection with DEH application to cathodically- protected steel pipes. AC corrosion mechanism of AlZnIn anodes remains yet to be established, and the following work is suggested for this purpose.

- It is suggested to perform several in-situ measurements to obtain knowledge of reaction kinetics and processes that occur on the electrode surface under AC corrosion. In this

way, the mechanism of AC corrosion can be elucidated. Firstly, in–situ impedance measurements in a frequency range are suggested to characterize the properties of the surface and their changes when under influence of AC. A frequency response analyzer with large AC amplitude range (e.g. Solartron 1260A), is recommended for such experiments. In combination with a modelling of the electrode-solution interface by an equivalent circuit, the technique can provide an insight into the AC corrosion mechanism. Secondly, in-situ potential measurements by an oscilloscope is suggested as an alternative (to the instruments evaluated in this thesis) to measure automatically the potential and current parameters of interest, but also to obtain information about the current response and phase shift during AC testing at a frequency of 50 Hz. An oscilloscope can thus elucidate the magnitude and change in time of the faradaic and capacitive component. Martin Høyer-Hansen in Sintef has utilized such equipment with success in his investigation of AC corrosion. Finally, an oscilloscope can also be used to obtain in-situ measurements of the ohmic resistance. Such measurements can possibly provide an insight into the processes that occur at the surface such as hydrogen trapping in pores and formation of oxide/hydroxide.

- It is suggested to measure the pH level, both in the bulk and especially locally at the surface in future AC experiments. An estimation of the pH level at the test sample surfaces can possibly elucidate the processes that are relevant during AC corrosion.
- Electrochemical testing (i.e. polarization experiments by a potentiostat) is recommended to further elucidate the AC influenced changes in electrochemical behaviour.
- The influence of alloying elements is well known in relation to the anode performance in a CP system in seawater under DC conditions. However, its influence in relation to AC corrosion is unknown. It is suggested to perform identical AC testing of pure aluminium samples. A comparison with AC testing of AlZnIn anodes can possibly provide an insight into the influence of alloying elements indium and zinc on AC corrosion of this alloy.
- Based on experimental observations, it appears that the surface activity ceases with time and that corrosion occurs mainly in the initial period of testing. It is therefore suggested to study the time dependency of AC corrosion by performing AC testing for shorter and longer periods. This aspect is considered especially relevant for investigating the performance of AlZnIn anodes under influence of AC in an actual situation where DEH is applied to subsea pipelines.
- It is suggested to measure the mean DC (couple) potential for a longer time after removal of the applied AC, to verify the drastic drop in mean DC potential in experiments involving only anodes, and to clarify the stability of this potential change.

With regard to the equipment and methodology for investigation of AC corrosion, the following are suggestions for any further work.

- The experimental work in this thesis involved application of, and an evaluation of, three logging instruments for investigation of AC corrosion. The NI logger was proven the most functional and focus should therefore be put on a further development of this logging system.
- In particular, a further optimization and improvement of the software associated with this instrument is recommended. In relation to this, managing signal interference from the surroundings is essential.

The following are proposed methods in further surface analyses of surface deposits and corroded surfaces.

- An analysis of test samples and surface deposits by glow discharge optical emission spectroscopy (GDOES) is highly recommended to determine the chemical composition of surface deposits and the surfaces of test samples. Such an analysis can confirm or disprove activation of the anode surface by indium enrichment and identify the composition of the calcareous deposits and other surface deposits such as corrosion products that form under application of AC. A depth profile by GDOES analysis can provide information about any variation in the inner and outer layer of the deposit in terms of e.g. protectiveness (i.e. the Ca/Mg ratio). This analysis in complementation with XRD analysis and/or with energy-dispersive X-ray spectroscopy (EDS) analysis is recommended to verify the changes reported here in chemical composition of the calcareous deposits under influence of AC.
- Study hydrogen and/or possible hydride absorption into the aluminium alloy by e.g. secondary ion mass spectrometry (SIMS) or X-ray photoelectron spectroscopy (XPS).

6 Conclusions

- Application of AC to steel – AlZnIn anode couples strongly affects the corrosion behaviour of the sacrificial AlZnIn anodes. Corrosion of the anodes, resulting from current provided for the protection of the steel and self-corrosion, occurred at an increasing rate with applied AC level. High self-corrosion rates were attributed to a successive alkalization (explained by hydrogen evolution) and acidification of the anode surface in each AC cycle, which destabilized the protective oxide layer. The limitation in weight loss increase of anodes found at high AC levels is thought to be related to the hydrogen blanketing of the anode surface and by hydrogen trapped within pores of the hydroxide surface film.
- AC corrosion of the AlZnIn anode was strongly dependent on the anode-steel area ratio (AR), as well as on the magnitude of applied AC. In experiments where AC was applied to two identical anode-steel pairs, the steel samples were shorted out at AR of 100, i.e., the system functioned as an anode - anode galvanic couple, and connection to steel thus had no influence on AC corrosion of the AlZnIn anodes. Such a system was characterized by significantly suppressed mean DC (couple) potentials in the negative direction. This condition caused a significant increase in the self-corrosion rate of the anodes.
- In experiments where AC was applied to an anode-steel couple, the mean DC (couple) potential was polarized to more positive levels within 20 hours, closer to (but still lower than) the DC operation potential of the AlZnIn anode (-1.05 V_{SCE}), explained by hydrogen evolution on steel. The time until the positive shift increased with applied AC level and increased area of steel (i.e. decreased AR). Increased hydrogen evolution on the steel (increased current demand for cathodic protection) was the cause for increased corrosion rate of the anode in this case; the increase was dramatic for an AR of 10. These results suggest that the lifetime of the CP system at high levels of AC ($V_{AC} \geq 2$ V AC or $i_{AC} \geq 30$ A m^{-2}) may become significantly reduced in relation to the expected lifetime under DC conditions.
- Unexpectedly negative mean DC (couple) potentials observed for large anode-steel area ratio (AR of 100) and applied AC level ≥ 40 A m^{-2} and large self-corrosion rate of the anode is attributed to alkalization of the anode surface. Formation of aluminium hydride is suggested as an added factor contributing to the anode corrosion rate under these conditions.
- The AC and DC components of the cell current (i_{AC} and i_{DC}) for the anode-steel couple increased with applied AC. However, these parameters decreased in a stepwise manner with the time of exposure. Both the time until the decrease and the amount of decrease was related to the applied AC level and the AR. The decrease of current with time is

explained by the build-up of a protective calcareous deposit on the steel surface and the formation of corrosion products on the anode surface. For the high levels of applied AC, the cell current did not decrease appreciably with time. This is attributed to the destruction and instability of calcareous deposits due to vigorous gas evolution and a possible change in the reaction kinetics by alkalization of the electrode surfaces.

- The cathodic conditioning under DC to form calcareous deposits on the steel surface was found to have no clear influence on the corrosion of anodes by subsequent application of AC. Although the initial current requirements were lower in presence of pre-developed calcareous deposits, these differences disappeared with time. Increased water reduction and destabilization of the calcareous deposits by vigorous gas evolution and reduced protectiveness by inhibition of $CaCO_3$ formation, question the importance of calcareous deposits in a CP system where AC is applied. The reduced amount of $CaCO_3$ in the calcareous deposits is explained by the increased cathodic reaction rate and resulting increased pH at the steel surface, which favours the formation of $Mg(OH)_2$. No calcareous scale were found to deposit on the anode surfaces, and the surface deposits are thought to be dominated by amorphous $Al(OH)_3$.
- Pitting corrosion was documented on anode samples. Pits increased in quantity and depth with AC level and with larger area of coupled steel sample. At applied AC densities ≥ 40 A m^{-2} large areas of the anode surface was affected, recognized by pit coalescence and high weight loss. The high rates of pitting corrosion documented in this thesis challenges the lifetime of anodes under influence of AC levels $i_{AC} \geq 30$ A m^{-2}.
- Steel samples were seen to be sufficiently protected by sacrificial anodes under influence of AC. A high uncertainty is related to the calculated steel corrosion rates by the standardized HCl cleaning procedure for removing the corrosion products, which questions the reliability of weight loss testing for evaluating AC corrosion of steel.

7 References

1. A. Nysveen, H. Kulbotten, A. Børnes, and M. Høyer-Hansen. *Direct electrical heating of subsea pipelines-technology development and operating experience*. in *Petroleum and Chemical Industry Conference, 2005. Industry Applications Society 52nd Annual*. IEEE.
2. K. Forthun, *Cathodic Protection of Steel under Alternating Current.* Specialization project (TMT 4500), 2012, NTNU.
3. L.S. Lilleby, *Effect of AC current on calcareous deposits.* Master's thesis, 2009, NTNU.
4. E.O. Strandheim, *AC Induced Corrosion of Carbon Steel in 3.5 wt% NaCl Electrolyte.* Master's thesis, 2012, NTNU.
5. DNV, *DNV-RP-B401 "Cathodic Protection of Structures"*. 2010.
6. DNV, *DNV-OS-F101 Offshore Standard* in *Submarine pipeline systems*. 2012.
7. ISO, *ISO 15589-2:2012 Petroleum, petrochemical and natural gas industries - Cathodic protection of pipeline transportation systems - Part 2: Offshore pipelines*. 2012.
8. K. Nisancioglu, *Lecture Notes for the course 53523 Korrosjonslære*. 1994, Trondheim: Norges Tekniske Høgskole, Institutt for Teknisk Elektrokjemi.
9. J.R. Davis, *Corrosion of aluminum and aluminum alloys*. 1999: ASM International.
10. G. Perrault, *The Role of Hydrides in the Equilibrium of Aluminum in Aqueous Solutions.* Journal of The Electrochemical Society, 1979. 126(2): p. 199-204.
11. K. Nisancioglu, *Corrosion Science and Engineering of Light Metals: Past, Present and Future.* Keikinzoku Gakkai Taikai Koen Gaiyo, 2006. 111: p. 313-314.
12. K. Nisancioglu, *Corrosion and protection of aluminium alloys in seawater*, in *Corrosion behaviour and protection of copper and aluminium alloys in seawater*, D. Féron, Editor. 2007, CRC Press. p. 145-155.
13. S. Gudić, J. Radošević, I. Smoljko, and M. Kliškić, *Cathodic breakdown of anodic oxide film on Al and Al–Sn alloys in NaCl solution.* Electrochimica acta, 2005. 50(28): p. 5624-5632.
14. S. Adhikari, J. Lee, and K.R. Hebert, *Formation of aluminum hydride during alkaline dissolution of aluminum.* Journal of The Electrochemical Society, 2008. 155(1): p. C16-C21.

15. S. Adhikari and K.R. Hebert, *Participation of aluminum hydride in the anodic dissolution of aluminum in alkaline solutions.* Journal of The Electrochemical Society, 2008. 155(5): p. C189-C195.
16. J. Radošević, M. Kliškić, P. Dabić, R. Stevanović, and A. Despić, *Processes on aluminium on the negative side of the open-circuit potential.* Journal of electroanalytical chemistry and interfacial electrochemistry, 1990. 277(1): p. 105-119.
17. A. Despić, D. Dražić, J. Balakšina, L. Gajić-Krstajić, and R. Stevanović, *Investigation of oxidation potentials of substances accumulated during cathodic polarization of aluminium.* Electrochimica Acta, 1990. 35(11): p. 1747-1755.
18. C. Breslin and L. Friery, *The synergistic interaction between indium and zinc in the activation of aluminium in aqueous electrolytes.* Corrosion science, 1994. 36(2): p. 231-240.
19. C. Breslin, L. Friery, and W. Carroll, *The electrochemical behaviour of Al Zn In and Al Zn Hg alloys in aqueous halide solutions.* Corrosion science, 1994. 36(1): p. 85-97.
20. C.B. Breslin and W.M. Carroll, *The activation of aluminium by indium ions in chloride, bromide and iodide solutions.* Corrosion science, 1993. 34(2): p. 327-341.
21. W. Carroll and C. Breslin, *Activation of aluminium in halide solutions containing 'activator ions'.* Corrosion science, 1992. 33(7): p. 1161-1177.
22. B. Graver, A.T.J. van Helvoort, and K. Nisancioglu, *Effect of heat treatment on anodic activation of aluminium by trace element indium.* Corrosion science, 2010. 52(11): p. 3774-3781.
23. J. Gundersen, A. Aytac, J. Nordlien, and K. Nişancıoğlu, *Effect of heat treatment on electrochemical behaviour of binary aluminium model alloys.* Corrosion science, 2004. 46(3): p. 697-714.
24. A. Munoz, S. Saidman, and J. Bessone, *Corrosion of an Al–Zn–In alloy in chloride media.* Corrosion science, 2002. 44(10): p. 2171-2182.
25. W. Wilhelmsen, T. Arnesen, Ø. Hasvold, and N. Størkersen, *The electrochemical behaviour of AlIn alloys in alkaline electrolytes.* Electrochimica acta, 1991. 36(1): p. 79-85.
26. B. Graver, A. van Helvoort, J.C. Walmsley, and K. Nisancioglu. *Surface segregation of indium by heat treatment of aluminium*. in *Materials science forum*. 2006. Trans Tech Publications.

27. B. Graver, A.T. van Helvoort, and K. Nisancioglu, *Effect of heat treatment on anodic activation of aluminium by trace element indium.* Corrosion science, 2010. 52(11): p. 3774-3781.
28. S. Gudić, I. Smoljko, and M. Kliškić, *The effect of small addition of tin and indium on the corrosion behavior of aluminium in chloride solution.* Journal of alloys and compounds, 2010. 505(1): p. 54-63.
29. M. Reboul, P. Gimenez, and J. Rameau, *A proposed activation mechanism for Al anodes.* Corrosion, 1984. 40(7): p. 366-371.
30. K. Nisancioglu, *Personal communication* 2013
31. R. Johnsen, *Cathodic Protection*. 2008, Trondheim: Institute of Engineering Design and Materials.
32. R.A. Gummow, R.G. Wakelin, and S.M. Segall, *AC corrosion - a new threat to pipeline integrity?* CORROSION/98, 1998. Paper No. 566: p. 443-453.
33. Z. Ahmad, *Principles of corrosion engineering and corrosion control*. 2006: Elsevier.
34. S. Elbeik, A. Tseung, and A. Mackay, *The formation of calcareous deposits during the corrosion of mild steel in sea water.* Corrosion Science, 1986. 26(9): p. 669-680.
35. W.H. Hartt, C.H. Culberson, and S.W. Smith, *Calcareous deposits on metal surfaces in seawater-a critical review.* Corrosion, 1984. 40(11): p. 609-618.
36. S. Rossi, P. Bonora, R. Pasinetti, L. Benedetti, E. Sacco, and M. Draghetti, *Laboratory and Field Characterization of a New Sacrificial Anode for Cathodic Protection of Offshore Structures.* Corrosion, 1998. 54(12).
37. T. Okstad, Ø. Rannestad, R. Johnsen, and K. Nisancioglu, *Significance of hydrogen evolution during cathodic protection of carbon steel in seawater.* Corrosion, 2007. 63(9): p. 857-865.
38. T. Okstad, *Hydrogenutvikling ved katodisk beskyttelse av karbonstål i naturlig sjøvann.* Master's thesis, 2005, NTNU.
39. W. Sun, G. Liu, L. Wang, and Y. Li, *A mathematical model for modeling the formation of calcareous deposits on cathodically protected steel in seawater.* Electrochimica Acta, 2012. 78: p. 597-608.
40. R.A. Berner, *The role of magnesium in the crystal growth of calcite and aragonite from sea water.* Geochimica et Cosmochimica Acta, 1975. 39(4): p. 489-504.
41. A. Neville and A.P. Morizot, *Calcareous scales formed by cathodic protection—an assessment of characteristics and kinetics.* Journal of crystal growth, 2002. 243(3): p. 490-502.

42. C. Deslouis, A. Doncescu, D. Festy, O. Gil, V. Maillot, S. Touzain, and B. Tribollet, *Kinetics and characterisation of calcareous deposits under cathodic protection in natural sea water.* Materials Science Forum, 1998. 289-292: p. 1163-1180.
43. K. Nisancioglu, *Design Techniques in Cathodic Protection Engineering*, in *Modern Aspects of Electrochemistry* B.E. Conway, R.E. White, and J.O. Bockris, Editors. 1992, Plenum Press: New York.
44. W.H. Hartt, C.H. Culberson, and S.W. Smith, *Calcareous Deposits on Metal Surfaces in Seawater—A Critical Review.* Corrosion, 1984. 40(11): p. 609-618.
45. C. Barchiche, C. Deslouis, O. Gil, P. Refait, and B. Tribollet, *Characterisation of calcareous deposits by electrochemical methods: role of sulphates, calcium concentration and temperature.* Electrochimica Acta, 2004. 49(17–18): p. 2833-2839.
46. M.E. Orazem and B. Tribollet, *Electrochemical impedance spectroscopy*. 2011: Wiley-Interscience.
47. S.N. Victoria and S. Ramanathan, *Effect of potential drifts and ac amplitude on the electrochemical impedance spectra.* Electrochimica Acta, 2011. 56(5): p. 2606-2615.
48. NACE, *AC Corrosion State-of-the-Art: Corrosion Rate, Mechanism, and Mitigation Requirements*. 2010, NACE International Task Group 327.
49. D.A. Harrington, *Theory of electrochemical impedance of surface reactions: second-harmonic and large-amplitude response.* Canadian journal of chemistry, 1997. 75(11): p. 1508-1517.
50. R.W. Bosch and W. Bogaerts, *A theoretical study of AC-induced corrosion considering diffusion phenomena.* Corrosion science, 1998. 40(2): p. 323-336.
51. B. Hirschorn, B. Tribollet, and M.E. Orazem, *On Selection of the Perturbation Amplitude Required to Avoid Nonlinear Effects in Impedance Measurements.* Israel Journal of Chemistry, 2010. 48(3-4): p. 133-142.
52. I. Stamnes, *AC-korrosjon av rørstål.* Master's thesis, 2010, NTNU.
53. S. Goidanich, L. Lazzari, and M. Ormellese, *AC corrosion. Part 2: Parameters influencing corrosion rate.* Corrosion Science, 2010. 52(3): p. 916-922.
54. L. Nielsen and P. Cohn, *AC-Corrosion and Electrical Equivalent Diagrams.* Proc CeoCor, 2000.
55. J.F. Williams, *Alternating Current and Aluminium.* Materials Protection, 1967: p. 50-52.
56. W.H. French, *Alternating Current Corrosion of Aluminum.* IEEE Transactions on Power Apparatus and Systems, 1973. PAS-92(6): p. 2053-2062.

57. E. Belland, *Alternating Current Corrosion of Carbon Steel.* . Master's thesis, 2011, NTNU.
58. S. Goidanich, L. Lazzari, and M. Ormellese, *AC corrosion – Part 1: Effects on overpotentials of anodic and cathodic processes.* Corrosion Science, 2010. 52(2): p. 491-497.
59. S.M. Hesjevik, *Interim Report AC Corrosion Testing*. 2009, Statoil.
60. M.A. Pagano and S.B. Lalvani, *Corrosion of mild steel subjected to alternating voltages in seawater.* Corrosion Science, 1994. 36(1): p. 127-140.
61. L.S. Lilleby, S. Olsen, and S.M. Hesjevik. *Effects from alternating current on cathodic protection of submarine pipelines.* 2011. Paper No 11055: NACE International.
62. J. Drugli and U. Steinsmo, *AC Influenced Corrosion Revised 1997-02-12*. 1997, SINTEF report STF24 F97206.
63. U. Steinsmo and J. Drugli, *A study of the influence of alternating currents on the corrosion of pipelines*. 1991, SINTEF Report STF34 F91183.
64. T. Tan and D.T. Chin, *Polarization of Aluminum during AC Corrosion in Sulfate Solutions.* Journal of The Electrochemical Society, 1985. 132(4): p. 766-773.
65. T. Tan and D.T. Chin, *Effect of Alternating Voltage on the Pitting of Aluminum in Nitrate, Sulfate, and Chloride Solutions.* Corrosion, 1989. 45(12): p. 984-989.
66. D.-K. Kim, S. Muralidharan, T.-H. Ha, J.-H. Bae, Y.-C. Ha, H.-G. Lee, and J.D. Scantlebury, *Electrochemical studies on the alternating current corrosion of mild steel under cathodic protection condition in marine environments.* Electrochimica Acta, 2006. 51(25): p. 5259-5267.
67. M. Bjordal and J. Drugli, *AC-influenced corrosion of aluminium anodes*. 1999, SINTEF report STF24 F00223.
68. ASTM, *D1141-98 (2008) Standard Practice for the Preparation of Substitute Ocean Water*. 2008.
69. A. Torstensen, *AC Corrosion on cathodically protected steel*. Master's thesis, 2012, NTNU.
70. L. Lazzari, F. Bolzoni, S. Lazzari, and M. Ormellese, *Laboratory Test Results of AC Interference on Polarized Steel.* CORROSION, 2003.
71. ASTM, *G1-03, 2003 Standard practice for preparing, cleaning and evaluating corrosion test specimens*. 2003.

72. M. Kliskic, J. Radosevic, and L. Aljinovic, *Behaviour of Al-Sn alloy on the negative side of the open-circuit potential.* Journal of applied electrochemistry, 1994. 24(8): p. 814-818.

APPENDICES

A. Calculations

This section presents the equations and physical data used in calculation of corrosion rates and anode efficiency.

A.1 Physical data

Table A.1.shows the physical data used in the calculations.

Table A.1. Physical data.

Property	Value	Unit
Faraday constant, F	96485	C mol^{-1}
Density of steel, ρ_{Fe}	7.86	g cm^{-3}
Density of AlZnIn, ρ_{Al}	2.72	g cm^{-3}
Molar weight Al, M_{Al}	26.98	g mol^{-1}
Molar weight Fe, M_{Fe}	55.85	g mol^{-1}

A.2 Corrosion rates

The total corrosion rate (CR) in mm $year^{-1}$ of both materials was calculated by

$$CR = \frac{k \cdot \Delta m}{A \cdot \rho \cdot t} \tag{A.1}$$

where the constant k is equal to 8.76, Δm is the weight loss in grams, A and ρ corresponds to the area [m^2] and density [g cm^{-3}] of the tested sample respectively, and t is the test period in hours.

A.3 Numerical integration

Corrosion rates by numerical integration

In the case of the AlZnIn anode, calculation of both the corrosion rate due to protection of the steel sample and the amount of self-corrosion was calculated by numerical integration. The

total charge transfer due to protection of the steel (A.2) was approximated by a summation of the Simpson's integrals over the time interval [a, b] (A.3). The current was logged every two minutes, thus the entire test period was divided into intervals with size (b-a) equal to 240 seconds.

$$Q = \int I \cdot dt \tag{A.2}$$

$$\int_a^b I \cdot dt \approx \frac{b-a}{6} \cdot \left[I(a) + 4 \cdot I\left(\frac{a+b}{2}\right) + I(b) \right] \tag{A.3}$$

where I is the direct current (DC) at a given time. Based on the total charge transfer estimation, the weight loss of the anode due to protection of the steel was calculated by

$$\Delta m = \frac{M \cdot Q}{n \cdot F} \tag{A.4}$$

where M is the molar weight of the anode, Q is the total charge(A.2), n is the number of moles of electrons transferred for every mole of oxidized aluminium and F is the Faraday constant given in Table A.1.

Calculation of charge related to the reduction reaction on anode

The total charge was found by numerical integration as outlined above(A.2). The charge related to the reduction reaction on the anode, Q_{red} (A.6), was calculated by a consideration of the net current i_{net} (A.5).

$$|i_{net}| = i_{korr} - |i_{red}| \tag{A.5}$$

Where i_{red} and i_{corr} are the current densities for the reduction reactions at the anode surface and corrosion of the anode respectively. i_{net} is thus the protection current to the steel structure. The charge transfer due to corrosion, Q_{corr} and the net charge transfer, Q_{net} (related to i_{net}) was found by weight loss measurements and numerical integration, respectively. The charge related to the reduction reaction on the anode is then given by

$$Q_{red} = Q_{corr} - Q_{net} \tag{A.6}$$

A.4 Anode capacity and efficiency

The anode capacity [Ah kg^{-1}] was calculated by

$$\varepsilon = \frac{Q}{3.6 \cdot \Delta m} \tag{A.7}$$

where Q [As] is the charge transfer found by numerical integration (A.2) and Δm is the weight loss [g] of the anode sample. The current (or anode) efficiency, S, was accordingly found by

$$S(\%) = \frac{I_{net}}{I_{corr}} = \frac{\Delta m_{prot}}{\Delta m_{tot}} \cdot 100 \tag{A.8}$$

B. Elemental analyses of AlZnIn anodes

The elemental composition of AlZnIn test materials was determined by spark optical emission spectroscopy (Spark-OES), glow discharge mass spectrometer (GDMS) and energy dispersive X-ray analysis (EDS) analysis. Elemental analysis by EDS was performed at the department of Materials Science and Engineering at NTNU. By this method, only one anode sample supplied from BEME Corrosion was analyzed at eight areas on the sample. The results are given in Table B. 1 (weight % of Al, Zn and In). Because alloy elements are present in solid solution, but also as particles, the method cannot find the absolute composition of the test sample, and the result of the analysis merely gives an indication of the actual composition. Spark-OES was performed at Hydro (Karmøy) on three anode samples of which are designated by the supplier of the test material (Table B. 2). Spark-OES provides an accuracy of ± 10 ppm. In addition, analysis by GDMS was performed at the department of Materials Science and Engineering at NTNU. Table B. 3 shows the average composition of three measurements obtained from GDMS analysis. Note that due to an incomplete analysis of reference samples, the results presented in Table B. 3 are only semi-quantitative.

Table B. 1. Results of compositional EDS analysis of one anode sample, supplied from BEME Corrosion International [wt %].

No.	Al	Zn	In	Total
1	91.416	2.851	0.018	94.285
2	93.061	2.812	0.018	95.891
3	93.152	3.033	0.021	96.206
4	92.968	2.807	0.011	95.786
5	93.968	2.923	0.015	96.906
6	92.817	2.831	0.019	95.667
7	92.278	2.895	0.022	95.195
8	94.81	2.837	0.024	97.671
Avg.	93.059	2.874	0.019	95.951
Sigma	1.02	0.076	0.004	1.028

Table B. 2. Elemental analysis by Spark-OES of three anode samples from Statoil and BEME Corrosion International [wt %].

Element	Si	Fe	Cu	Mn	Mg	Cr	Ni	Zn	Ti	V	B
Statoil *	0.03317	0.07518	0.00026	0.00093	0.00203	0.00048	0.00354	4.53995	0.00292	0.00523	0.00008
Statoil	0.03406	0.04189	-0.00015	0.00093	0.00002	0.00017	0.00165	3.74384	0.01896	0.01329	0.00106
BEME	0.04885	0.07552	0.00044	0.00093	0.00002	0.00029	0.00538	2.64995	0.00718	0.01187	0.00002

Element (cont.)	Be	Bi	Ca	Cd	Co	Ga	In	P	Pb	Sb	Zr	Bulk
Statoil *	0.00009	0.00008	0.00038	0.00022	0.00026	0.01278	0.02459	0.00023	0.00017	0.00296	0.00471	95.28692
Statoil	0.00010	0.00008	0.00033	0.00017	0.00026	0.01238	0.01504	0.00026	0.00007	0.00179	0.00245	96.10985
BEME	0.00010	0.00008	0.00030	0.00021	0.00026	0.01187	0.02580	0.00027	0.00007	0.00184	0.00158	97.15475

Table B. 3. Elemental analysis by GDMS of three anode samples from Statoil and BEME Corrosion International. Results are only semi quantitative [wt %].

Element	Fe	Cu	Zn	Cd	In	Pb	Si
Statoil *	0.024	3.53E-05	1.077	2.59E-06	0.0026	1.27E-04	0.0104
Statoil	0.023	6.22E-05	0.861	3.28E-06	0.0027	2.59E-04	0.0065
BEME	0.051	0.000305	0.915	4.77E-06	0.0032	2.64E-04	0.0142

* Anode sample from a batch used during AC testing in an earlier specialization project by the author.

C. XRD analysis

Additional XRD patterns of the calcareous deposits on the steel samples and the surface deposits on anode samples are presented in this section.

C.1 XRD analysis of calcareous deposits on steel

The results of the XRD analyses of calcareous deposits from many steel samples revealed that the deposits consisted mainly of brucite ($Mg(OH)_2$). Moreover, it revealed that application of AC clearly influenced the amount of aragonite ($CaCO_3$) in the deposits, shown by a reduced amount, and ultimately a complete exclusion of this component in the deposit, with increasing levels of applied AC. In the following figures, additional X-ray diffractograms of calcareous deposits from steel samples tested for one week at different levels of AC are presented.

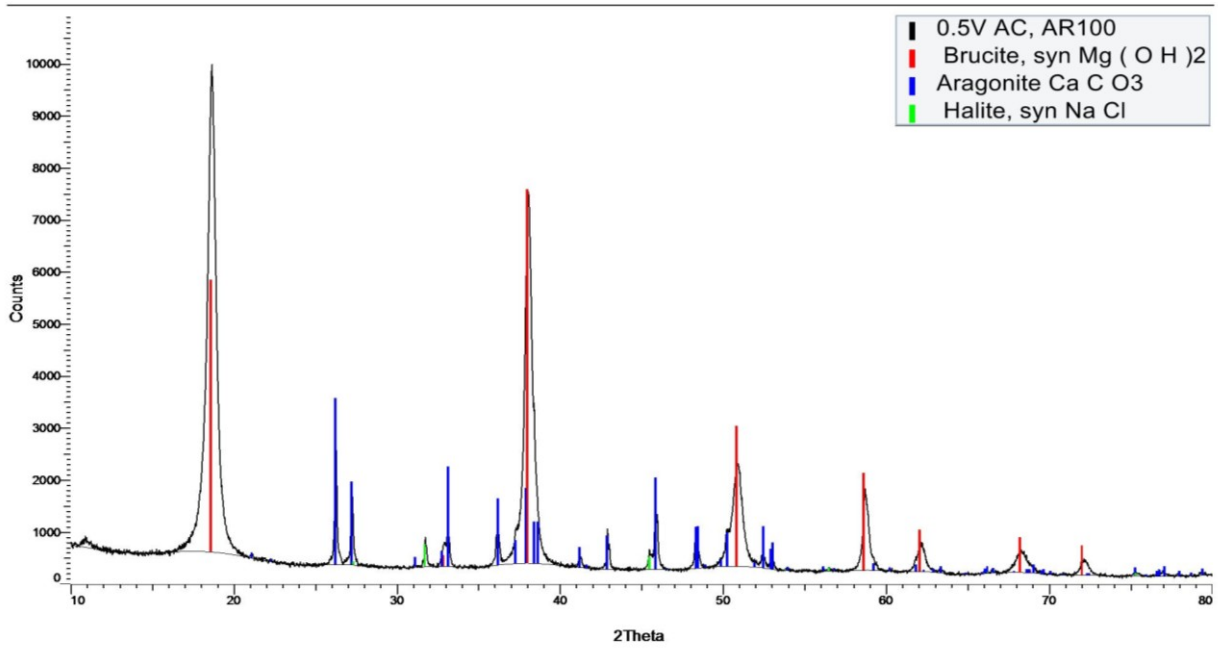

Figure C. 1. X-ray diffractogram of deposits after testing at 0.5 V AC. Peaks match the crystal structure of $Mg(OH)_2$, $CaCO_3$ and NaCl.

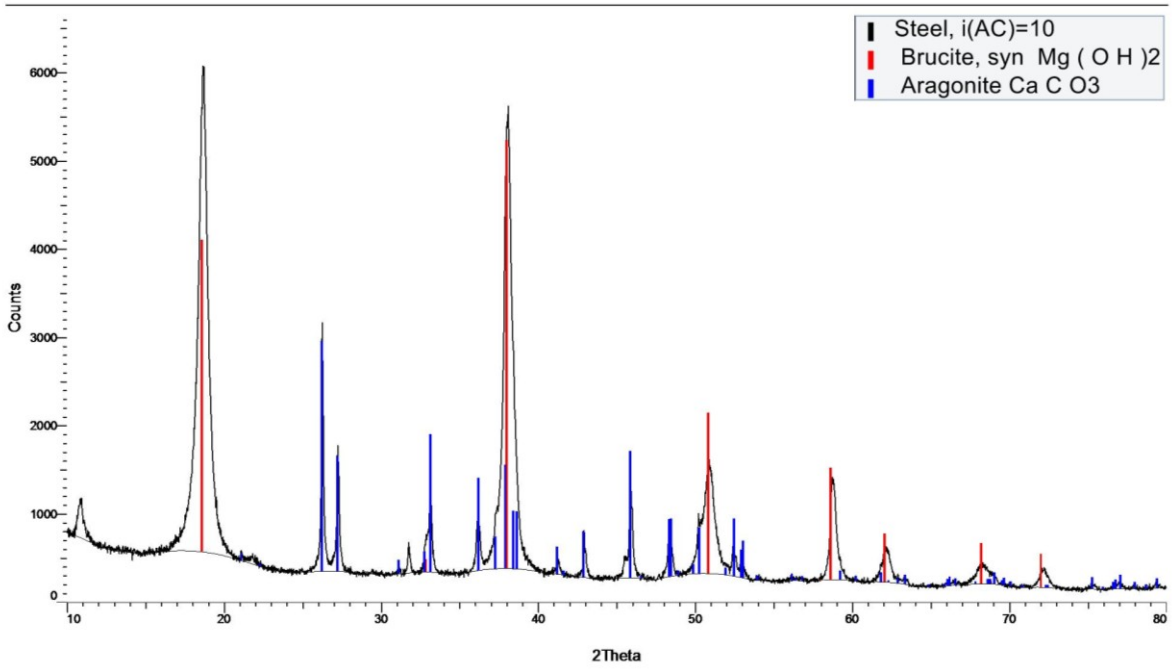

Figure C. 2. X-ray diffractogram of deposits after testing at i_{AC}=10 A m^{-2}. Peaks match the crystal structure of $Mg(OH)_2$ and $CaCO_3$.

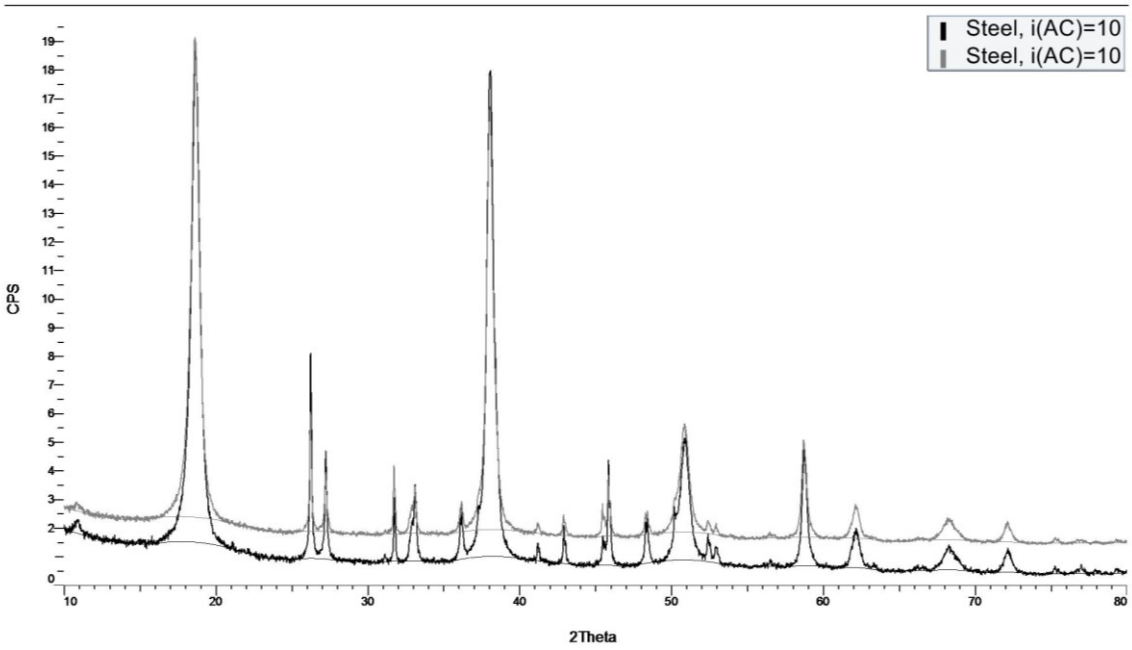

Figure C. 3. X-ray diffractogram of deposits after testing at i_{AC}=10 A m^{-2}. Peaks are identical to the X-ray diffractogram in Figure C. 2.

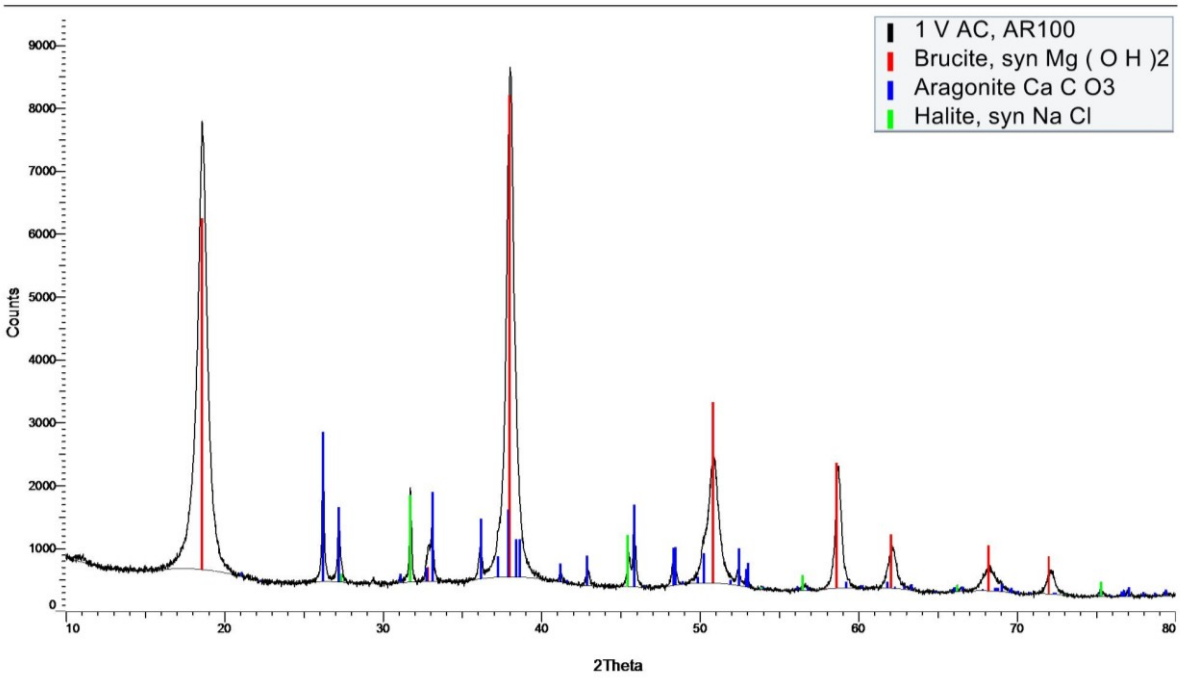

Figure C. 4. X-ray diffractogram of deposits after testing at 1 V AC. Peaks match the crystal structure of $Mg(OH)_2$, $CaCO_3$ and NaCl.

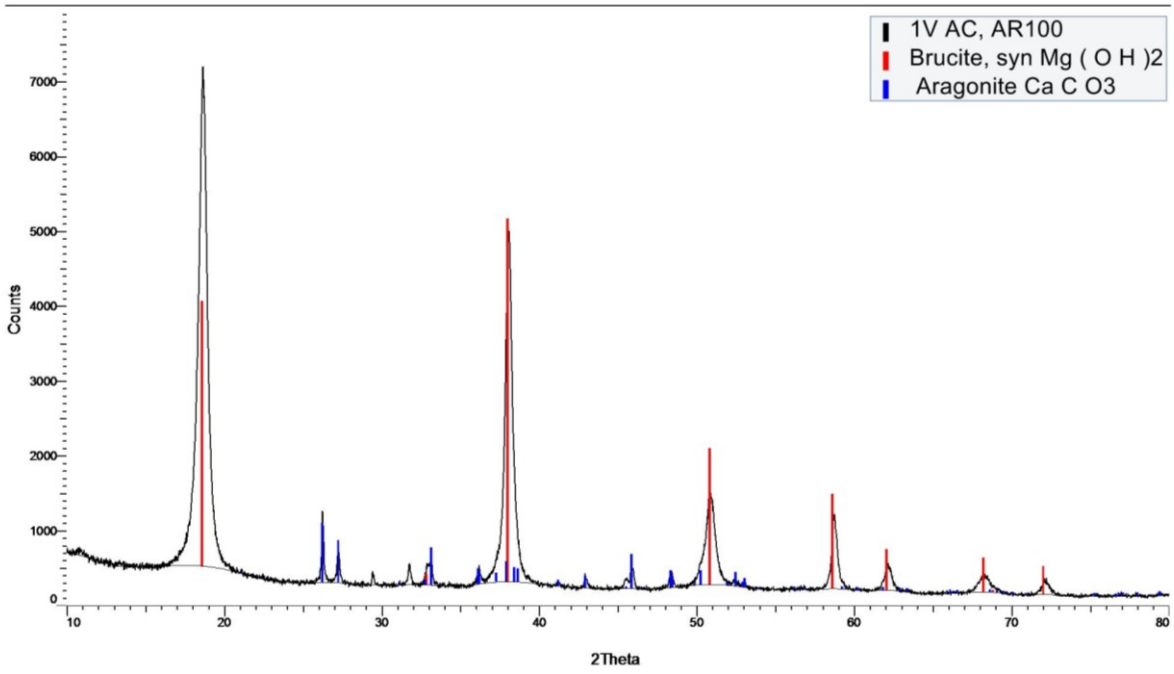

Figure C. 5. X-ray diffractogram of deposits after testing at 1 VAC. Peaks match the crystal structure of $Mg(OH)_2$ and $CaCO_3$.

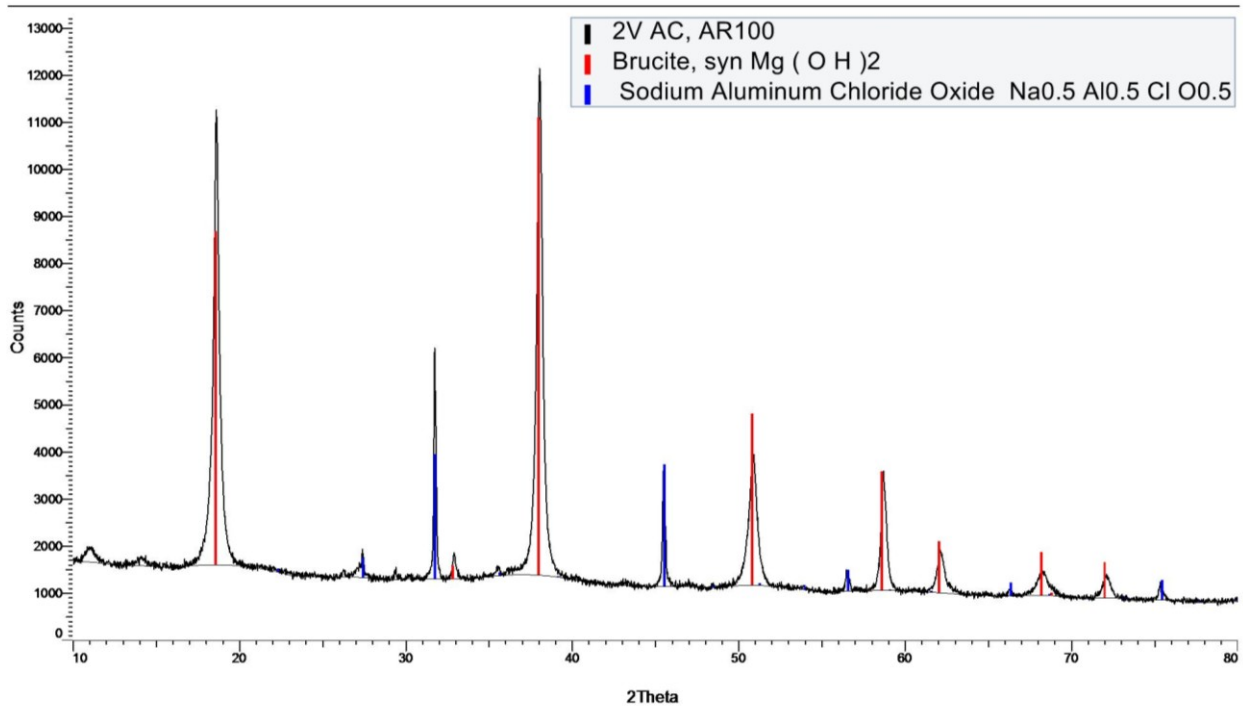

Figure C. 6. X-ray diffractogram of deposits after testing at 2 V AC. Peaks match the crystal structure of $Mg(OH)_2$ and $Na_{0.5}Al_{0.5}ClO_{0.5}$.

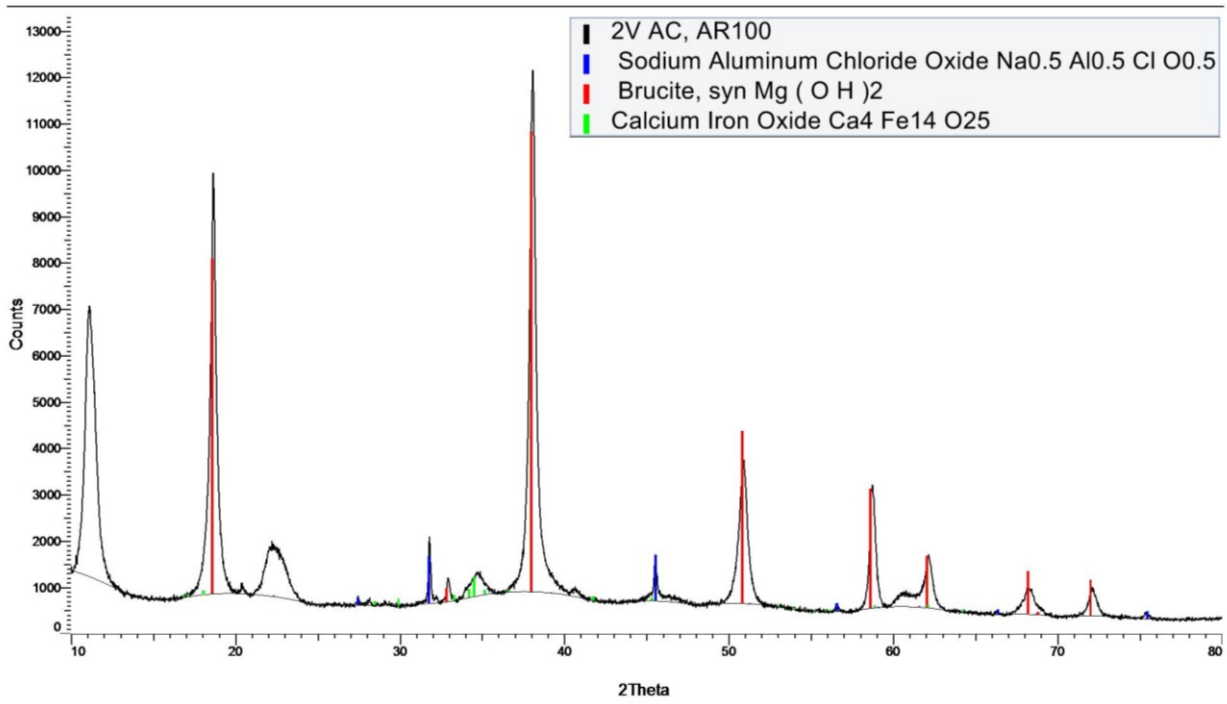

Figure C. 7. X-ray diffractogram of deposits after testing at 2 V AC. Peaks match mainly the crystal structure of $Mg(OH)_2$ and possibly $Na_{0.5}Al_{0.5}ClO_{0.5}$.

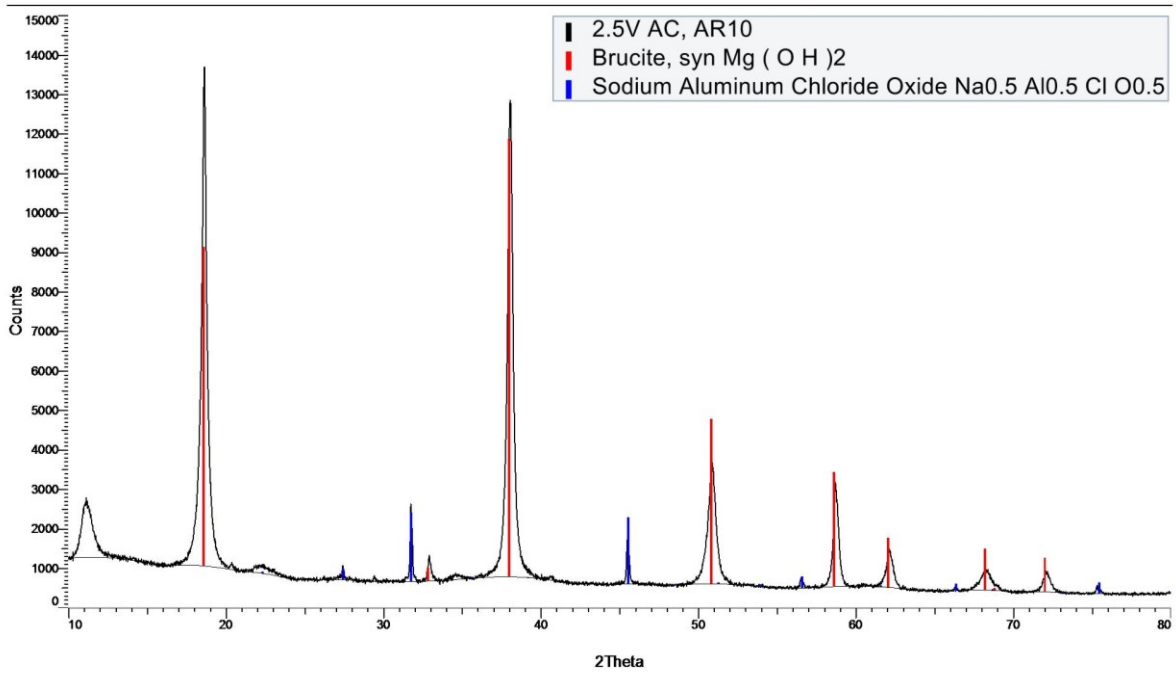

Figure C. 8. X-ray diffractogram of deposits after testing at 2.5 V AC. Peaks match the crystal structure of $Mg(OH)_2$ and $Na_{0.5}Al_{0.5}ClO_{0.5}$.

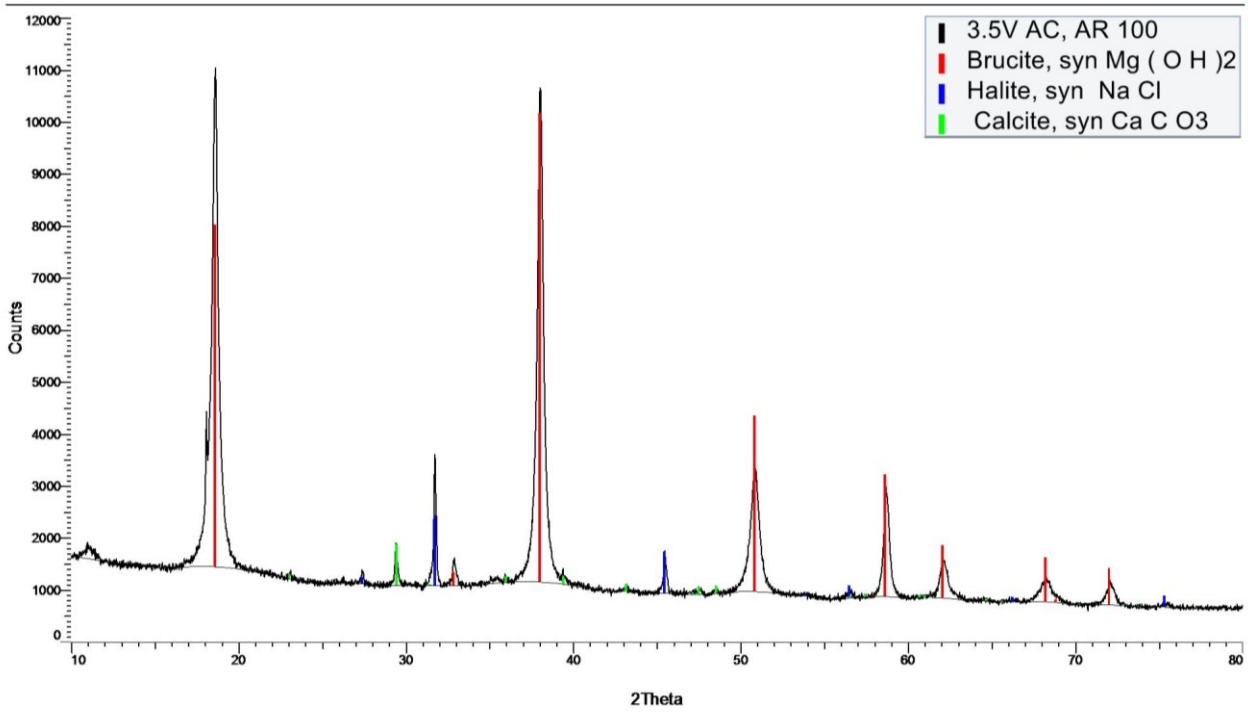

Figure C. 9. X-ray diffractogram of deposits after testing at 3.5 V AC. Peaks match the crystal structure of $Mg(OH)_2$, NaCl and possibly $CaCO_3$.

C.2 XRD analysis of deposits on anode samples

The surface deposits on anode samples were found by XRD analysis to consist of mainly halite, bayerite and sodium aluminium chloride oxide. The corrosion product on the anode samples are believed to consist of mainly amorphous $Al(OH)_3$. The large variation in the obtained XRD spectra of Figure C. 11 and Figure C. 12, which are spectra of surface deposits from the same tested anode sample, indicates that the major component in the surface deposits is an amorphous compound, considering the fact that a XRD analysis identifies only crystalline compounds.

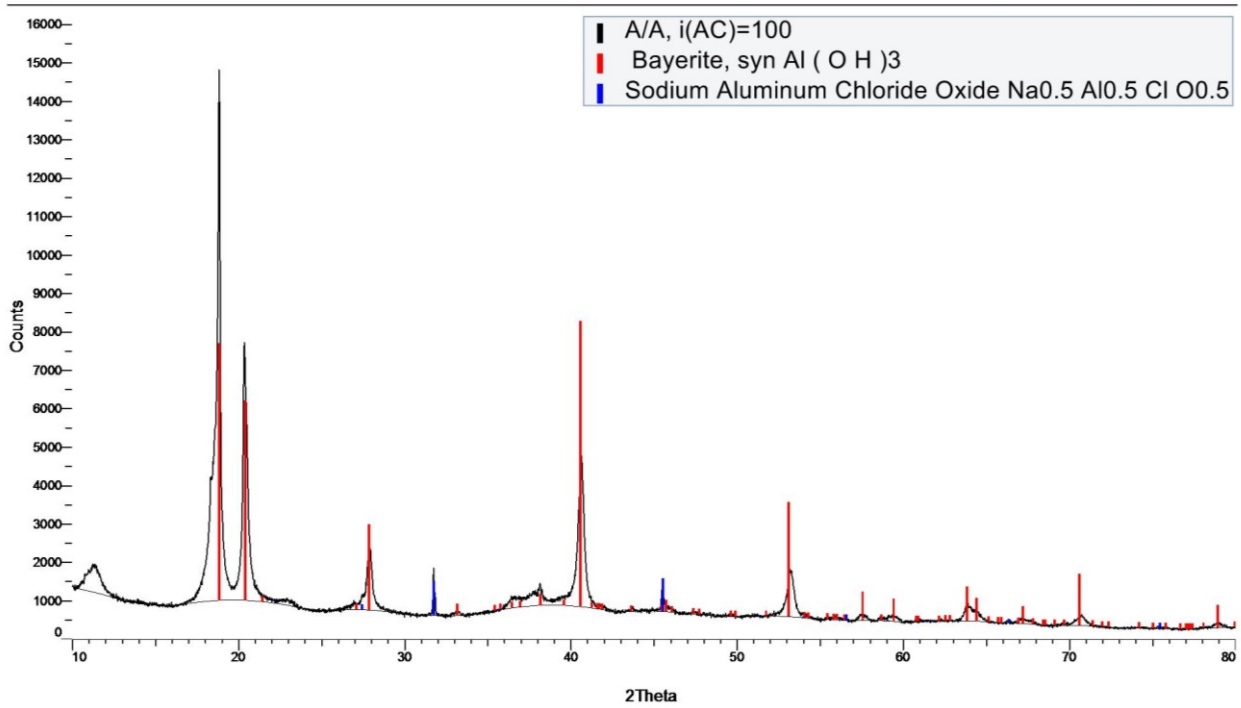

Figure C. 10. XRD spectrum of the corrosion product removed from an anode sample tested at 100 A m^{-2}. Peaks match the crystal structure of mainly bayerite, but also possibly a minor amount of sodium aluminium chloride oxide.

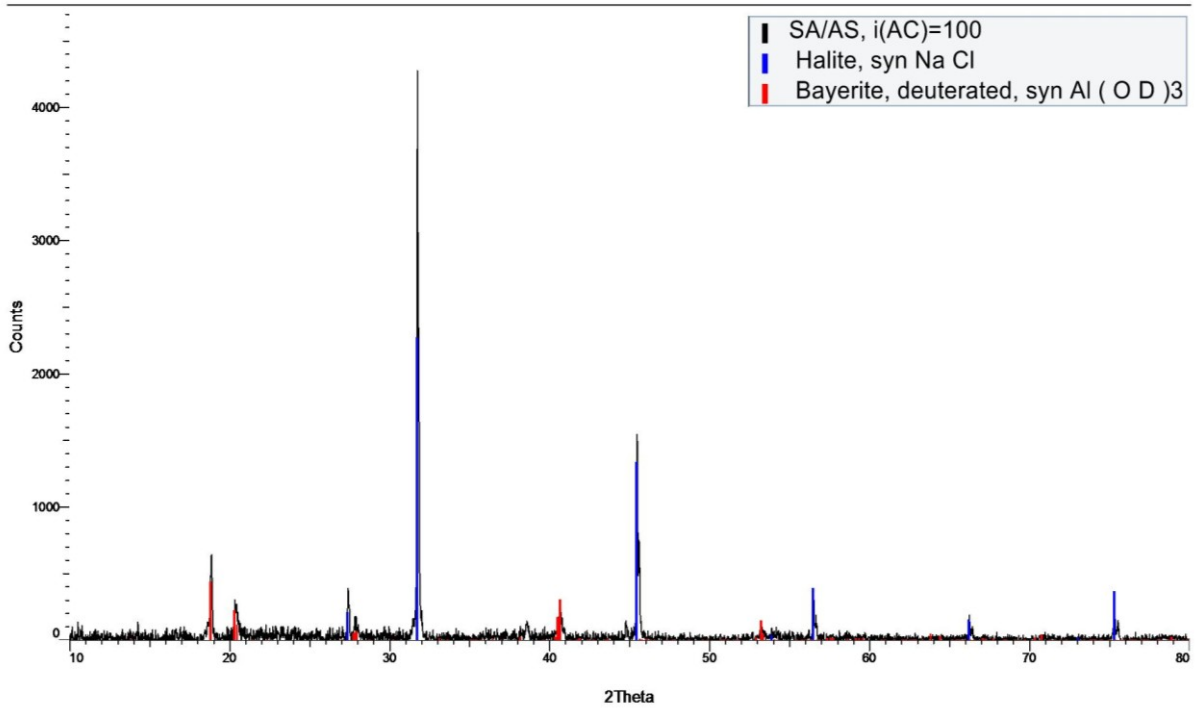

Figure C. 11. XRD spectrum of the corrosion product removed from an anode sample tested at 100 A m^{-2}. Peaks mainly match the crystal structure of halite, but also a minor amount of bayerite.

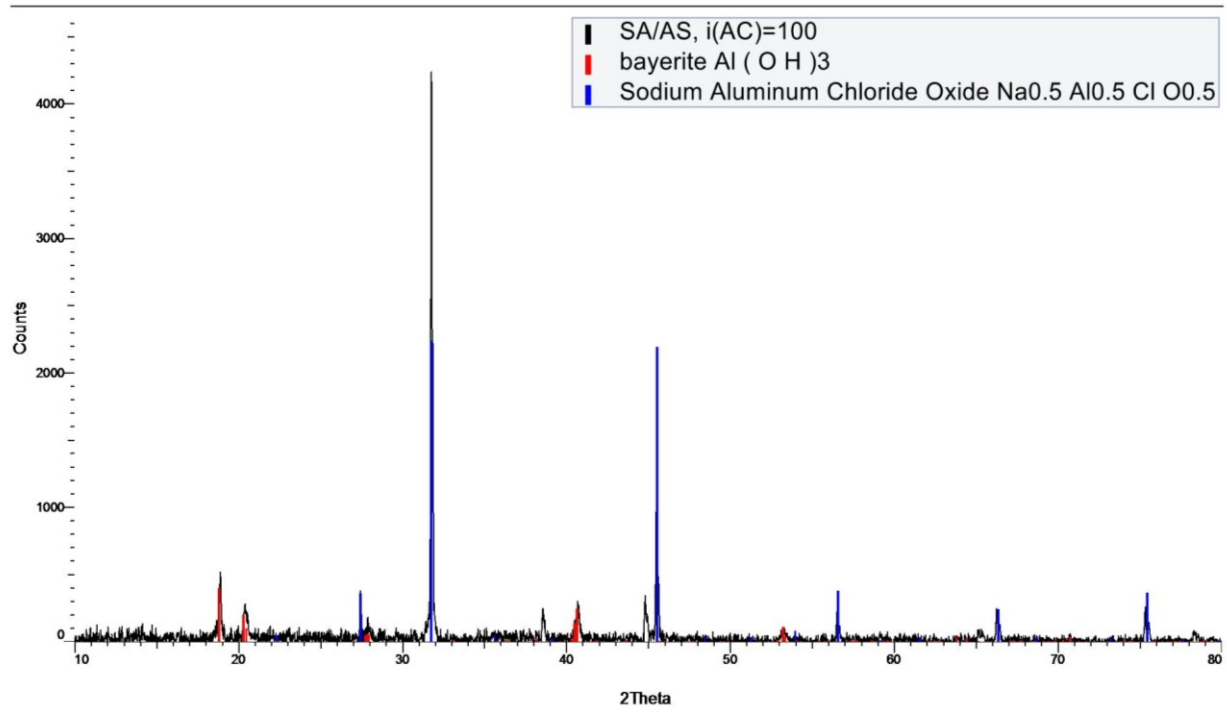

Figure C. 12 XRD spectrum of the corrosion product removed from an anode sample tested at 100 A m^{-2}. Peaks mainly match the crystal structure of sodium aluminium chloride oxide, but also a minor amount of bayerite.

D. Results from earlier work

Earlier work by the author involved AC testing of a coupled anode-steel pair (i.e. A/S experiments) with an area ratio (AR) of 10. Contrary to the experiments in this thesis, a preconditioning of steel to CP was performed for at least two weeks, to form calcareous deposits. Measurements of current density parameters (i.e. i_{DC} and i_{AC}) for a number of these earlier experiments are included here for comparison (Figure D. 1 and Figure D. 2). Both parameters conform well to the results in this thesis, and thus function as to provide a verification of new test apparatus and to evaluate the importance of calcareous deposits for the corrosion behaviour of AlZnIn anodes under influence of AC.

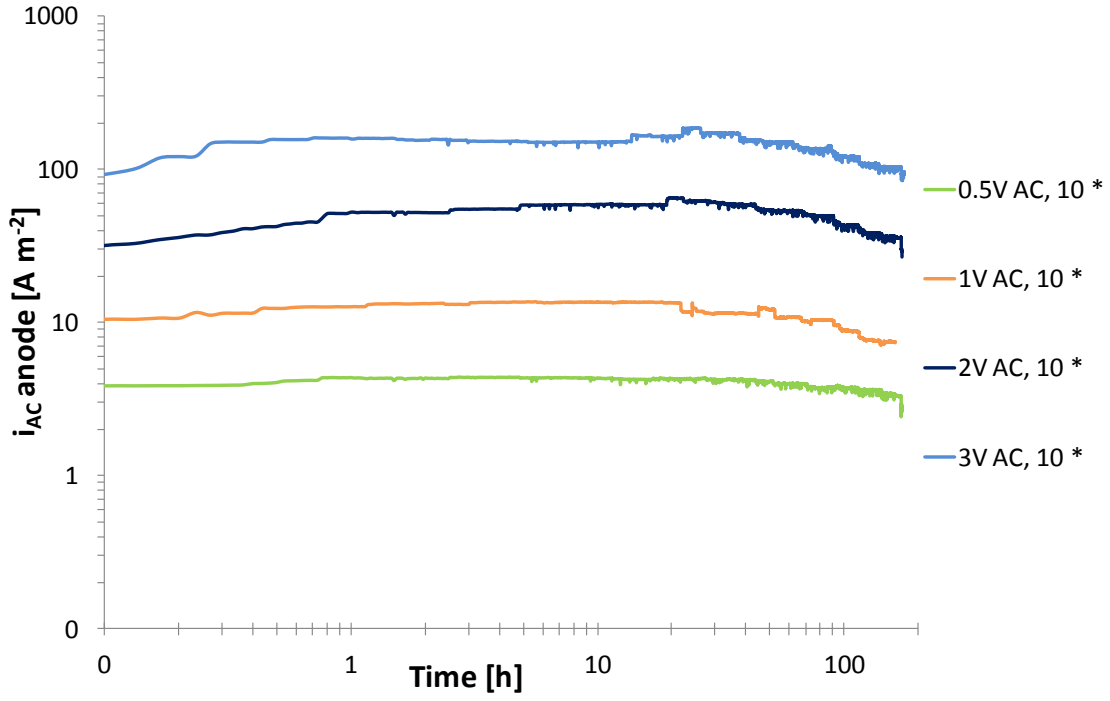

Figure D. 1. AC density of anode specimens in A/S experiments with an area ratio (AR) of 10 and various applied AC levels. Note that i_{AC} of steel samples are 10 times higher. From earlier work by the author [2].

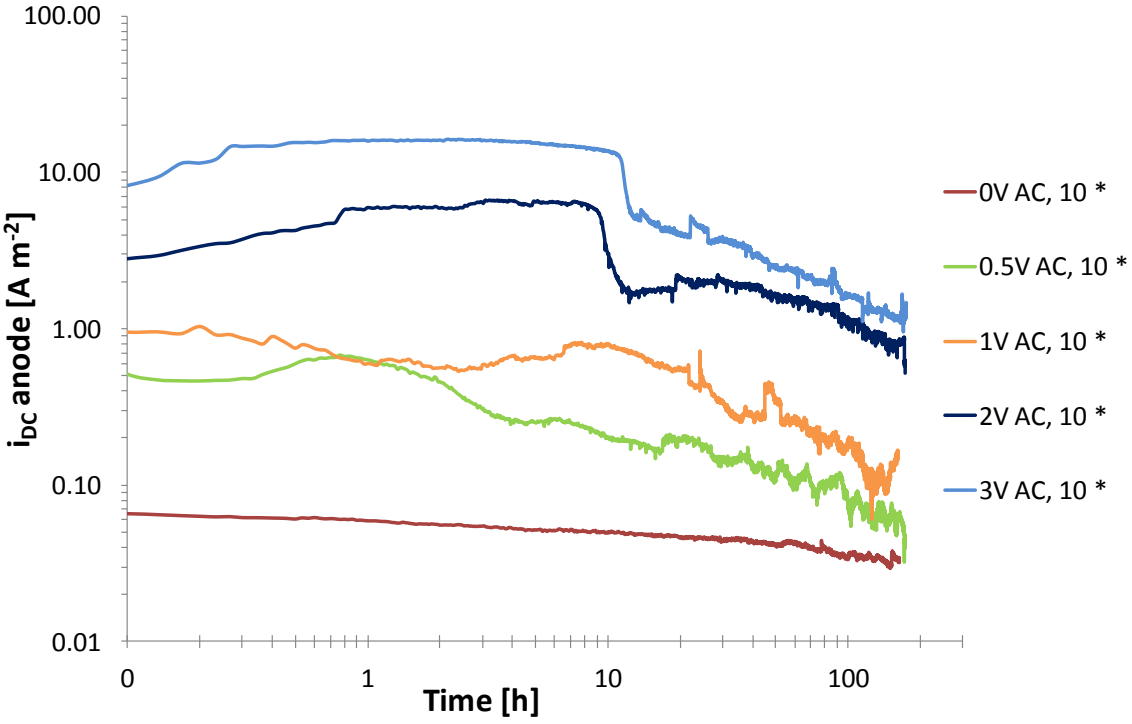

Figure D. 2. DC density of anode specimens in A/S experiments with an area ratio (AR) of 10 and various applied AC levels. Note that i_{DC} of steel samples are 10 times higher. From earlier work by the author [2].

A comparison of current measurements from earlier and present work in Figure D. 3 and Figure D. 4 at two different AC levels, demonstrates no clear impact on magnitude and change in i_{AC} by the presence of pre-developed calcareous deposits on steel. Whereas i_{AC} is generally higher in the experiment at 3 V AC involving preconditioning of steel, there is no apparent difference in i_{AC} at 2 V AC between the two experiments. One the other hand, a difference is apparent when comparing measurements of i_{DC} from experiments at the same AC level. DC current values are in general higher for experiments with no preconditioning. However, as evident from experiments at 2 V AC, the difference appear to cease in time, as both DC values decrease and stabilize at low levels.

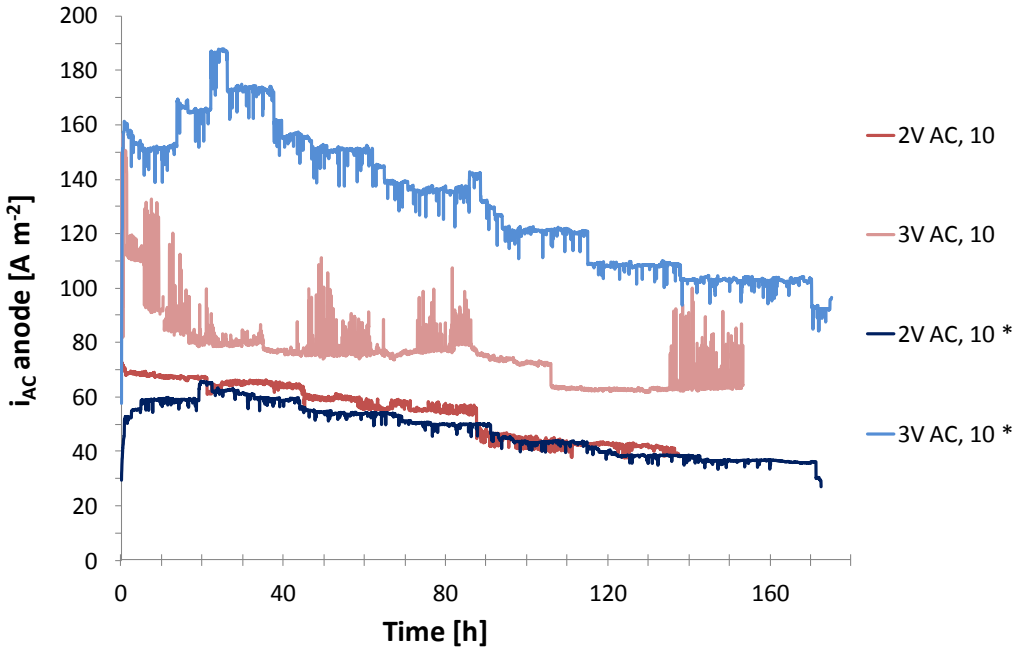

Figure D. 3. Comparison of measured AC density on anode specimens in A/S experiments at 2 V AC and 3 V AC, with an area ratio (AR) of 10. Earlier work [2] designated by *, is compared to work in this project to evaluate the importance of calcareous deposits on steel under influence of AC. Note that i_{AC} of steel samples are 10 times higher.

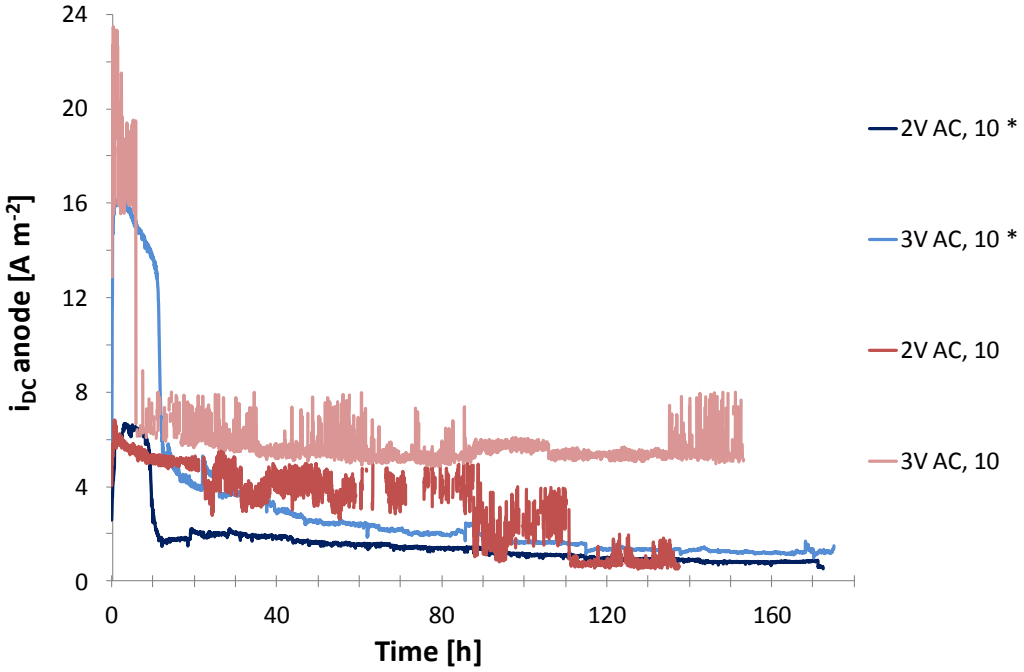

Figure D. 4. Measured DC density for anode specimens in A/S experiments at 2 V AC and 3 V AC, with an area ratio (AR) of 10. Earlier work [2] designated by *, is compared to work in this project to evaluate the importance of calcareous deposits on steel under influence of AC. Note that i_{DC} of steel samples are 10 times higher.

The corrosion rates of steel in a number of earlier experiments are included for comparison in Figure D. 5. The anode corrosion rates in Figure D. 5 are identical from those already included in section 4.2.2.

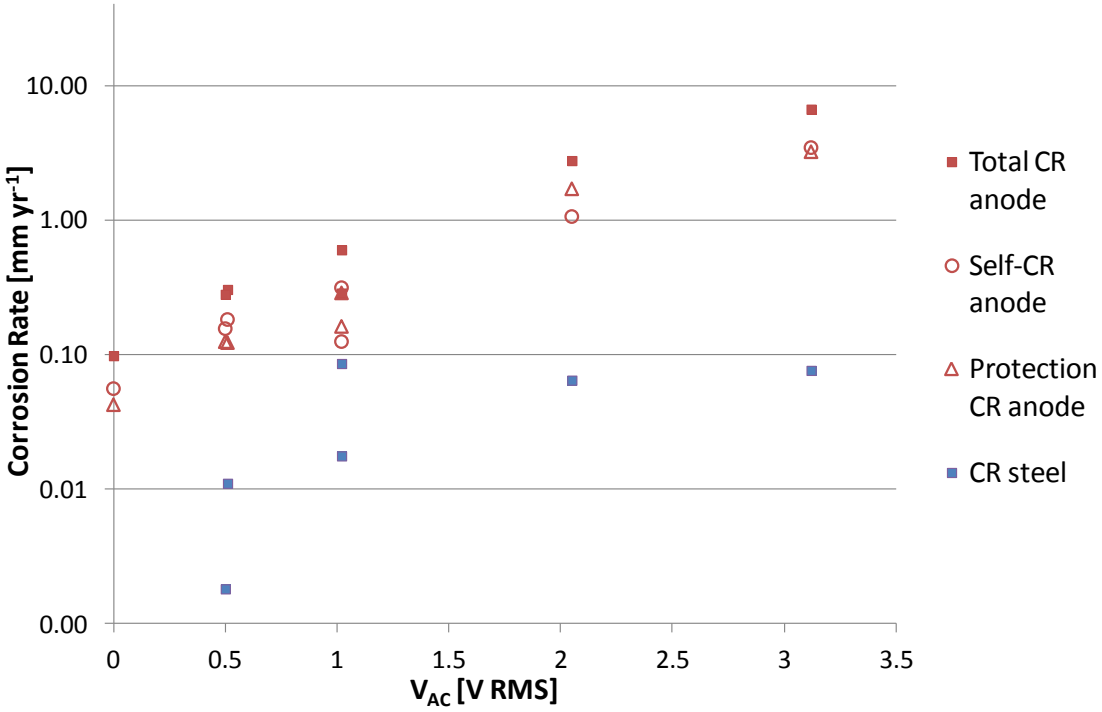

Figure D. 5. Anode and steel corrosion rates at various applied AC levels. Results from earlier A/S experiments with an area ratio (AR) of 10 and preconditioning of steel by CP to form calcareous deposits [2].